universität wien

DISSERTATION / DOCTORAL THESIS

Titel der Dissertation /Title of the Doctoral Thesis

„Towards radiolabeled peptides for imaging the immune checkpoint target PD-L1 “

verfasst von / submitted by

Nedra Jouini

angestrebter akademischer Grad / in partial fulfilment of the requirements for the degree of

Doktorin der Naturwissenschaften (Dr.rer.nat.)

Wien, 2022 / Vienna 2022

Studienkennzahl lt. Studienblatt / degree programme code as it appears on the student record sheet:	UA 796 605 419
Dissertationsgebiet lt. Studienblatt / field of study as it appears on the student record sheet:	Doktoratsstudium Naturwissenschaften Chemie
Betreut von / Supervisors:	Assoz. Prof. Dr. Thomas Mindt, Privatdoz. o. Univ.-Prof. Dr. Dr. Bernhard Keppler

Acknowledgement

Dear Reader,

If you have landed on this page, you must have contributed, in your own way, to the achievement of this work. For that reason, I would like to express my deep sense of gratitude towards your oversight, support, help, guidance, teachings, advice and most importantly for your valuable time and contribution to this journey. With it soon coming to an end, I would like to whole-heartedly thank you for everything you have done, built, drew, written, graded, and voiced to witness this doctoral thesis coming to light. These two words, we can never say enough; so, Thank you!

Cordially,

Nedra

Abstract

Molecular imaging and nuclear medicine have contributed to the evaluation and characterization of biological processes on the cellular level through radionuclide imaging. This technique is useful in managing and treating several diseases, most notably cancer. The advancement of radiopharmaceuticals targeting solid tumors for the radionuclide imaging modalities Positron Emission Tomography (PET) and Single Photon Emission Computed Tomography (SPECT) have facilitated diagnosis at early stages of the disease. It has also supported patient stratification for therapy (personalized medicine), thus improving the quality of primary care.

In the early phases of cancer diagnosis, choosing therapies that activate the innate responses of the immune system to eliminate lesions and malignancies is substantial. Immunotherapy has emerged as a new type of treatment that enables the body to suppress cancer cells by re-establishing its natural defences. Immune checkpoints, e.g., the Programmed cell Death receptor-1 (PD-1)/ligand 1 (PD-L1), are an immunotherapy target highlighted as an essential biomarker for both cancer diagnosis and treatment. The interaction between PD-1 (found on T cells) and PD-L1 (found on cancer cells) leads to T cells anergy and, therefore, tumor evasion and proliferation. Imaging immune checkpoints and PD-L1 with targeted radiopharmaceuticals gives valuable insight into the adequate inhibition therapy and the prediction of treatment response for many cancer patients.

With a PET/SPECT radiotracer targeting PD-L1, an expanded global use accounting for the different healthcare infrastructures would spread the benefits of immune checkpoint imaging and inhibition (ICI) therapy. This doctoral thesis has therefore explored the possibility of developing a novel peptide-based radiotracer for PD-L1 imaging with PET and SPECT as a novel ICI therapy probe. Macrocyclic peptides reported in the patent literature (from *Bristol Myers Squibb*) were selected to be synthesized, modified with a chelator, radiolabeled, and evaluated *in vitro* as potential radiotracers. The radiolabeling with either a PET-radionuclide gallium-68 (^{68}Ga) or a SPECT-radionuclide indium-111 (^{111}In) was made possible using the universal chelator DOTA.

Furthermore, a systematic investigation was conducted on the SPECT-radiometal ^{111}In to overcome the formation of unknown [^{111}In]In-species that affected the radiochemical yields of the radiolabeling experiments. The formation of the unwanted species has been circumvented by adding chloride ions to the [^{111}In]$InCl_3$ stock solution, allowing, therefore, for its recovery. Similar behaviour of [^{111}In]$InCl_3$ solution has rarely been reported, making it an important finding to the radiochemistry/pharmacy community. Consequently, the project continued with the PET radionuclide, and the synthesized macrocyclic peptide's radiolabeling with ^{68}Ga was successful. Despite the promising values reported in the patent, the low binding affinity of the selected macrocyclic peptide in radioactive receptor-binding experiments with PD-L1-expressing cell lines was observed. The loss of affinity could be explained by the modifications introduced to the initial peptide structure and the metal-complexation to the chelator

as indicated by the IC_{50} values from cellular assays. Nevertheless, we were able to establish the therapeutic potential of a macrocyclic peptide that inhibits the PD-1/PD-L1 interaction along with a novel standardized *in vitro* testing system, serving as a reference assay for newly developed PD-L1 radiotracers. The radioactive and the fluorescence-based *in vitro* evaluation of the peptide represented a significant key finding in this thesis, as our results may incite researchers to optimize this class of peptide immunomodulators for future radiopharmaceutical applications.

Zusammenfassung

Molekulare Bildgebung und Nuklearmedizin haben zur Auswertung und Charakterisierung biologischer Prozesse durch radionuklide Bildgebung auf zellulärer Ebene beigetragen. Diese Technik ist hilfreich bei der Behandlung verschiedener Krankheiten, insbesondere bei Krebs. Die Weiterentwicklung von Radiopharmazeutika, die auf solide Tumore abzielen, für radionuklide Bildgebungsmodalitäten Positronen-Emissions-Tomographie (PET) und Single-Photon-Emissions-Computertomographie (SPECT), haben eine frühe Diagnose der Krankheit erleichtert. Desweiteren hat sie die Patienteneinteilung für die Therapie (personalisierte Medizin) unterstützt und damit die Qualität der Primärversorgung verbessert.

In den frühen Phasen der Krebsdiagnose ist die Wahl von Therapien, die die angeborenen Reaktionen des Immunsystems aktivieren, um Läsionen und Malignome zu beseitigen, von wesentlicher Bedeutung. Solche Immuntherapien haben sich zu einer neuen Art der Behandlung entwickelt, die es dem Körper ermöglicht, Krebszellen zu unterdrücken, indem er seine natürlichen Abwehrkräfte wiederherstellt. Immuncheckpoints, wie z. B. der programmierte Zelltod-Rezeptor-1 (PD-1) und sein Ligand-1 (PD-L1), sind ein Ziel der Immuntherapie. Solche entscheidenden Biomarker werden sowohl für die Krebsdiagnose als auch für die Behandlung aufgezeigt. Die Wechselwirkung zwischen PD-1 (zu finden auf T-Zellen) und PD-L1 (zu finden auf Krebszellen) führt zu einer T-Zellen-Anergie und damit zur Proliferation von Tumoren. Die Bildgebung mit zielgerichteten Radiopharmaka von Immuncheckpoints, insbesondere von PD-L1, gibt für viele Krebspatienten wertvolle Einblicke in die geeignete Inhibitionstherapie und die Vorhersage, wie sie auf die Behandlung ansprechen werden.

Mit einem PET/SPECT-Radiotracer für PD-L1 würde eine erweiterte globale Verwendung, unter Berücksichtigung der verschiedenen Gesundheitsinfrastrukturen, die Vorteile der Immuncheckpoint-Bildgebung und -Inhibitionstherapie (ICI) ausweiten. Diese Doktorarbeit hat daher die Möglichkeit untersucht, einen neuartigen peptidbasierten Radiotracer als ICI-Therapiesonde für die PD-L1-Bildgebung mit PET und SPECT zu entwickeln. Makrocyclische Peptide, beschrieben in der Patentliteratur (von Bristol Myers Squibb), wurden ausgewählt, synthetisiert, mit einem Chelatbildner modifiziert, radioaktiv markiert und als potenzielle Radiotracer in vitro evaluiert. Die Radiomarkierung mit entweder dem PET-Radionuklid Gallium-68 (^{68}Ga) oder dem SPECT-Radionuklid Indium-111 (^{111}In) wurde unter Verwendung des universellen Chelatbildners DOTA ermöglicht.

Darüber hinaus wurde eine systematische Untersuchung des SPECT-Radiometalls ^{111}In durchgeführt, um die Bildung unbekannter [^{111}In]In-Spezies zu vermeiden, die die radiochemischen Ausbeuten der Radiomarkierungsexperimente beeinflussten. Die Bildung der unerwünschten Spezies wurde umgangen, indem der [^{111}In]$InCl_3$-Stammlösung Chloridionen zugesetzt wurden, wodurch ihre Rückgewinnung ermöglicht wurde. Ein solches Verhalten der [^{111}In]$InCl_3$-Lösung wurde bisher selten beschrieben, was es zu einer wichtigen Erkenntnis für die Radiochemie-/Pharmazie-Gesellschaft macht.

Das Projekt wurde mit dem PET-Radionuklid fortgesetzt, was zu einer erfolgreichen radioaktiven Markierung des synthetisierten makrozyklischen Peptids mit ^{68}Ga führte. Trotz der im Patent berichteten vielversprechenden Werte wurde eine geringe Bindungsaffinität des ausgewählten makrozyklischen Peptids in radioaktiven Rezeptor-Bindungsexperimenten mit PD-L1-exprimierenden Zelllinien beobachtet. Der Affinitätsverlust, angezeigt durch die zellulären Assays, könnte durch die Modifikationen und durch die Metallkomplexierung mit dem Chelatbildner erklärt werden, die in die anfängliche Peptidstruktur eingeführt wurde. Dennoch konnten wir das therapeutische Potenzial eines makrozyklischen Peptids, das die PD-1/PD-L1-Interaktion hemmt, zusammen mit einem neuartigen standardisierten in vitro-Testsystem etablieren, das als Referenzassay für neu entwickelte PD-L1-Radiotracer dienen wird. Sowohl die radioaktive als auch die fluoreszenzbasierte in vitro-Evaluierung des Peptids stellen eine wichtige Schlüsselerkenntnis dieser Dissertation dar, da unsere Ergebnisse Forscher dazu anregen könnten, diese Klasse von Peptid-Immunmodulatoren für zukünftige radiopharmazeutische Anwendungen zu optimieren.

Résumé

L'imagerie moléculaire et la médecine nucléaire ont contribué à l'évaluation et à la caractérisation des processus biologiques au niveau cellulaire grâce à l'imagerie des radionucléides. Cette technique est utile dans la gestion et le traitement de plusieurs maladies, notamment le cancer. L'avancement des radiopharmaceutiques ciblant les tumeurs solides pour les modalités d'imagerie par radionucléides, la tomographie par émission de positrons (TEP) et la tomographie par émission de photons uniques (SPECT) ont facilité le diagnostic aux premiers stades de la maladie. Ces techniques ont également soutenu la stratification des patients pour la thérapie (médecine personnalisée), améliorant ainsi la qualité des soins primaires.

Dans les premières phases du diagnostic du cancer, le choix des thérapies qui activent les réponses innées du système immunitaire pour éliminer les lésions et les tumeurs malignes est important. L'immunothérapie est apparue comme un nouveau type de traitement qui permet à l'organisme d'éliminer les cellules cancéreuses en rétablissant ses propres défenses naturelles. Les points de contrôle immunitaires, par exemple le récepteur de mort cellulaire programmée-1 (PD-1) /ligand 1 (PD-L1), sont une cible d'immunothérapie mise en évidence comme un biomarqueur essentiel pour le diagnostic et le traitement du cancer. L'interaction entre PD-1 (trouvé sur les cellules T) et PD-L1 (trouvé sur les cellules cancéreuses) conduit à l'anergie des cellules T et, par conséquent, à l'évasion et à la prolifération tumorales. L'imagerie des points de contrôle immunitaire et de PD-L1 avec des radiopharmaceutiques ciblés communique des informations précieuses sur la thérapie d'inhibition adéquate et la prédiction de la réponse au traitement pour de nombreux patients atteints de cancer.

Avec un radiotraceur PET/SPECT ciblant PD-L1, une utilisation mondiale élargie tenant compte des différentes infrastructures de soins de santé permettrait de diffuser les avantages de la thérapie d'imagerie et d'inhibition des points de contrôle immunitaire (ICI). Cette thèse de doctorat a donc exploré la possibilité de développer un nouveau radiotraceur peptidique pour l'imagerie PD-L1 avec PET et SPECT en tant que nouveau moyen de thérapie et d'imagerie ICI. Des peptides macrocycliques rapportés dans la littérature des brevets (de *Bristol Myers Squibb*) ont été sélectionnés pour être synthétisés, modifiés avec un chélateur, radiomarqués et évalués *in vitro* en tant que radiotraceurs potentiels. Le radiomarquage avec soit un PET-radionucléide gallium-68 (^{68}Ga) soit un SPECT-radionucléide indium-111 (^{111}In) a été rendu possible grâce au chélateur universel DOTA.

En outre, une enquête systématique a été menée sur le SPECT-radiométal ^{111}In pour surmonter la formation d'espèces [^{111}In]In inconnues qui affectaient les rendements radiochimiques des expériences de radiomarquage. La formation des espèces indésirables a été contournée en ajoutant des ions chlorure à la solution mère [^{111}In]$InCl_3$, permettant ainsi sa récupération. Un comportement similaire de la solution [^{111}In]$InCl_3$ a rarement été rapporté, ce qui en fait une découverte importante pour la communauté radiochimie/pharmacie. Par conséquent, le projet s'est poursuivi avec le radionucléide PET et le radiomarquage du peptide macrocyclique synthétisé avec ^{68}Ga a été couronné de succès. Malgré

les valeurs prometteuses rapportées dans le brevet, la faible affinité de liaison du peptide macrocyclique sélectionné dans des expériences de liaison aux récepteurs radioactifs avec des lignées cellulaires exprimant PD-L1 a été observée. La perte d'affinité pourrait s'expliquer par les modifications introduites dans la structure initiale du peptide et la complexation du métal avec le chélateur, comme indiqué par les valeurs IC_{50} des essais cellulaires. Néanmoins, nous avons pu établir le potentiel thérapeutique d'un peptide macrocyclique qui inhibe l'interaction PD-1/PD-L1 avec un nouveau système de test *in vitro* standardisé, servant de test de référence pour les radiotraceurs PD-L1 nouvellement développés. L'évaluation *in vitro* radioactive et basée sur la fluorescence du peptide a représenté une découverte clé importante dans cette thèse, car nos résultats pourraient inciter les chercheurs à optimiser cette classe d'immunomodulateurs peptidiques pour de futures applications radiopharmaceutiques.

Table of content

Introduction

1. Molecular Imaging and Nuclear Medicine

1.1 Role of molecular imaging in nuclear medicine

Throughout the past years, non-invasive molecular imaging within nuclear medicine has provided valuable clinical information at both cellular and molecular levels. It has significantly contributed to the healthcare sector and the assessment of disease via well-targeted radioactive probes accumulating in specific areas in the body.[1] Imaging has laid the ground for a better understanding of various functional processes: from tissue blood flow, metabolic activity, interactions between proteins, expression of cell-surface receptors, neurotransmitters, and neurochemical activity, to tissue proliferation.[2] The collection of such diverse information allows for a more accurate treatment choice, leading to coherent prognostic statements for patients. As described by the Society of Nuclear Medicine and Molecular Imaging (SNMMI) and its Molecular Imaging Centre of Excellence: "*Molecular imaging is the visualization, characterization and the measurement of biological processes at the molecular and cellular levels in humans and other living systems*".[3]

Different non-invasive molecular imaging modalities can be distinguished within the field of nuclear medicine: computed tomography (CT) imaging, ultrasound imaging (US), optical imaging (OI), magnetic resonance imaging (MRI), and radionuclide imaging.[4] Computed tomography (CT) imaging involves using a computer-processed combination of X-rays measured from different angles and forming a tomographic cross-sectional image. High-resolution small animal CT, which is often relied on in preclinical research, allows for imaging skeletal and soft tissues.[5] Ultrasound imaging is a form of tomography that uses ultrasound to probe soft tissues and help detect the early stages of the disease. With the advances in the ultrasound contrast agent field, ultrasound sensitively depicts specific molecular targets. It can be used for both diagnostic and therapeutic ends.[6]

Furthermore, optical imaging includes both fluorescence and bioluminescence imaging, which are light-using imaging modalities and thus relatively safe.[7] In OI, bioluminescence imaging (BLI) relies on the light produced by enzymatic oxidation of luciferase and coming from the tissue unlike the fluorescence, making BLI a more sensitive method. Moreover, MRI employs strong magnetic fields and radio waves to produce images of different organs in the body.[8] MRI requires introducing an imaging contrast agent, a ferromagnetism contrast agent (lanthanide chelate such as gadolinium-DTPA) or a paramagnetic one (paramagnetic iron oxide). Lastly, radionuclide imaging is a technique that relies on the intravenous administration of a radiotracer.[9] With the progress in radiochemistry and molecular biology, radionuclide imaging provides high sensitivity (see Table 1) and specificity as it has found numerous clinical applications. It incorporates radioactive substances in the therapy and diagnosis of certain diseases. A radiopharmaceutical (or radiotracer) is usually composed of a radionuclide attached to a biomolecule via a linker/chelator system (or a prosthetic group) and is injected intravenously. It maps the defected tissues by following the circulatory system and localizing lesions.[10]

Table 1: Spatial resolution and sensitivity of imaging modalities in nuclear medicine. [19-22]

Imaging Modality	Spatial Resolution (mm)	Target sensitivity (mol/L)
Computed Tomography (CT)	0,5-2 (clinical CT) 0,2-0,3 (animal CT)	10^{-2}-10^{-3}
Magnetic Resonance Imaging (MRI)	0,5-1,5 (1.5 T MRI) 0,01-0,1 (small animal MRI)	10^{-3}-10^{-5}
Positron Emission Tomography (PET)	4-10 (clinical PET) 1-2 (micro-PET)	10^{-11}-10^{-12}
Single Photon Emitting Tomography (SPECT)	7-15 (clinical SPECT) 0,5-2 (micro-SPECT)	10^{-10}-10^{-11}
Optical Imaging	1-5	Biolum: 10^{-15}-10^{-17} Fluo: 10^{-9}-10^{-12}
Ultrasound Imaging	0,05-0,5	Not characterized

Positron Emission Tomography (PET) and Single Photon Emission Computed Tomography (SPECT) are the two nuclear imaging modalities discussed in-depth in the following text.[11,12] Overall, these imaging techniques are used to evaluate certain disease-states while providing a whole-body mapping of the target tissues. Nonetheless, they present various strengths and weaknesses, among which exposure to harmful ionizing radiation is of high relevance. PET is relatively more expensive than SPECT and CT. It also suffers from long acquisition times and low spatial resolution, similarly to SPECT. However, CT lacks in good contrast when it comes to imaging soft tissues. Despite these setbacks, PET, SPECT and CT offer unlimited depth of penetration and the possibility to image the whole body. Unlike the quantitative molecular imaging provided by PET and SPECT, CT can only provide anatomical imaging. As far as MRI, US and OI are concerned, these techniques do not use any ionizing radiation. MRI provides excellent contrast of soft tissues, high spatial resolution, full-body imaging. Nonetheless, MRI remains an expensive imaging tool with a long acquisition time. US and OI, however, can offer real-time imaging with short acquisition times while maintaining an excellent spatial resolution and a high sensitivity. Although imaging the whole body is not possible with US and OI, OI presents a limited penetration depth.[13] The contrast microbubbles of the US can only be limited to the vasculature.

Furthermore, these imaging modalities help elucidate different biological processes that other medical techniques failed to evaluate, such as specific organ function, enzyme activity, and, most importantly, disease progression. Multimodality imaging - the combination of more than one imaging technique - leads to synergistic effects and can compensate for the drawbacks of each method.[14] For instance, PET/CT, SPECT/CT and PET/MRI are highly efficient multimodality imaging techniques.[15] They can provide both anatomical and functional information, allowing for successful clinical evaluation. For

instance, the PET/CT scans of ^{18}F-FDG show the accumulation of the tracer in high-metabolic tumor lesions, while locating them anatomically with the CT scan.[16] Moreover, CT is more sensitive than PET and SPECT; therefore, the combination of both yields better results.[17] OI/US is another well-known combination as the high resolution of US can complement the high specificity and sensitivity of OI.[18]

1.2 Imaging modalities in nuclear medicine

In the case of cancer diagnosis with PET and SPECT, the scans show the different parts of the lesions where the disease has proliferated (see Figure 3). Within this non-invasive imaging technique, the radioactive particles emitted by the injected radiotracer from within the body, are detected by gamma cameras and reconstructed to form a 3-D image.[23] The radioactive decay leads to the emission of either electromagnetic radiation (gamma rays, γ) or of radioactive particles (α, β^+, β^-). Gamma rays, X-rays and β^+ particles are used to diagnose certain diseases using SPECT, CT, and PET. However, α particles and β^- have found numerous applications in therapy as they have a short travelling distance when injected into soft tissues and are more likely to damage cancer cells.[24]

1.2.1 SPECT

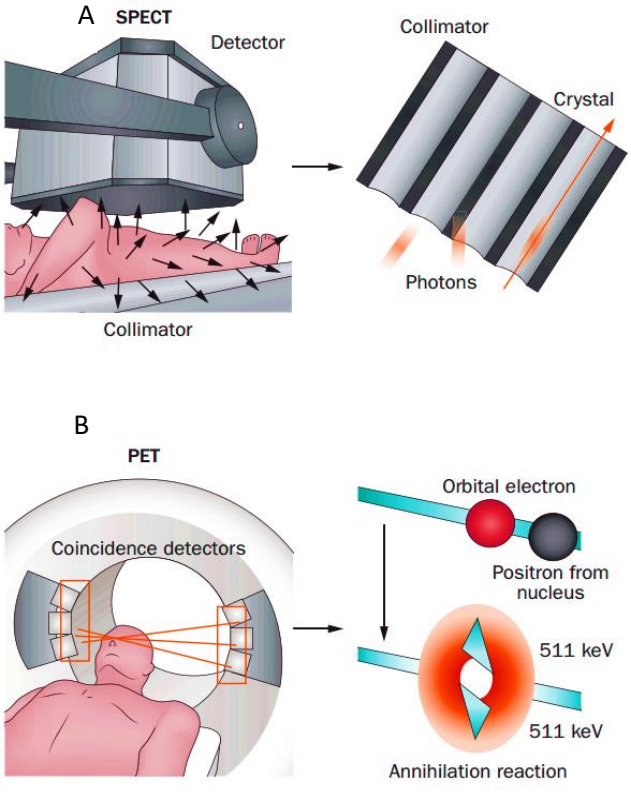

Figure 1: A) An illustration of the SPECT machine and the incoming gamma radiation the collimators detect from various angles B) The coincidence detectors of a PET scanner and the annihilation event taking place between a positron and an electron, releasing gamma rays within the line of response (in orange). Image adapted from *Hicks, R. J. et al. Nat. Rev. Clin. Oncol. 2012, 9 (12), 712–720*.[25]

SPECT is a nuclear imaging modality that directly detects gamma rays. It requires, therefore, a gamma-emitting radiotracer that is administered to patients through intravenous injection. In SPECT, gamma emitters, such as indium-111 (^{111}In), technetium-99m (^{99m}Tc) or iodine-123 (^{123}I) are used (see Table 2).[25] Despite the direct emission of gamma-rays detected by a rotating multi-headed camera, PET presents the advantage of offering more radiation localization events. This creates a better spatial reconstruction with higher resolution than SPECT.[26,27] However, SPECT scans are relatively more cost-effective than PET, mainly due to the use of longer-lived radionuclides; they are easier to obtain than PET radionuclides, and they enable the performance of longitudinal studies. Moreover, SPECT is less sensitive than PET which is due to the process of photon-detection: the radiation detector in

SPECT and PET cameras relies on scintillator crystals (usually thallium- doped sodium iodide (NaI(Tl)) that converts ionizing radiation into photons.[28] In their turn, these photons can be captured by the photomultiplier tubes and transformed into an electric signal (see Figure 2).[29-31] In pre-clinical SPECT, pinhole collimators that magnify specific organs are used. As for the clinical SPECT cameras, the parallel collimators can only capture certain ionizing particles. Therefore, anything that did not travel along the collimator axis is rejected and is not accounted for in signal processing. Due to the accurate 3-D space localization, SPECT can be used for localized organ functions such as brain imaging, cardiac imaging, and more specifically, myocardial perfusion imaging (using ^{99m}Tc radiotracers, Figure 3).[32]

The 2-D scintigraphy has also allowed for accurate bone imaging and further widening of the disease diagnosis array in nuclear medicine.

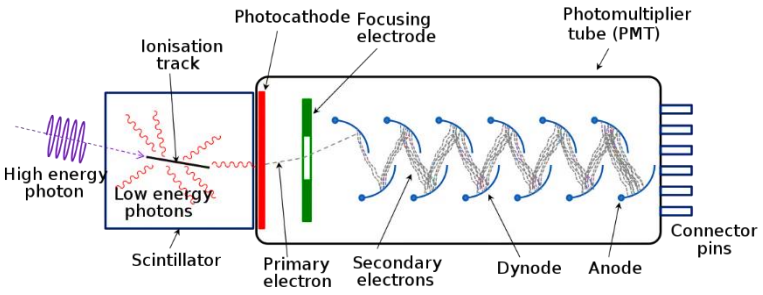

Figure 2: The principle of radiation detection in SPECT and PET cameras. The scintillator is composed of (NaI(TI)) crystals that would have an electron ejected by the incident gamma photon. A small flash of light is then produced when the electron finds stable energy levels (Compton effect). The PMT tubes detect these flashes (events) and amplify them so that they can be summed and converted into an electrical signal. Figure credit: Qwerty123uiop (CC BY-SA 3.0)[33]

1.2.2 PET

PET radiotracers are different from SPECT because of their detection method. In PET, the detection of gamma rays takes place via a physical phenomenon known as positron annihilation.[34] Moreover, PET radionuclides decay by emitting a positron (positive electron). It is emitted by the nucleus of the radionuclide and quickly pairs up with an electron in the neighbouring tissues, leading to annihilation. Annihilation is therefore observed when this collision converts the mass-energy of the two particles into photons, with 511 KeV each (see Figure 1B). These two gamma-rays photons maintain the momentum to travel in opposite directions. Since PET has more of a ring-shaped detector encircling the patient, the scintillating crystal detectors capture the photons emitted from various points, absorbing them, and converting them into an electric signal. The simultaneous detection of the photons in the detector (called coincidence) leads to the placement of a line between those two points (line of response), localizing, therefore, the annihilation event.[35] The numerous coincidence lines help to reconstruct a high-resolution three-dimensional scan. PET detectors are formed of many blocks of scintillation crystals arranged circularly in one or two rows, capturing the emerging 511 KeV photons from the line of response (see Figure 1B). The most used scintillators for PET detector types are Bismuth Germanate (BGO), Sodium Iodide (NaI), and Lutetium Oxyorthosilicate (LSO). However, Bismuth Germanate (BGO) is preferred to NaI(TI) since the attenuation coefficient is not enough for the high annihilation energy received. Furthermore, Lutetium Oxyorthosilicate (LSO) has better properties than NaI(TI) and BGO.[36]

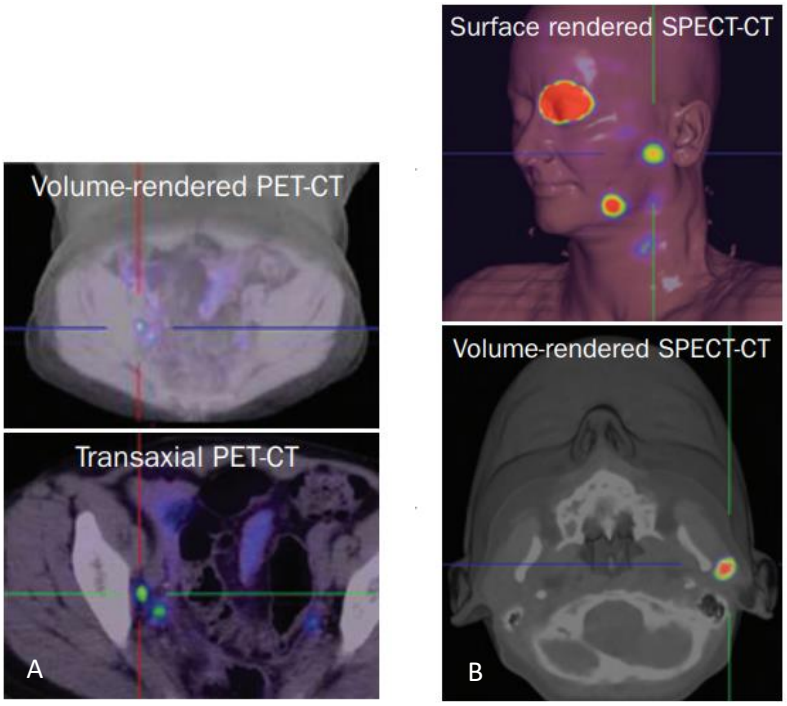

Figure 3: A) A PET-CT scan for ^{18}F-FDG for the detection of small malignant melanoma metastases B) A SPECT-CT scan of ^{99m}Tc-colloid for sentinel lymph-node detection. [25]

1.3 Radiopharmaceuticals in oncology

Radiotracers are the primary operative tool of radionuclide imaging in nuclear medicine**.** They have found various non-invasive applications in cancer diagnosis, staging, and predicting the response to therapy. It is known by clinicians that patients exhibit different types of lesions within the same cancer category and highly variable malignancies within the patient.[37] This heterogeneity is found in different morphological and physiological features, such as the expression of cell surface receptors or proliferative and angiogenic potential.[38,39] However, PET and SPECT have gained in the detection accuracies of specific lesions, leading to the optimized differentiation of cancer progression stages while shedding light on tumor heterogeneity.[40,41] The diagnosis can be achieved by targeted radiopharmaceuticals or by a combination of different ones, each bringing complementary information to fulfil the diagnostic process.

1.3.1 Theragnostic

Radiopharmaceuticals have a dual application in nuclear medicine: a radiotracer can be used in diagnosis and therapy, a concept known as the theragnostic approach.[42] The application can combine diagnostic imaging and therapy, using the same scaffold but interchanging the radionuclide (since α or β^- particles are needed for therapy) or injected into the patient in a different dose than the diagnostic one.[43] Historically, radioiodine has been the first successful theragnostic radiotracer to be used to diagnose and treat thyroid cancer, with ^{123}I for diagnosis and ^{131}I for therapy.[44] A theragnostic radionuclide can emit

gamma-rays and β particles such as lutetium-177 (^{177}Lu) and ^{131}I, as seen in Table 2. Moreover, different isotopes from the same element can be used, such as yttrium-86 (^{86}Y)/yttrium-90 (^{90}Y) (true matches), or even terbium isotopes; newly emerging radiometals: ^{152}Tb (β^+), ^{155}Tb (γ), ^{149}Tb (α) and ^{161}Tb (β^-).[45] Many theragnostic-based therapies have gained tremendous success, such as ^{90}Y for liver cancer therapy, ^{31}I for thyroid cancer and ^{177}Lu-PSMA radionuclide therapy for different types of prostate cancer. For instance, during the administration of the therapeutic ^{177}Lu-PSMA compound, SPECT scans can be taken to follow the progression of the uptake. [46,47]

Table 2: Repartition of diagnostic and therapeutic radionuclides as original, true matches or matched pairs of theragnostic radionuclides.

	Diagnosis	Therapy
Original theragnostic	^{177}Lu γ (SPECT)	β^- (therapy)
	^{131}I γ (SPECT)	β^- (therapy)
True matches	^{86}Y β^+ (PET)	^{90}Y β^- (therapy)
	^{64}Cu β^+ (PET)	^{67}Cu β^- (therapy)
Matched pairs	^{68}Ga β^+ (PET)	^{177}Lu β^- (therapy)
	^{99m}Tc γ (SPECT)	$^{186/188}$Re β^- (therapy)

1.3.2 Dosimetry of PET and SPECT applications

The intravenous administration of a radiopharmaceutical to a patient for diagnostic or therapeutic purposes leads to the absorption of ionizing radiation. Once absorbed, this ionization and excitation of atoms in human tissues lead to DNA damage, delayed cell division rate and health complications consequently.[48] Therefore, the benefits of the intervention must be balanced with the dangerous side effects of the procedure. The radiotracer's design needs to consider the following characteristics of the radioisotope: the half-life ($t_{1/2}$), the method and costs of production, the mode of decay, the coordination chemistry of the radioactive metal and its possible chelating agents. Dosimetry calculates this risk correlated with medical interventions relying on ionizing radiation. It calculates the amount of estimated radiation dose deposited in the human tissues. First, it is essential to determine the radiotracer distribution in different parts of the body and organs. This type of data is usually obtained during the preclinical evaluation of a novel radiopharmaceutical through *ex vivo* studies in animals.[49]

Furthermore, evaluation of the radiotracer (pharmacokinetics and biodistribution) in humans using whole-body imaging techniques such as PET and SPECT are carried out in clinical trials. Therefore, it is required to determine the radiation dose to every organ (equivalent dose, mSv) and to the whole body

(effective dose, mSv), then judge in comparison to the benefits that the patient receives from this medical intervention. Dosimetry is also a well-regulated subfield in nuclear medicine where national and international guidelines set the regulatory frameworks that must be respected and put in place.[50]

1.3.3 Types of radiotracers

Radiotracers can be divided into two distinct categories: 1st generation and 2nd generation radiotracers. The first category consists of radioactively labeled molecules that accumulate in the area/tissues of interest based on their physical properties. These radiotracers, known as perfusion tracers, are generally considered specific but do not target a specific receptor or a pathway. Examples include the ^{99m}Tc-MIBI for cardiac imaging, which imitates the transport of potassium ions into the heart muscle.[51,52] Another ^{99m}Tc-based tracer is HEDP (etidronic acid). This bone imaging tracer accumulates in hyperactive bone tissues by interacting with its calcium ions.[53] As far as the 2nd generation of radiotracers is concerned, they rely on molecular recognition of receptors, antigens, and other types of biological interactions (imitating endogenous ligands).[54] Specific radiolabeled probes are developed to target different tumor sites and elucidate various cancers' proliferation mechanisms.

Radiotracers are powerful molecular imaging tools for cancer diagnosis due to their high sensitivity. They usually consist of a biomolecule having a well-targeted physiological pathway or a receptor to which it binds with high affinity.[55] These well-targeted imaging probes can be small molecules or peptide-based such as ^{68}Ga and ^{111}In-labeled somatostatin peptide-analogues targeting the somatostatin receptors expressed by neuroendocrine tumours (DOTA-TATE/TOC for somatostatin receptor subtype 2).[56] ^{68}Ga, ^{18}F and ^{177}Lu (therapy) labelled PSMA ligands targeting prostate cancer have made their mark among many research teams and clinical investigations.[57]

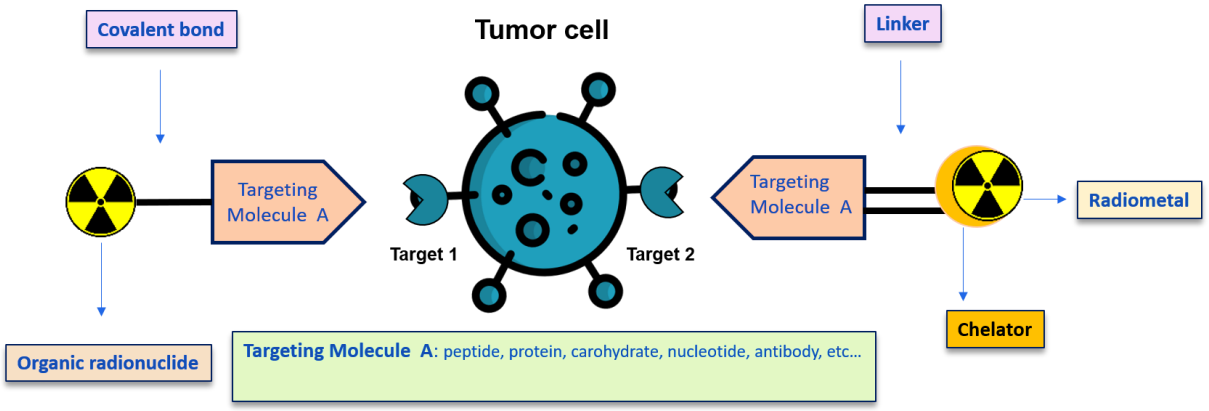

Figure 4: Schematic explanation of the various types of possible radionuclide conjugation systems and targeting molecules within a radiopharmaceutical.

Other peptide-based radiotracers, such as RGD peptides, are used for angiogenesis imaging (targeting $\alpha_v\beta_3$ integrin - refer to Table 6). Moreover, antibody/protein-based radiotracers such as ^{125}I-Trastuzumab (targeting the human epithelial growth factor receptor 2 HER2) and ^{89}Zr-Nivolumab targeting programmed cell death receptor 1 PD-1; are prominent examples that can be named among many.[58,59]

The biomolecular probe (proteins or peptides) should possess a modification site where the conjugation of a linker/chelator can be made possible (see Figure 4).

1.3.4 Types of radionuclides

We can distinguish between two types of radionuclides used in the development of radiotracers. Metal-based radionuclides (also called radiometals) such as ^{111}In, ^{99m}Tc, ^{68}Ga, ^{64}Cu, and ^{89}Zr. The second type is organic radionuclides, formed of ^{11}C, ^{18}F, ^{13}N and ^{15}O (see Table 3).[62,63]

1.3.4.1 Organic radionuclides

Organic atoms such as carbon, hydrogen, oxygen, and nitrogen, have many unstable radioisotopes that can substitute the stable atoms (forming covalent bonds with the bio vector as shown in Figure 4).

Table 3: Organic and metallic radionuclides and their characteristics. These radiotracers are used in oncology, CNS and brain, metabolism, and perfusion imaging.[60,61]

Radionuclide	Half-life	Decay mode	Energy (KeV)	Production route	Radiotracer
^{11}C	20.3 min	β^+ and Electron Capture (EC)	1982	Cyclotron ^{14}N (n, p)^{11}C	^{11}C-PHNO ^{11}C-PIB ^{11}C -AMT
^{13}N	9.97 min	β^+	1220.5	Cyclotron ^{16}O (p, α)^{13}N	^{13}N-N2
^{15}O	122.2 sec	β^+	1754	Cyclotron ^{14}N (d, n)^{15}O	^{15}O-water
^{18} F	109 min	β^+ and γ	6335	Cyclotron ^{20}Ne (d, α) ^{18}F	^{18}F-FDG ^{18}F-FET ^{18}F-FDOPA
^{99m}Tc	6.02 h	γ, Internal Transition	140	^{99}Mo/^{99m}Tc generator	^{99m}Tc-Demobesin1 ^{99m}Tc-MIBI
^{111} In	67.2 h	EC, Auger e$^-$	245.17	Cyclotron ^{111}Cd (p, n)^{111}In	^{111}In-Octreotide
^{68} Ga	67.7 min	β^+, EC	1889	^{68}Ge/^{68}Ga generator	^{68}Ga-PSMA ^{68}Ga-Pentixafor ^{68}Ga-FAPI
^{123} I	13 h	γ, EC	159	Cyclotron ^{122}Te (d, n)^{123}I	^{123}I-FP-CIT

These unstable isotopes can be used as PET radionuclides. ^{11}C and ^{18}F constitute the basis of many PET radiotracers with versatile chemistry.[62] ^{11}C is thoroughly used for brain imaging, such as ^{11}C-L-DOPA, an analogue of L-DOPA, a precursor for dopamine. As far as ^{18}F is concerned, 2-deoxy-2-(^{18}F)-fluoro-D-glucose (^{18}F-FDG) is a glucose analogue and has been extensively used for many diagnostic purposes.

^{18}F-FDG is, in fact, a metabolic activity probe that allows for early tumor detection when combined with other investigative tools. [64-66]

Despite their multiple uses in radiotracer development, organic radionuclides have found limited application. They can only be used in PET imaging (only diagnostic) due to their predominant emission type. Furthermore, these radionuclides do not have therapeutic analogues, unlike radiometals. Exceptionally, only the iodine isotopes ^{124}I (diagnostic; β+, ε) and ^{131}I (therapeutic; β−, γ) form a theragnostic pair within the organic radionuclide category. Sodium iodine symporter is used to diagnose and treat thyroid cancer and non-thyroidal neoplasms, among other thyroidal disorders.[67]Although, as a radionuclide, iodine is limited due to its deionization and subsequent uptake in thyroidal tissues. There are other less common organic radionuclides such as bromine (bromine-75 and bromine-76) based radiotracers for PET and SPECT as well as astatine-211, an alpha emitter that is more suited for therapy.[68] However, these radionuclides have yet to find frequent use and applications. That is mainly due to the high costs of production in nuclear reactors or particle accelerators, the availability of the targets that need to be irradiated, and the lack of the infrastructure (and regulatory framework) suitable for such productions across the world.[69]

1.3.4.2 Metallic radionuclides

Metallic radionuclides have witnessed tremendous growth in radionuclide imaging. Radioisotopes of transition metals such as ^{99m}Tc, ^{89}Zr, or ^{111}In and ^{68}Ga from the primary metals group from the periodic table. They are in frequent use due to their versatility and the vast range of characteristics. The use of targeted radiotracers depends on the biological half-life of the chosen molecule; antibodies tend to have a prolonged circulation time, so it is required to match them with a long-living metal radionuclide such as ^{89}Zr ($t_{1/2}$ =3.3 days) or ^{111}In ($t_{1/2}$ = 2.8 days).[70] Among the most used metallic radionuclides, ^{99m}Tc and ^{68}Ga, they are usually produced via ^{99}Mo/^{99m}Tc generators and ^{68}Ge/^{68}Ga generators. Scandium-44, which had started to gain popularity in recent years, can also be eluted from a Titanium-44 / Scandium-44 generator. As for most metallic radionuclides, their production requires irradiating a specific target in a cyclotron; ^{111}In, for instance, is produced by proton irradiation of a cadmium target, either ^{112}Cd (p,2n) or $^{\boldsymbol{111}}$Cd (p,n).[24,71]

Similarly, ^{89}Zr can be obtained *via* proton irradiation of natural yttrium targets ^{89}Y (p, n). Despite the straightforward methods used to produce metallic radionuclides, the lack of the appropriate infrastructure, low irradiation yields, and lack of available pure substances (target) constitute the limiting factors to their application. Among the less commonly used radionuclides, we can mention strontium-82, bismuth-213 or actinium-225, an alpha-emitter that is on the rise in the field of cancer radiation therapy. However, for diagnostic imaging, the decay mode of most metallic radionuclides needs to be mainly by β^+ particle (for PET) or via gamma rays 'emission (SPECT) to ensure the signal reception and

transmission through the gamma cameras. A chelator that matches the physical and chemical characteristics of the chosen metal needs to be selected and conjugated to the biomolecule.[72]

Most widely used radiometals such as ^{111}In and $^{67/68}$Ga are also called hard Lewis' acids, with a predominant oxidation state of +3 (hence their appellation M^{3+}) in aqueous solutions.[73] Chelators, which can be monodentate or multidentate/polydentate, have oxygen, nitrogen, or sulphur donor groups in carboxyl groups, phosphonates, and amines, form stable complexes with radiometals *in vivo*.[74]

The difference between the monodentate and the polydentate chelator is found in what is known as the '*chelate effect'*. It has been shown that on a thermodynamic level, multidentate chelators readily exchange ligands more than monodentate ones, making them more stable in forming a chelate-metal complex. A positive increase in entropy can be observed. At the same time, the enthalpy change is almost negligible, making this complexation favours the multidentate chelator.[75,76]

Furthermore, polydentate chelators that present a cyclic structure follow the same principle called the *'Macrocyclic effect'*. The rigid ring structure of the macrocyclic chelator (see DOTA, NOTA in Figure 6) makes the metal complex even more stable, diminishing, therefore, any conformational freedom for the metal-ligand construct. Macrocyclic chelators tend to have limited specificity for specific metal ions due to these constraining characteristics, which must be considered when choosing the proper chelating agent for a radiometal. [77,78]

Moreover, thermodynamic stability is not the only criterion that must be fulfilled for a metal-chelator complex in developing a radiotracer. Kinetic stability, defined as the ability of the chelator to replace its ligands with difficulty when the complex is inert, must be fulfilled. A labile complex with a fast exchange rate of its ligands can pose various drawbacks, especially *in vivo*: the chelator competes with naturally existing chelating agents circulating in the bloodstream, such as transferrin or human serum albumin.[79] That is why, generally, the formation constant LogK of the metal-chelator complex must be higher than that of the radiometal and the natural chelator found *in vivo*. Among the drawbacks of transchelation (i.e., one chelate group replaces the other) is the accumulation of non-chelated metallic radionuclide in living tissues, which needs to be avoided at all costs (e.g., ^{177}Lu and ^{90}Y are known as 'bone seekers' since they tend to cause bone marrow damage). [80]

Often in radiopharmacy, many metal-chelator complexes are thermodynamically unstable but kinetically inert (or robust) since the highest formation constant of a metal-chelator complex is not always matched with its right chelator. Nevertheless, the complexes show promising results after their *in vivo* evaluation.[81] For their conjugation to the radiotracer precursor, macrocyclic bifunctional chelating agents (BFCA) such as DOTA are commonly used and preferred for their increased stability. BFCAs are chelators that give strong complex stability while precisely controlling the modification and labelling sites. In a BFCA, the chelator complexes the metal and the functional group forms a covalent link to the biomolecule (Figure 4).[82,83] Furthermore, the radiometal-chelator complex is usually large, which may influence the biological properties of the whole radiotracer (e.g., CNS small-molecule radiotracers and CXCR4 targeting peptides).[84] That is why the binding affinity to the target receptor should be evaluated in the various steps of the chelator/radionuclide modification.

1.3.4.3 Choice of chelators and radiometals

1.3.4.3.1 Radiometals ^{68}Ga and ^{111}In

Developing a radiotracer that can be used for PET and SPECT imaging (same structure but different radionuclide) is a goal of many research teams. It becomes, therefore, more critical when the diagnostic radiotracer lays the ground for the choice of therapy and the patient's response to therapy while providing a whole-body mapping of the target cancer cells. Although PET has caught the most attention and development throughout the last years, SPECT remains the imaging modality that is more affordable and most available in hospitals worldwide. Therefore, a PET/SPECT radiotracer would benefit the clinics with its accessibility across a different cost range while allowing them to have the same diagnosis/therapeutic options.

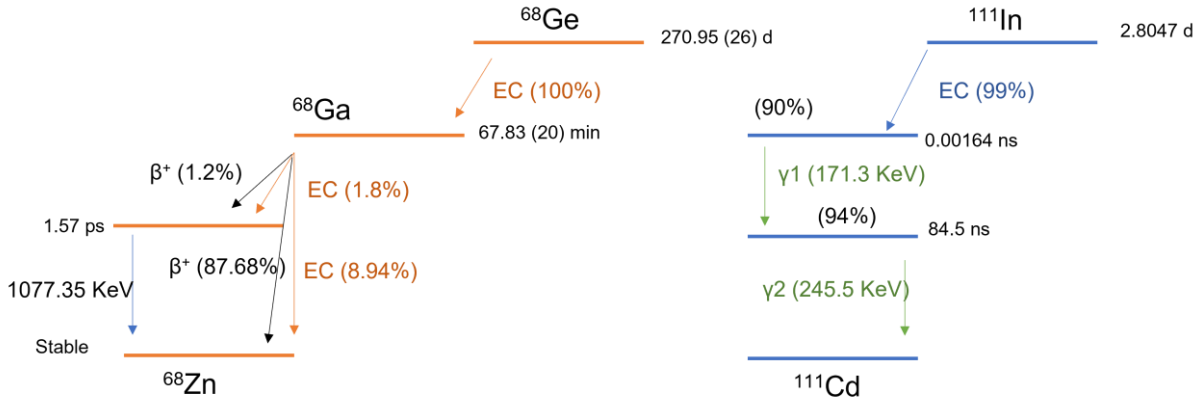

Figure 5: Decay characteristics of the PET radionuclide ^{68}Ga and SPECT radionuclide ^{111}In.[85,86]

Gallium-68 and Indium-111 have always formed a good radionuclide pair for PET and SPECT imaging modalities.[87] Somatostatin receptors (SSTRs) imaging performed with DOTA-TOC/DOTA-TATE, labelled with ^{111}In for SPECT/CT and ^{68}Ga for PET, have been quite widely used in many clinics and hospitals across Europe.[56] As seen in Figure 5, gallium and indium belong to the same group in the periodic table, thus sharing many characteristics (see Table 4). The most important radioisotopes of gallium are ^{67}Ga and ^{68}Ga. ^{67}Ga has a longer half-life, 3.3 days, than that of ^{68}Ga: 68 min. It emits gamma rays by electron capture, rendering it useful for SPECT imaging. As for ^{68}Ga, a positron emitter, its convenient production route using a ^{68}Ge/^{68}Ga Generator make it far more attractive and cost-effective as a radiometal in PET imaging. For greater quantities, ^{68}Ga can also be produced by proton bombardment of ^{68}Zn in low energy medical cyclotrons. Under physiological conditions, the oxidation state of gallium is 3+, with the possible coordination numbers 3, 4, 5, 6. The complexation of Ga^{3+} can be challenging since it tends to quickly form hydroxide complexes at pH higher than 3,5 in solution, besides its slow, complex formation kinetics. To overcome the slow kinetics and the Ga-hydroxide

formation, $GaCl_3$ that is eluted from the generator is first complexed with a weaker ligand such as acetate or citrate (in buffers) since it has faster formation kinetics with Ga^{3+} than with the hydroxides or larger organic ligands. Consequently, this prevents the precipitation of the radiometal, and the preparation of more stable complexes is made possible. ^{68}Ga is commonly complexed with DOTA at high temperatures, overcoming the slow kinetics of the complex formation. [88,89]

Table 4: Physico-chemical characteristics of gallium and indium.

Element	Electronic configuration	Oxidation potential (V)	Ionic Radius (A°) of M^{3+}	Coordination number (aq. M^{3+})
Ga	[Ar] $3d^{10}$ $4s^2$ 4p	$Ga \rightarrow Ga^{3+} + 3e^-$ E°=0.53	0.62	6
In	[Kr] $4d^{10}$ $5s^2$ 5p	$In \rightarrow In^{3+} + 3e^-$ E°=0.342	0.8	6

As for ^{111}In, it has a half-life of 2.8 days. Its emission type is gamma radiation and Auger electron emission, decaying to the stable cadmium-111. It can be produced in a cyclotron through proton irradiation of cadmium target (^{112}Cd (p, 2n) or ^{111}Cd (p, n)). Similarly, to ^{68}Ga, ^{111}In is formulated in $InCl_3$ solutions and presents the same coordination number, hence the possibility of using comparable chelator systems for both radionuclides. In SPECT imaging, ^{111}In radiotracers have found application in prostate cancer imaging (^{111}In-PSMA-617/PSMA-11) and somatostatin receptor with ^{111}In-Octreotide. In a different formulation for infectious disease detection, ^{111}In oxyquinoline (oxine) can be used to image blood cells, platelets, and leukocytes.[90,91]

^{111}In is usually delivered in a stock solution of [^{111}In]$InCl_3$ to radiopharmaceutical research labs or routine productions. However, solubility issues were encountered with some received batches with ^{111}In, leading to the formation of unknown ^{111}In[In]-species.[92,93]

1.3.4.3.2 Chelators for ^{68}Ga and ^{111}In

Having good thermodynamic stability and a high kinetic inertness *in vivo* is an important factor to consider. For that matter, the chelators chosen for this work were selected among the most known and trusted macrocyclic chelators for M^{3+} radiometals. Acyclic chelators derived from the structure of diethylenetriaminepentaacetic acid (DTPA) have indeed shown promising results in the past, especially for chelating ^{111}In. However, they were redeemed ineffective for stably complexing other radiometals due to *in vivo* instability.[94]

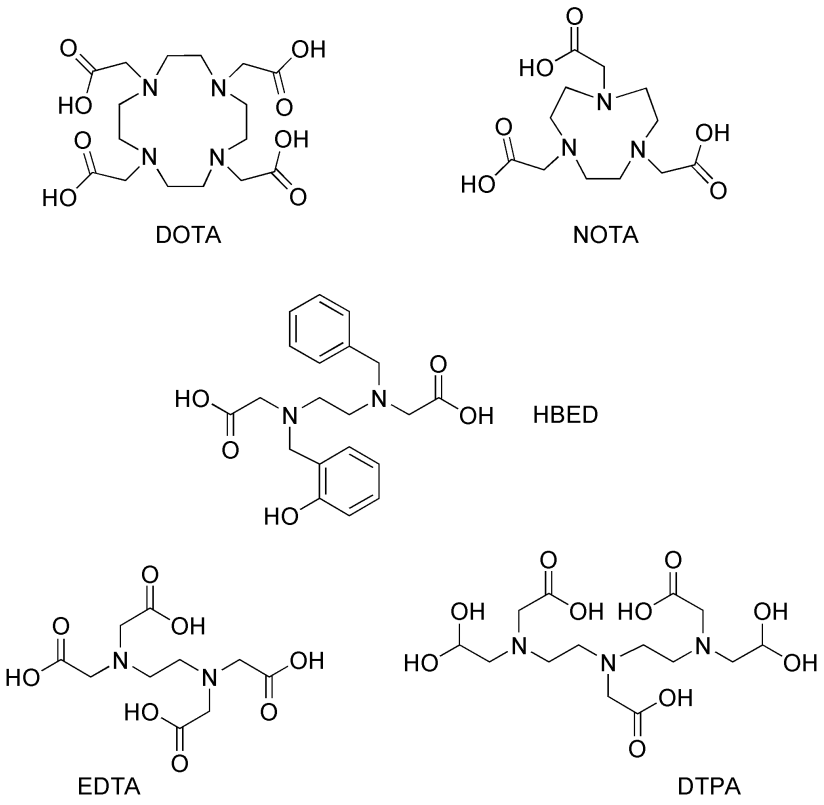

Figure 6: Structure of the mostly used cyclic and acyclic universal chelators.

Between the choice of the proper radiometal pair for PET and SPECT and the type of chelator that gathers the needed characteristics (i.e., stability and chelation properties for both metals), DOTA was a reasonable choice for ^{68}Ga and ^{111}In.[95-98] After the success ^{111}In-DOTA-NOC and ^{68}Ga-DOTA-TOC have witnessed in neuroendocrine tumor imaging, DOTA chelators and their derivatives have been readily available and suitable to any modification, labeling and conjugation to other biological molecules. Therefore, DOTA has been chosen in this project to chelate both ^{68}Ga and ^{111}In. Having faced radiolabeling issues with indium-111, we only moved forward with our preclinical evaluation with ^{68}Ga.[99]

1.4 Development of radiopharmaceuticals

1.4.1 The process of radiopharmaceutical development

Due to recent advances in radiochemistry, automation and cyclotrons miniaturization, the production of radiopharmaceuticals became more practical and versatile.[100] Hence their routine application in various diagnoses of diseases. In drug discovery, the focus of the process lies mainly on the repetitive cycle of screening for ‘’hits”, obtaining lead compounds and medicinal chemistry optimization. However, radiopharmaceutical development extends the work carried out in drug discovery by adding a radioactive element. The focus in developing novel radiopharmaceuticals resides in the *in vitro* evaluation of the compounds: testing their ability to generate a particular response, to target specifically and selectively

the receptor or the biological mechanism in question without damaging the surrounding tissues. Both disciplines are entirely complementary, yet sometimes some iterative steps and processes must be performed under different conditions due to the ionizing radiation generated by the radiotracer.

The first important step usually stems from an initial research question that answers the necessary needs of clinicians within the diagnosis and treatment of patients. Once the need for a novel diagnostic tool arises, the search for a suitable target with enough information on its expression and localization comes next. Screening for lead compounds that can show promising results (biological activity) towards the selected target is a significant step based on existing libraries and endogenous ligand structures.[101,102]

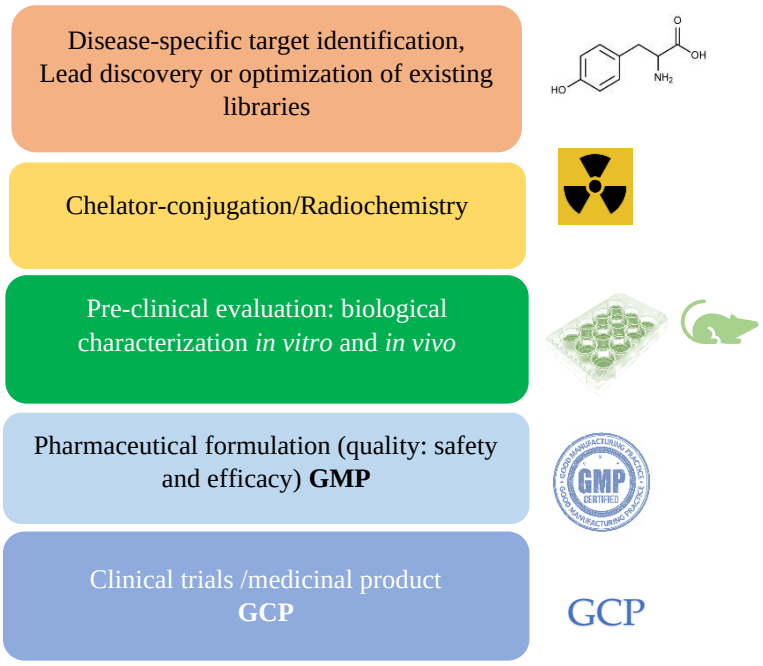

Figure 7: The process of radiopharmaceutical development for clinical use. Good Manufacturing practice (GMP) and good clinical practices (GCP) are guidelines and international quality standards.[103]

A lead compound is then transformed into a final compound which will undergo extensive structure-activity relationship (SAR) studies. Medicinal chemistry modifications would then allow for the optimization of the compound to increase its binding affinity, selectivity, and overall physicochemical properties.

To develop radiopharmaceuticals, studying the possible routes of radiosynthesis is essential. For instance, the conjugation of a BFCA and a spacer would allow radiolabeling with radiometals (see Figure 7). Then radiolabeling experiments to determine the right synthesis path and the highest labeling yield, radiochemical purity and specific activity are conducted and followed by *in vitro* evaluation of the obtained radiotracer: stability in physiological fluids, octanol-water partition coefficient that determines the lipophilicity of the radioligands, and most importantly cell-binding experiments. For diagnostic radiotracer development in oncology, the cell assays consist of cultured cancer cell lines incubated with the radiolabelled tracer to determine the uptake. Once the *in vitro* studies are carried out and the results are satisfactory, *in vivo* studies to determine the biodistribution and the tracer's pharmacokinetics are conducted (accumulation in target and nontarget tissues are essential parameters to investigate).

In summary, a diagnostic radiotracer must have the following characteristics: high specificity and selectivity, high plasma clearance and low plasma protein binding having a neutral and hydrophilic

nature to enhance elimination and reduce effective (radiation) dose, possibly known metabolism, low toxicity, and promising *in vivo* stability because of low metabolic clearance. As far as this current work is concerned, we have conducted *in vitro* assays and did not reach the animal experiment phase. First-in-human evaluation is expected for radiotracers that have successfully passed preclinical evaluation, followed by clinical trials.[104]

1.4.2 In vitro evaluation of radiopharmaceuticals

Radioligand binding assays are employed during radiotracer development to understand better the interactions between the radioligand and the receptors of interest. Here, three types can be distinguished: kinetic, competitive and receptor saturation assays. These assays are performed on cancer cell lines or primary cells. Besides kinetic experiments, membrane suspension bearing the target of interest can also be employed. By performing binding assays at several time points, information about the association and dissociation of the radiotracer from the receptor over time and internalization into the cell can be assessed. Receptor saturation and competitive experiments are performed to determine the extent of the binding of the ligand to the receptor (affinity) and the specificity of this interaction.

The binding of the radioligand/radiotracer to the receptor follows the Law of Mass Action according to the following equations 1 and 2.

$$R + L \leftrightarrow RL \qquad \frac{C_L C_R}{C_{RL}} = K_D \quad (1)$$

The radioligand binds to the receptor when the correct conformation and a suitable amount of energy are present. The rate of association of RL equals $C_R.C_L.k_{on}$ (where K_{on} is association rate constant Mol^{-1} min^{-1}, C_R and C_L are the concentrations of the receptor and the ligand). Ligand and receptor associate and form a ligand-receptor complex, or they may dissociate again. The dissociation rate equals $C_{RL}.k_{off}$ (where k_{off} is dissociation rate constant Mol-1 min-1, C_{RL} concentrations of the RL complex). Equilibrium is attained when the rate of formation of new RL complexes equals the dissociation rate of these complexes.

$$C_R \times C_L \times k_{on} = C_{RL} \times k_{off} = \frac{k_{off}}{k_{on}} = K_D \ (2)$$

Once equilibrium is reached, K_D-value, the equilibrium dissociation constant can be determined. This represents the radioligand concentration that occupies half of the receptors at equilibrium. When K_D is low, a low ligand concentration is needed to occupy the receptors, yielding a high binding affinity of the ligand and the receptor and vice versa.[105]

Every radioligand shows some degree of nonspecific binding. This can be caused by attaching to other nontarget receptors, membrane lipids, or even tubes and plates where the experiments were conducted. The non-target binding can be due to the radioactive compound's charge, lipophilicity, or lack of specificity (binding to receptor transporters and plasma proteins). The nonspecificity can be measured

when co-incubating with a high concentration of a competitor compound (-<100 x K_D or -<1000 x C_L), where this non-radioactive compound saturates more than 99,9% of specific sites so that the tracer can bind only non-specifically. Specific binding can be then calculated as a difference between total and nonspecific binding (summary found in Figure 8).[106]

Although most of the *in vitro* evaluation of a radiotracer must be performed with the radioactive compound, the behaviour of the non-radiolabeled compound can be evaluated beforehand. For this purpose, non-radioactive cellular assays can be employed: TR-FRET, cell viability assays, ELISA, among many others, can be employed.[107]

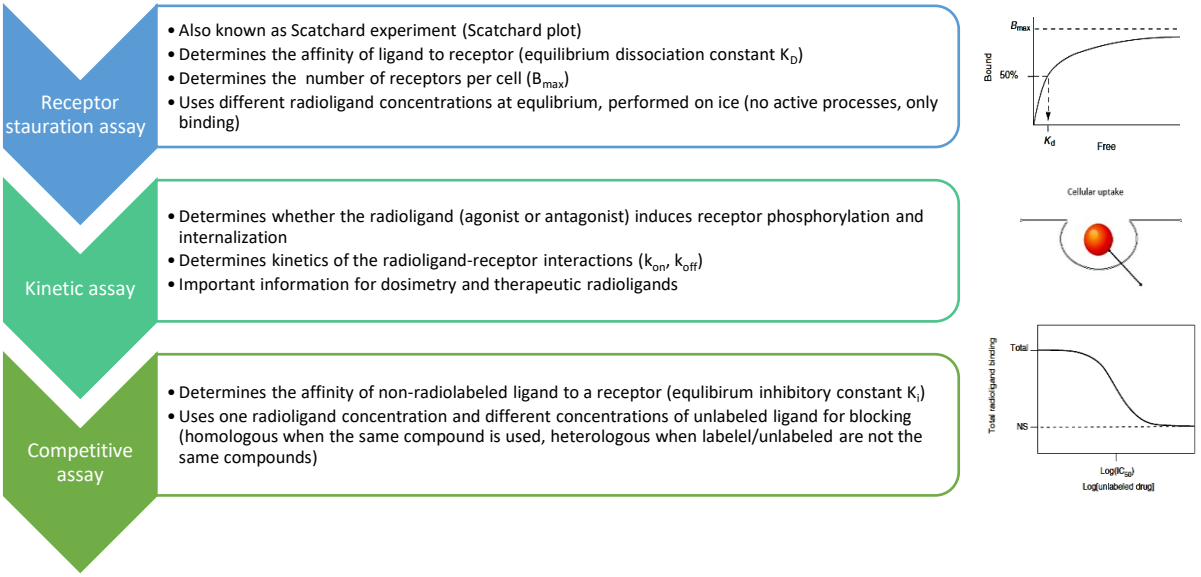

Figure 8: Representative scheme of the key characteristics and measured parameters in radioligand binding experiments.[103]

1.4.2.1 Fluroescence based cellular assays

TR-FRET based competitive assay (HTRF): Time-Resolved Fluorescence Energy Transfer (TR-FRET; Förster resonance energy transfer) has been a frequently used assay in drug discovery and developments. In addition to standard experiments, this technology was applied to quickly screen biologically active compounds while maintaining high sensitivity and reliability. Fluorescence intensity (FI) measurements generally use regular fluorophores such as fluorescein (a brief nanosecond emission). The excitation of the sample and the emission measurement take place simultaneously. Although microplate readers are very effective at removing excitation light from the emission measurement, this excitation light, along with the brief light emitted by materials in the well or sample, often contributes to noise, resulting in high background.[108]

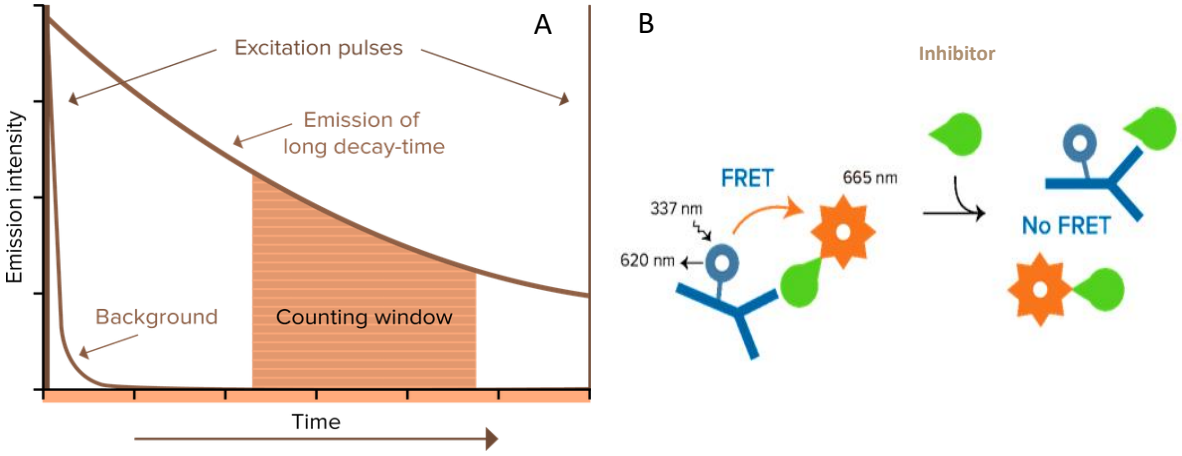

Figure 9: A) Determination of the counting window from the emission intensity over time curve. B) Demonstration of the FRET signal in presence or absence of an inhibitor.[108,109]

Time-resolved fluorescence (TRF) reduces background noise by using a lanthanide fluorophore, such as europium or terbium, which emits fluorescence for a more extended period. This long fluorescence lasts several milliseconds. Therefore, excitation of the fluorophore by a pulsed light source (e.g., flashlamp), followed by a delay, signal measurement, allows for the brief fluorescence (lasting a few nanoseconds) to attenuate before taking a measurement. Tests using time-resolved fluorescence yield significantly reduced signal-to-noise ratios (see Figure 9). The most frequently used lanthanides are europium, terbium and samarium. They are generally used as chelate or cryptate type complexes allowing good signal intensity and stability. TR-FRET combines time-resolved (TR) measurement with fluorescence resonance energy transfer (FRET) technology. In FRET assays, biomolecules (e.g., target proteins) are labeled with donor and acceptor fluorophores. When biomolecules interact, donor and acceptor fluorophores come together. When the donor (e.g., Europium cryptate) is excited, he can transfer his emission energy to the acceptor (XL665 or d2), emitting a fluorescent signal at a specific wavelength. Donor and acceptor fluorescence emissions have different wavelengths that can be differentiated from each other using a microplate reader, allowing quantification of biomolecular interaction. Furthermore, this assay can be used to determine the binding affinity of an antagonist targeted to block the interactions between the two tagged proteins. IC_{50} values are determined from signal to concentration curves that indicate the reduction of the FRET signal transfer.[110]

2. Immune Checkpoint Imaging and Therapy

2.1 Cancer diagnosis and therapy

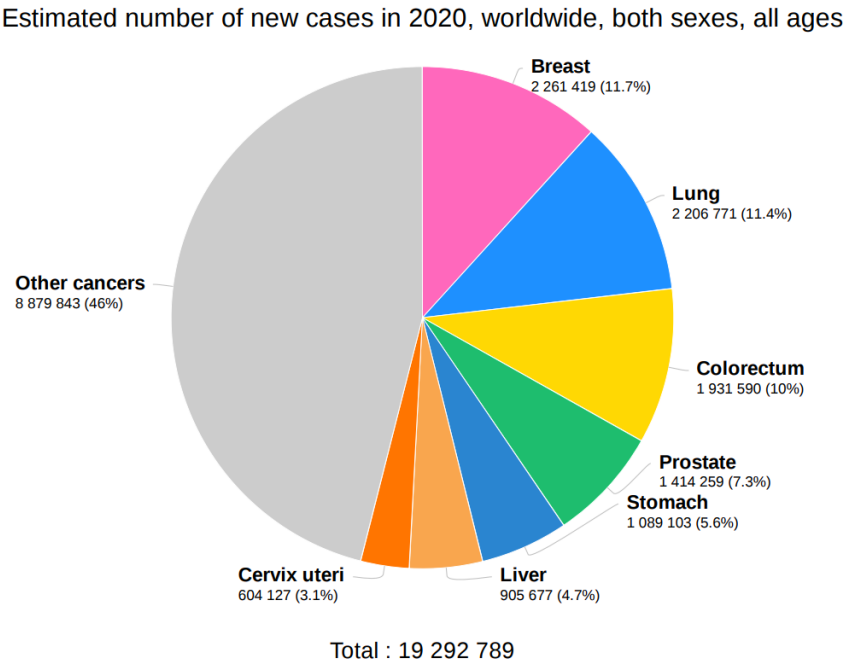

Figure 10: cancer incidence and mortality rates from 2020.[111]

The World Health Organization report states that cancer is among the leading causes of death worldwide, responsible for 10 million deaths in 2020. Lung, colorectal, breast, liver and prostate cancer are behind the highest rates of cancer-related deaths each year, among other types, in men and women (Figure 10).[112] More than 30% of deaths caused by cancer account for behavioural risk factors such as high body mass index (BMI), poor diet, lack of physical activity, tobacco and alcohol use. Tobacco use is the highest risk factor for cancer, causing over 20% of global cancer deaths.[113] Cancer stems from the rapid formation of abnormal cells that grow and expand beyond their usual limits. The turnover of the cells towards malignant ones may also be started by external agents and inherited genetic factors. Many clinicians strive to detect lesions before they spread to different parts of the patient's body with an early-stage diagnosis. Therefore, early diagnosis ensures a better chance for the patient to get the appropriate treatment. Regular health check-ups are recommended for specific high-risk categories. Symptomatic patients are prone to further evaluations and testing.[114] Among the tools that allow for screening of malignant lesions are the following imaging techniques: US, X-rays, MRI, CT, PET and SPECT, and histopathological methods (biopsies of cancer tissues and IHC analysis). For PET and SPECT imaging, a biomarker is identified to be in a tight relationship with a biological process that leads to the appearance of malignant tumours. Therefore, a specific radiotracer targeting that exact biomarker can efficiently map the underlying status of cell abnormality and deliver further insight into the patient's diagnosis.[115] Depending on the type and stage, cancer can be treated with surgery as a primary treatment. Adjuvant or neoadjuvant therapies to the primary treatment are constituted of chemotherapy, radiation exposure,

immunotherapy, hormone therapy, and targeted drug therapy, among other options. In most cases, cancer treatment is still partly dependent on radiation-based therapies that employ high doses of ionizing radiation to block the replication of cancer cells by damaging their DNA beyond repair. The radiation leads to the shrinking of their growth and size. Two types of radiation therapies can be discerned: the first one consists of a radioactive source in a machine targeted at a specific body part, constituting a local treatment called external beam radiation. The second radiation therapy is internal and called brachytherapy. It consists of a liquid or a solid radiation source that is put inside the body (swallowed in the case of a liquid source such as ^{131}I for thyroid cancer) and radiates near the tumor sites.[116] Decreasing the radiation burden of the patient is of high importance. Therefore, recent progress in research has paved the way to discovering novel cancer therapies that deliver optimal results while reducing the harmful effects of ionizing radiation. One of the novel cancer treatments is immunotherapy, which relies on restoring the body's defences to fight off cancer.

2.2 Immunotherapy as an emerging treatment

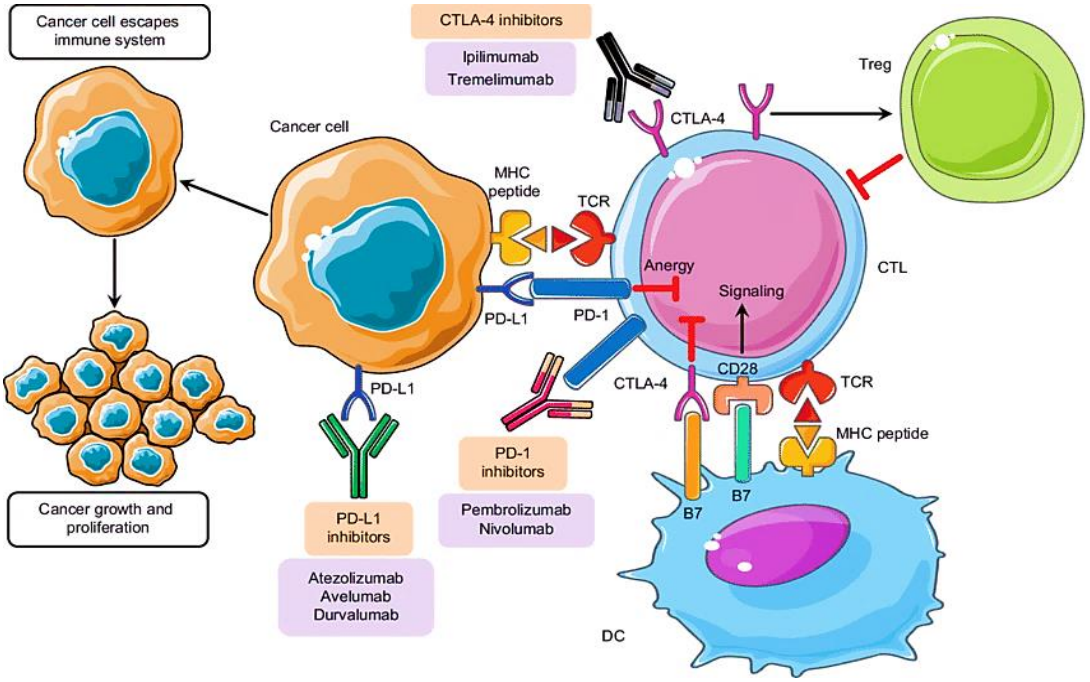

Figure 11: The implication of the immune checkpoint PD-1/PD-L1 and CTLA-4 in cancer's immune evasion and their antibody-based inhibitors.[117]

Immunotherapy is a biological therapy that has become an evolving and promising treatment for various types of cancer. This type of therapy stimulates the immune system. It allows the human body to take control of its defence mechanisms to ward off cancer. There are three main types of immunotherapies: immune checkpoint blockade therapy, Chimeric Antigen Receptor (CAR) T cell therapy and cancer vaccines.[118] The latter option, cancer vaccines, has been explored in precision medicine and personalized treatment; it aids the immune system in recognizing cancer antigens and fighting them. The CAR-T cell therapy works similarly, but the T cells are engineered and optimized, then reinjected into the patient to

exterminate tumor cells. As for immune checkpoint blockade therapy, it reactivates the T cells and helps them recognize cancer cells, leading to their elimination.

Immune checkpoints regulate the immune system. They are essential for immunotolerance by preventing immune cells from attacking other cells at random. Immune checkpoint molecules fall into two categories: stimulatory checkpoints, part of the tumor necrosis factor (TNF) receptor superfamily, and inhibitory ones (Cytotoxic T-Lymphocyte-Associated protein 4-CTLA4, Programmed cell Death receptor 1 PD-1), belonging to the immunoglobulin superfamily.[119]

Tumor cells must successfully evade the immunosurveillance by cloaking themselves from the immune cells for cancer to grow and proliferate (see Figure 11). Over the recent years, Immune Checkpoint Inhibition (ICI) as an immunotherapy treatment has gained attention and achieved desirable results among patients suffering from the following types of cancer: lymphoma, melanoma, leukaemia, kidney, liver, lung, colorectal, brain, head and neck, breast, bladder, non-small cell lung carcinoma as well as prostate cancer.[120] Approved inhibitors for CTLA4/PD-1 and PD-L1/PD-1 are currently only antibody-based, and they are already used in clinics, showing favourable results.[121] The results from over 150 clinical trials with ICI therapy on PD-1/PD-L1, for instance, have shown better tumor response and a higher overall survival rate for patients than traditional treatment options. The variance between the objective response rates was high between the different types of cancers treated and the status of PD-L1 expression in patients. Despite generating a good response in both PD-L1 positive or negative patients, it has been reported that the PD-1/PD-L1 blockade therapy decreases the risk of death in both patients compared to conventional therapy, justifying therefore its choice as a first-line therapy in recent years.[122,123]

2.3 Targeting the immune checkpoint PD-1/PD-L1

The immune checkpoint PD-1/PD-L1 is a widely researched inhibitory immune checkpoint. The interaction between PD-1 and PD-L1 deactivates the T cells, putting the immune system on breaks, and no further actions against foreign invaders (i.e., cancer) can be taken. Programmed cell death protein 1, PD-1 also known as CD279 (cluster of differentiation 279), is a surface receptor protein critical for regulating the function of T cells during the immune response and immune tolerance.[124] First, it promotes apoptosis (programmed cell death) of antigen-specific T cells in lymph nodes. Second, it reduces apoptosis in regulatory T cells (anti-inflammatory, suppressive T cells). PD-1 has two ligands: Programmed cell Death Ligand 1 (PD-L1) and 2 (PD-L2). Only the interaction of PD-1/PD-L1 has been considered during this work since PD-L2 has not been demonstrated to be involved in crucial immune-compromising pathways.[124] Moreover, PD-L1, also known as CD274 or B7-H1, is a 40 kDa transmembrane protein expressed on immune-related lymphocytes, such as T cells, B cells, and myeloid cells.

It has also been proven that PD-L1 is overexpressed on tumor cells. The overexpression of the ligand on the surface of cancer cells facilitates its evasion from the host immune system. The ligation of PD-1 and PD-L1 sends signals that inhibit the TCR-mediated activation of interleukin-2 (IL-2, a type of cytokine) production and the inhibition of the rapid growth of T cells.[125] The blockade of the interaction between PD-1 and PD-L1 can be achieved on either target (cancer and T cells) and is now a successful treatment adopted in immune-oncology. FDA approval of PD-1 and PD-L1 therapeutic antibodies has reached a high level compared to the previous decade. Table 5 and Figure 11 show the different types of antibodies in clinics sometimes even as first-line therapy.[122,126,127]

Several probing tools have been used to evaluate which patients are more likely to respond well to the immune checkpoint blockade therapy. To start, immunohistochemistry staining (IHC) for PD-L1 expression is a well-established method that allows for predicting a patient's response to treatment. Not all patients can benefit from checkpoint blockade therapy, regardless of their high tumor PD-L1 expression (and its absence thereof).[128] The limitations of the IHC method can be related to the tissue sampling techniques since it cannot reflect the tumor heterogeneity in a single collected biopsy from a specific region. Furthermore, the tissue handling processes through the staining can alter the expression of the receptor and thus delivering faulty conclusions. Therefore, the need for a non-invasive PD-L1 expression evaluation tool will provide novel insights, thus optimizing the existing treatments and their possible combinations.[129,130]

2.3.1 PET imaging of PD-L1

Imaging immune checkpoints, PD-L1 specifically, using radioactive probes have benefited not only clinicians but also patients due to the heterogeneity of the target and the difficulty of understanding the expression levels of PD-L1 using just IHC. Many radiotracers have been developed from already established therapeutic antibodies to evaluate the whole-body status of PD-L1. Throughout the past years, imaging PD-L1 with antibodies, a technique known as ImmunoPET, has gained interest and further development.[124] The focus, however, has been directed towards imaging PD-L1, as most researchers diverted from targeting PD-1 with radioactive probes since it is mainly found on T cells. Baring a radionuclide that matches the antibody's half-life, immunoPET imaging probes such as ^{89}Zr-Atezolizumab have shown promising results during clinical studies.[126] The clinical trial's outcome of patients subject to immunotherapy treatments indicates that the response was better correlated with the pre-treatment PET results (PET/CT scans) than with the IHC outcome.[122,123] Therefore, these findings have propelled the research in PET and SPECT radiotracer development for PD-L1 imaging and encouraged the use of a non-invasive technique for a better prediction of the treatment response. The advances in research have somehow deviated from the frequent use of labeled antibodies and turned towards molecular probes that are smaller in size. This change stemmed from the problematic characteristics of an antibody-based radiotracer: as radiotracer-biomolecules, antibodies take a longer time to clear out from non-target tissues, have poor tissue penetration, and are relatively large and expensive to produce.[131] These pharmacokinetic drawbacks lead to a long waiting period until the

background signal from the unbound radiotracer clears out from the circulation (and other types of tissues), rendering it challenging to make a prompt decision regarding therapeutic options.

With medium-sized probes, rapid mapping of the *in vivo* target while gaining in time and radiation burden can be achieved.[132] That is why many PD-L1-targeted small molecules and peptides have been radiolabeled and evaluated *in vitro* and *in vivo*. Although most of the developed compounds have been rather trialled as drugs and not as radiopharmaceuticals, there has been some recent development regarding a specific class of peptides (anti-PD-L1), with highly interesting results from a first-in-human study (see the paragraph *Macrocyclic peptides*).

2.3.1.1 PD-L1 PET radiotracers

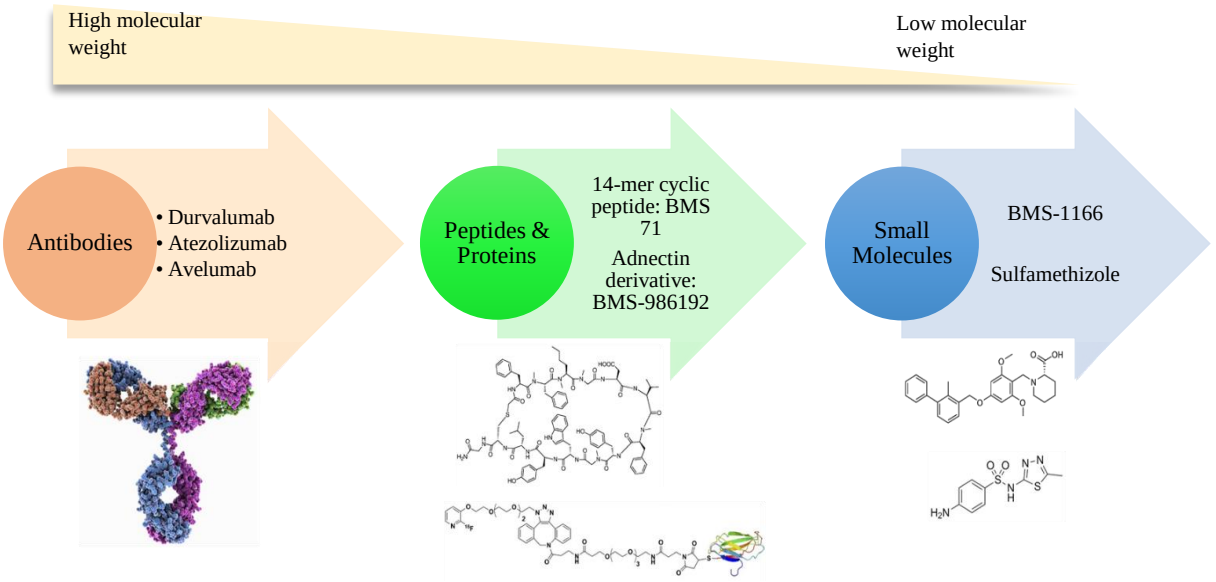

Figure 12: Molecular categories of PD-L1 targeting biomolecules.

The efforts carried towards developing a novel imaging tool for the immune checkpoint PD-1/PD-L1 are considerable (Figure 12 shows the most relevant general classes of molecules targeting PD-L1). After establishing antibodies for both treatment and diagnosis (Durvalumab, Atezolizumab and Avelumab), PD-L1 radiotracers are expanding to reach different molecular size categories. Peptides and proteins have rapidly emerged as alternative imaging tools: linear, macrocyclic peptides (BMS-71), protein-derivatives baring similar amino acid sequences to PD-1 such as adnectins (BMS-986192),[133] and small molecules inhibitors have been reported to efficiently block the PD-1/PD-L1 interaction. Although imaging with small molecules is relatively novel, peptides and proteins have already entered clinical trials as summarized in table 5, constituting, therefore, the next generation of PD-L1 radiotracers.

2.4 Peptide-based radiotracers for PD-1/PD-L1

2.4.1 Peptides in radiopharmacy

Peptides, derived from the Greek word *peptós*, meaning 'digested', are amino acid chains ranging from two to fifty residues forming peptide bonds. This class of biomolecules has been of high value in drug discovery and development. As pharmaceutical compounds, peptides present the advantage of being placed between small molecules and proteins yet are different in their biochemistry and therapeutical benefits from both classes.[139]

Table 5: radiotracers for PD-L1 imaging in preclinical and clinical stages.[134-138]

Agent	Class	Reactivity	Modality	Stage
^{18}F-BMS-986192	Adnectin	Human/Cynomolgus	PET	Clinical
^{18}F-NOTA-ZPDL1-1	Affibody	Human/macaque	PET	Preclinical
^{64}Cu-DOTA-HAC-PD1	HAC-PD1	Human	PET	Preclinical
^{111}In/^{64}Cu/^{89}Zr - Atezolizumab, NIR-Atezolizumab	Humanized IgG1	Human	PET, SPECT, optical	Clinical
^{89}Zr-C4	Humanized IgG1	Human/murine	PET	Preclinical
^{111}In-PD-L1.3.1	Murine IgG1	Human	SPECT	Preclinical
^{111}In-DTPA-anti-PD-L1	mAb	Murine	SPECT	Preclinical
^{99m}Tc-Nbs	Single domain antibody	Murine	SPECT	Preclinical
^{99m}Tc-NM-01	Single domain antibody	Human	SPECT	Clinical
Apdl16gnps	Nanoparticle	Murine	CT	Preclinical
^{64}Cu/^{68}Ga/^{18}F -WL12	Peptide	Human	PET	Clinical
^{18}F-LG-1	Small molecule	Human	PET	Preclinical
^{68}Ga-DOTA-SETSKSF	Peptide	Human	PET	Preclinical

In radiopharmacy, peptides have been considered a valuable precursor for developing radiotracers. That is due to their accessibility and cost-effective synthesis (manual or automated). Second, peptides are versatile biologics as they are the closest to our natural "template" and endogenous ligands. Furthermore, unless immunogenic, peptides are non-toxic, with sequences' lengths going beyond 10-20 amino acids.[140-142] *In vivo*, peptides present a high favourable pharmacokinetic profile and a better tissue penetration because of their relatively small size compared to antibodies and larger molecules. Peptide-based radiotracer precursors can be divided into linear amino acid chains that vary in length, peptides

with turns such as the proline induced turns, helices (peptide chains with alpha-helical turns) and finally cyclic peptides. The latter category presents various advantages as precursors in the drug development field. Cyclic peptides are conformationally constrained, which enhances their affinity and improves their stability *in vivo*.[141] They are metabolically stabilized; the exopeptidases require recognizing the end of the peptide to proceed with the degradation, which is omitted in a cyclic form. Moreover, cyclic peptides are often bioavailable or modified to become bioavailable.

Overall, peptides have found numerous applications in radiopharmacy and targeted cancer screening.[143] The most used peptide categories with their corresponding PET/SPECT radiotracers in pre-clinical/clinical stages can be summarized below (Table 6). The corresponding target receptors, mainly G-protein coupled receptors (GRPR), have been proven to provide important information that is relevant for diagnostic (tumor staging) and therapeutic ends.

Table 6: The different classes of peptides (some already approved by authorities) targeting important receptors on various cancer cells.[144,145]

Peptide	Radiotracer	Receptor	Tumor expression
Somatostatin (SST)	^{68}Ga-DOTA-TOC ^{68}Ga-DOTA-NOC ^{68}Ga-DOTA-TATE	Somatostatin receptor subtype-2 (SST2)	Neuroendocrine (breast, brain small cell lung cancer)
Bombesin (BBN)/Gastrin Releasing Peptide (GRP)	^{68}Ga/^{111}In-DOTA-RM2	Bombesin receptor subtype-2 (BB2)	Prostate, breast, pancreas, colorectal
α- Melanotropin (α - MSH)	^{111}In- DOTA-NAP-amide	Melanocortin-1 receptor (MCI1R)	Melanomas
Neuropeptide Y (NPY)	^{18}F-Labeled Argininamide-type Neuropeptide (^{18}F-23)	Neuropeptide receptor Y1 (Y-1)	Ovary, adrenal, kidney, Ewing's sarcoma
Cholecystokinin (CCK), minigastrin (MG)	^{111}In-DOTA-PP-F11 ^{111}In-DTPA-MG0	Cholecystokinin-B (CCK-B)	Small cell lung, medullary thyroid cancer, astrocytomas
Arg-Gly-Asp (RGD)	^{99m}Tc-2P-RGD2 ^{18}F-galacto-RGD	$A_v\beta_3$ integrin	Ovarian, lung carcinoma, glioblastomas, breast cancer

2.4.2 Peptides targeting PD-L1

Many efforts have been devoted to developing novel peptide structures targeting PD-L1 in the past years. Numerous peptide scaffolds have been developed based on the findings reported on the type of interactions PD-1 and clinical antibodies have towards PD-L1. Furthermore, since the disclosure of the X-ray structure of the human PD-1/PD-L1 complex (http://www.rcsb.org/structure/4ZQK), as well as the most critical binding motifs (found mainly on the CC′FG β-sheet), [146] the synthesis of peptides of suitable affinity with an average molecular weight has been carried. Phage-display was among the methods used, along with virtual screening and molecular dynamics studies, that complemented the research on finding novel PD-L1 targeting peptides.

Aurigene discovery™ have been disclosing different peptides and peptidomimetics targeting PD-L1. AUNP-12, their 'star' compound, gathered three active linear peptide sequences derived from the PD-1 binding interface in its structure (see Figure 13A). This 29-mer has been extensively studied *in vivo*. It has successfully restored the proliferation and effector function in an IFN-γ production assay, meaning that it has successfully inhibited the interaction between PD-1 and PD-L1. It has also reduced the tumor size of lung metastasis (in cell line B16F10) in mice. Moreover, AUNP-12 has been clinically evaluated to reduce advanced tumors and lymphomas in many studies.[147]

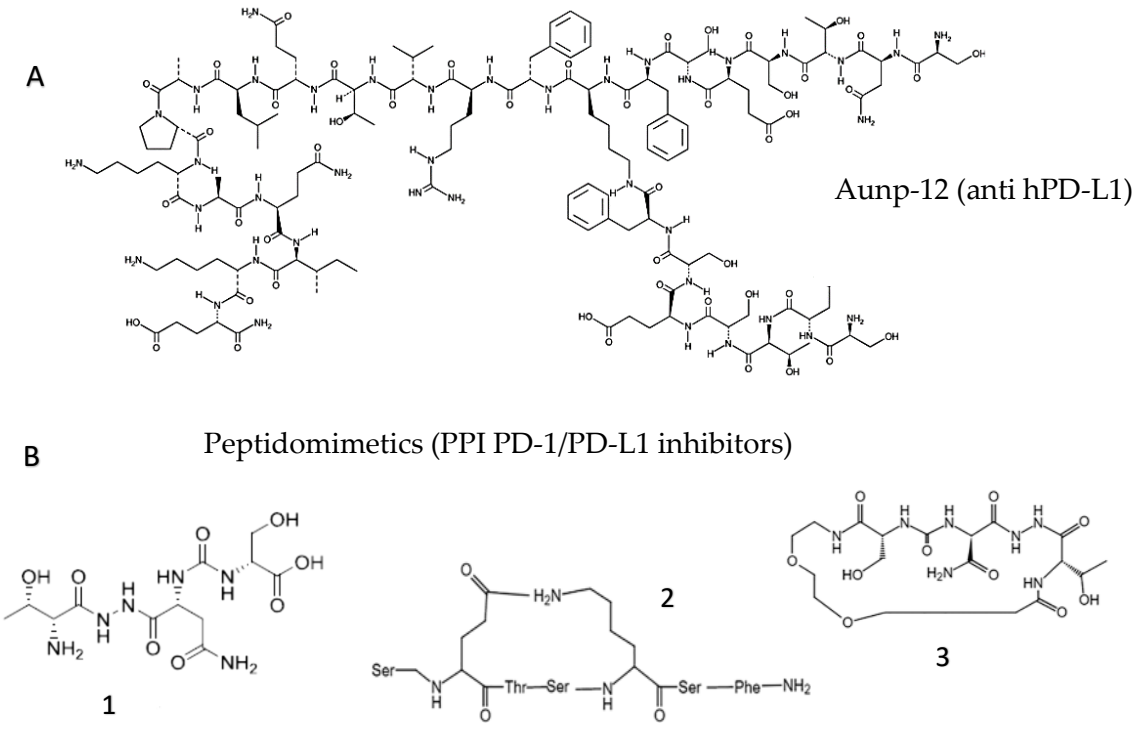

Figure 13: Structural difference in peptides inhibiting the PD-1/PD-L1 interaction. A) Structure of Aurigene's Aunp-12. B) Structure of the peptidomimetics PPI inhibitor.[149,150]

Furthermore, Aurigene scientists have also screened for modified short-chain peptides and peptidomimetics to serve as PD-L1 inhibitors or radiotracer precursors.

Tripeptide peptidomimetics, seen in Figure 13B, composed of diacylhydrazine and urea linker, can inhibit the PD-L1 signalling pathways with IC_{50} values in the nanomolar range (measured in the splenocyte effector function assay). The peptidomimetics exhibited *in vivo* efficacy by the inhibitory rate of 46% in a CT-26 colon cancer mouse model. Although many studies have been conducted on Aurigene compounds to evaluate their therapeutical potential, no further research has been undertaken to optimize their structures for radiopharmaceutical applications. [147,148]

Among the newly developed PD-L1 targeting peptides with shorter chains, we mention PD-L1Pep-1(CLQKTPKQC) and PD-L1Pep-2 (CVRARTR). These 7-9 mer linear peptide sequences were developed after screening of phage-display peptide-based antagonist libraries for cell surface PD-L1. Both peptides were found to bind with good affinity to the extracellular target (K_D= 373 ± 114 nM for Pep-1 and 281 ± 92 nM for Pep-2). PD-L1Pep-1 is of particular interest since many of its amino acid residues replicate those of PD-1 in the same binding interface of PD-1 to PD-L1, rendering it a valuable inhibitor of this interaction.[151] Similar short peptide sequences were also developed by mirror image phase-display techniques in the solid and liquid phase, yielding a D-peptide named H12. This peptide underwent optimization aided by molecular dynamics simulations. It was, therefore, able to inhibit PD-1/PD-L1 and induce an anti-tumor response, making it among the first orally bioavailable peptides (proteolysis resistant) targeting PD-L1.[152]

Furthermore, despite the advances in developing short-chain linear peptides as potential PPI inhibitors, another class of peptides have received the most attention: the PD-L1 targeting macrocyclic peptides with radiopharmaceutical translation developed by Bristol Myers Squibb (see Figure 14). We will discuss the BMS peptides in the following paragraph.

The past few years have witnessed revolutionary progress in peptide-based inhibitors for immune checkpoint therapy. From proteolysis-resistant oral peptides to lengthy 30-mer multi-linear sequences, the application and the use of this class of biologics in a relatively new target would bring forth valuable insight into cancer therapy and diagnosis.

2.4.3 Macrocyclic peptides inhibitors of PD-1/PD-L1

Many peptides are currently in the preclinical stages of their development for PD-L1 imaging (see Table 5). One of these peptides has recently entered clinical trials and demonstrated promising results (WL12),[153] making this class of compound the topic of many research projects. We find different macrocyclic peptide-classes published in patents by the pharmaceutical company Bristol Myers Squibb.[154] Within the patents, three distinct categories of macrocyclic peptides are presented. Each has a distinctive amino acid sequence, ranging between 12 and 15 residues (see model amino acid chain for each category in Figure 13). The noticeable differences in these categories consist of the unnatural amino

acids, amide bond methylation, cyclized rings within the sequence, or the cyclization procedure itself. Two of the most promising categories contain thioether bonds (used for cyclization). These peptides were tested for their affinity towards PD-L1(antagonists) and their inhibitory effect on the interaction between PD-1 and PD-L1. A selection of the most potent peptides was made after thorough literature reviewing (the alanine-scan was performed based on results from literature patent).

Other research groups have been showing interest towards this novel class of anti-PD-L1 inhibitors. Some studies conducted on the BMS peptides have evaluated their claimed potency and selectivity.[155-158] The co-crystal structures of the hPD-L1/macrocyclic peptides complex indicate valuable information regarding the binding motif and the different residues that are not interacting with the binding pocket (**PDB ID**:5O45, 5O4Y). Seeing room for modification in these peptides is crucial since attaching a linker and a chelator is needed for radiolabeling purposes.

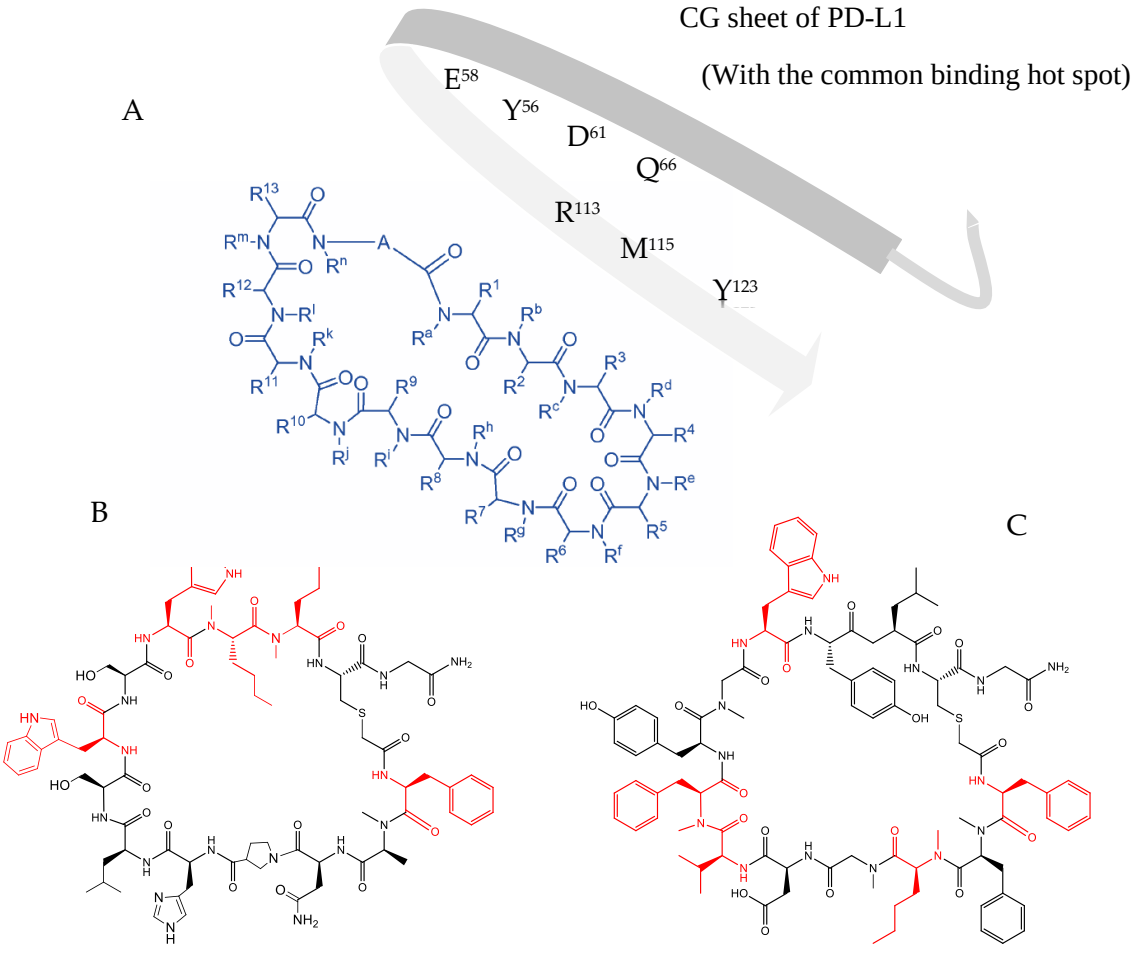

Figure 14: A) General structure of the BMS macrocyclic peptides binding to the CG sheet of PD-L1. B) Peptide 71 from category II C) peptide 57 from category I are two examples of the most prominent compound categories from BMS patent. $R_{c, f, h, I, m, n}$ are all hydrogens. $R_{a, e, j, k}$ is either a hydrogen or a methyl. $R_{1\text{-}2}$ till R_{13} are independently selected natural/unnatural amino acid side chains. Hydrophobic AA, participating in the binding to PD-L1, are coloured in red.

The peptides seem to interact with PD-L1 just like the original receptor, PD-1, according to in-depth pharmacophore mapping performed on BMS peptides. Most of the interactions are hydrophobic, with some hydrogen bonding and low-energy interactions between specific residues. According to published pharmacophore models,[159] peptide 71 (Figure 13B) interacts with PD-L1 via hydrogen bonds between Leu^{12} and Glu^{58} on PD-L1, with an intramolecular hydrogen bond generated between Asp^{5} and Tyr^{8}. Val^{6} from peptide 71 seems to interact with Ile^{54} on PD-L1 via hydrophobic bonds. More hydrophobic bonds can be observed between Trp^{10} peptide 71 and Ala^{121} on PD-L1, $^{m}Phe^{7}$ on peptide 71 and Met^{115} on PD-L1. The following residues on PD-L1 are essential in these hydrophobic interactions; Ile^{54}, Arg^{113}, Met^{115}, Ala^{121}, and Tyr^{123}, making this valuable information for further structural modifications.[159] Although a second pharmacophore modelling of two BMS peptides indicated the necessity of including a positive ionizable point (e.g., arginine), BMS peptide 71 seems to be an excellent candidate that can be further optimized for radiotracer development: finding a point of attachment for the linker/chelator system and evaluating the overall binding affinity. Despite being a challenging PPI to inhibit with medium-sized molecules,[160] PD-1/PD-L1 targeted peptides constitute the next generation of immune-oncology radiotracers and therapeutics. For that reason, the synthesis, modification, and evaluation of BMS peptides as a potential PET/SPECT radiotracer constituted the basis of this doctoral thesis.

Aims

Novel molecular imaging techniques have enhanced the treatment of cancer by significantly improving the diagnostic tools and refining the choice of suitable therapeutic approaches. For solid tumors, such as lung cancer and colorectal cancer specifically, the recent breakthroughs in the development of radiopharmaceuticals for PET and SPECT imaging have allowed for the possibility of early disease detection. Immune checkpoints (e.g., PD-1/PD-L1) were found to be among the biological processes that detect and predict the progression of the disease as well as the most suitable immunotherapy options. Since PD-L1 has been reported to be an important biomarker in immuno-oncology, the development of both gallium-68 (PET) and indium-111 (SPECT) PD-L1 tracers constituted the purpose of this doctoral thesis, with specific aims divided as follow:

Therefore, the aims of this doctoral thesis constitute the following points:

- The first aim of this work consists of selecting a macrocyclic peptide structure from a published library of PD-L1 antagonists, synthesizing the chosen compound by SPPS, optimizing the peptide´s stability, evaluating the possible modification-sites for chelator attachment and conjugating the suitable linker/chelator for radiolabeling purposes.
- Radiolabeling of the macrocyclic peptide with the PET and SPECT radionuclides ^{68}Ga and ^{111}In represents the second aim. The choice of the suitable radiometals and the bifunctional chelator were made after thorough considerations of their intrinsic characteristics.
- The chosen SPECT radionuclide, indium-111, presented difficulty in its handling due to the formation of an identified [^{111}In]In-species in the stock solutions, thus investigating the unknown formed [^{111}In]In-species in order to overcome the issue and carry on the indium-111 radiolabeling experiments constituted our third aim
- The Fourth aim of our study is to evaluate the binding affinity of the $^{nat/68}$Ga-labeled macrocyclic peptide with both fluorescence-based cellular assays (HTRF) and radioligand binding assays in CHO-K1 hPD-L1 cells, using a reference radiopeptide (WL12), along with the establishment of a validated *in vitro* test system for the evaluation of future PD-L1 radiotracers.

Published manuscripts

First manuscript: Carolina Giammei[1], Nedra Jouini[1], Marie R. Brandt, Stefanie Frey, Thomas L. Mindt, Jens Cardinale, Unexpected transformation of n.c.a. [^{111}In]$InCl_3$ in stock solutions into an unreactive [^{111}In]In-species,Applied Radiation and Isotopes, Volume 180, 2022, 110037 (DOI: 10.1016/j.apradiso.2021.110037) ……42-53

Second manuscript: Nedra Jouini[1], Jens Cardinale, Thomas L. Mindt. Evaluation of a Radiolabeled Macrocyclic Peptide as Potential PET Imaging Probe for PD−L1, ChemMedChem 2022, e202200091 (DOI: 10.1002/cmdc.202200091)……..54-75

Applied Radiation and Isotopes 180 (2022) 110037

Contents lists available at ScienceDirect

Applied Radiation and Isotopes

journal homepage: www.elsevier.com/locate/apradiso

Unexpected transformation of n.c.a. [^{111}In]$InCl_3$ in stock solutions into an unreactive [^{111}In]In-species

Carolina Giammei [a,b,c,1], Nedra Jouini [a,b,c,1], Marie R. Brandt [a,c], Stefanie Frey [a,b], Thomas L. Mindt [a,b,c,*], Jens Cardinale [a]

[a] Ludwig Boltzmann Institute Applied Diagnostics, General Hospital of Vienna, Währinger Gürtel 18-20, 1090, Vienna, Austria
[b] Department of Inorganic Chemistry, Faculty of Chemistry, University of Vienna, Währinger Straße 42, 1090, Vienna, Austria
[c] Department of Biomedical Imaging and Image-Guided Therapy, Division of Nuclear Medicine, Medical University of Vienna, Währinger Gürtel 18-20, 1090, Vienna, Austria

ARTICLE INFO

Keywords:
Indium-111
DOTA ^{111}In-labeling
Transformation
Impurities
Radiochemical yield

ABSTRACT

While performing multiple indium-111 labeling of DOTA-modified peptides from a single batch of [^{111}In]$InCl_3$, inconsistent radiochemical yields were observed. We found that the formation of a radioactive impurity in the [^{111}In]$InCl_3$ stock solution hampered the reactivity of the indium-111 during radiolabeling reactions. The formation of this unknown ^{111}In-species could be successfully suppressed by increasing the concentration of chloride ions in the stock solution and [^{111}In]$InCl_3$ was "recovered". Radiolabeling of DOTA-peptides with the stabilized [^{111}In]$InCl_3$ resulted again in acceptable radiochemical yields. In addition, we report convenient iTLC systems that allow distinguishing between [^{111}In]$InCl_3$, the formed unknown ^{111}In-species, radiocolloids, and radiolabeled peptides (DOTANOC).

1. Introduction

Indium-111 (^{111}In) is an important radionuclide with suitable decay radiation for applications in the field of Single Photon Emission Computed Tomography (SPECT) imaging(Blower et al., 2019; Lahiri et al., 2013; Wadas et al., 2010). Due to its comparatively long physical half-life ($t_{½}$ = 2.8 days), it has found wide application for the labeling of peptides and proteins since early 1970s. Nowadays it is still used in research and in the clinic as a radiolabel of different radiotracers, e.g., ^{111}In-Pentetreotide (Octreoscan®).

In general, the radiochemistry of ^{111}In is well-known and established (Blower et al., 2019; Moerlein and Welch, 1981). In most cases, the radiometal is coordinated *via* a chelator (e.g., DTPA or DOTA), which is conjugated to a pharmaceutical targeting vector. As for other metals of the boron group (group 3 metals; triels), elevated pH-values have to be avoided during handling due to the potential formation of insoluble In$(OH)_3$ eventually leading to the formation of radiocolloids(Moerlein and Welch, 1981). Under the condition suggested e.g., by Moerlein and Welch, a large number of molecules have been radiolabeled with ^{111}In in the past leading to reliable routine applications. However, during the development of ^{111}In-radiopharmaceuticals in our lab, we observed inconsistent radiochemical yields (RCYs), especially when performing multiple labeling reactions with the same batch of [^{111}In]$InCl_3$ at different time points after first usage. A closer look at the available literature revealed some hints that such "multi-sampling" of [^{111}In]$InCl_3$ stock solutions might be an issue(Blower et al., 2019). This is also in line with observations made by Brom et al., who found that RCYs dropped when "aged" solutions of [^{111}In]$InCl_3$ were used for radiolabeling reactions. However, this study was more related to the optimization of the molar activity (Brom et al., 2012), which is less of an issue for the clinically used ^{111}In-based radiotracers Octreoscan (Olsen et al., 1995), oxine (Kurantsin-Mills et al., 1989) and DTPA (Collins et al., 1999). Since multi-sampling of aged [^{111}In]$InCl_3$ stock solutions was inevitable for our research for economic reasons, we started a systematic investigation in order to solve the issues. After approximately 10 months, during which we were only able to perform a single reliable radiolabeling from a batch of [^{111}In]$InCl_3$ immediately after opening the vial of the stock solution, the encountered issues suddenly did not occur anymore. This could be related to a change in the production and/or formulation. We were thus not able to complete our investigations.

* Corresponding author. Ludwig Boltzmann Institute Applied Diagnostics, General Hospital of Vienna, Währinger Gürtel 18-20, 1090, Vienna, Austria.
E-mail address: Thomas.mindt@lbiad.ac.at (T.L. Mindt).
[1] Contributed equally.

https://doi.org/10.1016/j.apradiso.2021.110037
Received 8 June 2021; Received in revised form 7 November 2021; Accepted 21 November 2021
Available online 1 December 2021

Nevertheless, we want to report our findings that might be helpful to the radiochemistry/-pharmacy community as the problems may reoccur in the future.

2. Results and discussion

During the course of our work directed towards the development of ^{111}In-labeled DOTA-peptide conjugates, we observed a low reproducibility of our γ-HPLC-based RCYs (results not shown). Consequently, we set up an additional instant thin layer chromatography (iTLC)-based analysis to look for potential radiocolloids or other side products. The check for ^{111}In-radiocolloids was negative (<3%), however, we were able to identify a second ^{111}In-species in our crude product. The latter was not unreacted [^{111}In]$InCl_3$ but somewhat behaved like a different lipophilic ^{111}In-complex (R_f of approx. 0.8 while [^{111}In]$InCl_3$ had an R_f of 0, respectively; see Supporting Information (SI) for details). Most importantly, we were able to detect this impurity also in the [^{111}In]$InCl_3$ stock solution, indicating that the newly formed ^{111}In-species might be the cause of the low reproducibility of RCYs.

Our observations were confirmed by Phil Blower and co-workers who reported potential issues with multi-sampling of [^{111}In]$InCl_3$ stock solutions in a recently published book chapter (Blower et al., 2019). Thus, we set out to study the formation of this ^{111}In-species and its effect on RCYs. The ^{111}In-labeling of DOTANOC was used as a model reaction and RCYs were determined by iTLC as the quantification by γ-HPLC was not possible (the unknown ^{111}In-species eluted together with unreacted [^{111}In]$InCl_3$ in the injection peak using reversed-phase HPLC columns).

In a first attempt, we tried to avoid the formation of the ^{111}In-species by introducing precautions as suggested by Phil Blower. These precautions included the application of glass instead of plastic pipette tips and thorough washing with acetone and HCl before the experiments (Blower, 2019; Giersing, 2000). Using this experimental set-up, four ^{111}In-labeling reactions of DOTANOC were conducted from a single batch of [^{111}In]$InCl_3$ at different time points after the opening of the delivery vial. A significant decrease of the RCYs of ^{111}In-DOTANOC was observed after the second reaction >1 h after the opening of the vial of the [^{111}In]$InCl_3$ stock solution (Table 1). Therefore, it became apparent that washing the glass pipette tip before and after each sampling did not solve the problem of low RCY at later time points.

At this stage, we had neither clear evidence of what the impurity in the [^{111}In]$InCl_3$ stock solution might be, nor its potential origin. The most obvious assumption was the hydrolysis of [^{111}In]$InCl_3$, leading to the formation of mixed chloride/hydroxide and/or aqua complexes of indium and, eventually, to [^{111}In]$In(OH)_3$ (Blower et al., 2019; Moerlein and Welch, 1981).

$$InCl_{3(aq)} + H_2O \rightleftharpoons In(OH)_{3-x}Cl_{y(aq)} + yH_3O^+ + (3-x)*Cl^- \rightleftharpoons In(OH)_3\downarrow + 3HCl \quad (1)$$

Equation (1): Simplified reaction equilibrium for the hydrolysis of indium chloride in water; x = 1,2; y = 1,2.

According to a study by Moerlein and Welsh, such hydrolysis should not lead to the "precipitation" of [^{111}In]$In(OH)_3$ under the acidic conditions as found in the stock solution (0.02 M HCl; pH approx. 1.7) due to the very low concentration of the metal under n.c.a. conditions (Moerlein and Welch, 1981). However, the solubility product Moerlein and Welsh used for their calculation might be in part inaccurate due to the non-trivial coordination behavior of the group 3 metals (Tuck, 1983). Extensive but often only theoretical descriptions of the hydrolysis behavior of metals, in particular of group 3 metals, are available in the meantime (Brown and Ekberg, 2016). In aqueous and chloride-containing solutions, the predominant indium complex is strongly pH-dependent. (Baes et al., 1976) However, these calculations are usually descriptions of ideal systems without any potential disturbance by the presence of other trace metals, e.g., residual cadmium ions from the cyclotron target workup in the case of ^{111}In. We realized that the available literature did not provide sufficient information to explain the formation of the unknown ^{111}In-species. Instead, we pursued a practical approach. We postulated that an increased chloride concentration could stabilize the [^{111}In]$InCl_3$ complex in the stock solution in accordance with the mass action law (based on equation (1)). This postulate was supported by a diagram showing the hydrolysis/dissociation behavior of $InCl_3$ (Fig. S5, supporting information). (Baes et al., 1976) Moreover, the increased chloride concentration could also be capable of reverting the transformation of [^{111}In]$InCl_3$ to the unknown ^{111}In-species provided that this process – may it be the formation of hydroxides or not – is reversible. It should be noted that from here on we again worked with normal pipette tips.

To verify our postulate, the remaining [^{111}In]$InCl_3$ stock solution from the "glass tip experiment" was split into two parts. One part was diluted with 0.02 M HCl (the same HCl concentration as in the stock solution) while the second part was diluted with 1.5 M NaCl in 0.02 M HCl to achieve a final chloride concentration of approx. 0.75 M. Indeed, the ^{111}In of the solution with the elevated chloride concentration behaved again like the original [^{111}In]$InCl_3$ according to iTLC ($R_f = 0.0$). This recovery of [^{111}In]$InCl_3$ from the unknown unreactive species requires several hours at room temperature and can be followed by iTLC (no kinetics were investigated). The results are shown in Table 2.

Subsequent labeling of DOTANOC using the "untreated" and the "stabilized" [^{111}In]$InCl_3$ stock solutions was conducted and [^{111}In]In-DOTANOC was obtained in a RCY of 9.7% and 86.8%, respectively. This experiment demonstrates that the transformation of [^{111}In]$InCl_3$ in the stock solutions to the unreactive ^{111}In-species can not only be reverted but also provides a radiolabeling precursor of higher quality for radiometal complexation experiments.

Encouraged by these results, we next investigated the effect of an increased chloride concentration on the RCY when applied to an unused stock solution of [^{111}In]$InCl_3$. Therefore, a fresh batch of [^{111}In]$InCl_3$ was again split into two portions; one was stabilized by adjusting the chloride concentration to 0.75 M NaCl and the other one was simply diluted with 0.02 M HCl to provide a reference. Labeling reactions of DOTANOC with both solutions were conducted in parallel at different time points without any additional precautions. The RCYs overtime after opening of the stock solution vial are shown in Fig. 1. The labeling of DOTANOC with the non-stabilized [^{111}In]$InCl_3$ resulted in a significant decrease in the RCYs already after a few hours. However, the stabilized [^{111}In]$InCl_3$ (0.75 M NaCl) provided acceptable and reproducible RCYs of 81 ± 4% (n = 8).

In order to reproduce the previously achieved results, and to further identify the formed troublesome ^{111}In-species some weeks later, we

Table 1
Results from ^{111}In-labeling of DOTANOC using thoroughly washed glass pipette tips at different time point after opening (and first usage) of the $^{111}InCl_3$ stock solution.

Species	[%] after			
	0 h	1 h	2 h	3 h
Formed unknown ^{111}In-species	3.8	7.0	50.0	65.8
[^{111}In]radiocolloids & [^{111}In]$InCl_3$	2.9	3.0	2.3	1.4
[^{111}In]In-DOTANOC	93.3	90.0	47.7	32.8

Table 2
Composition of [^{111}In]$InCl_3$ solution in presence of different chloride concentrations directly 0 h and 18 h after dilution as determined by iTLC.

Diluent	^{111}In-species (0 h)	[^{111}In] $InCl_3$ (0 h)	^{111}In-species (18 h)	[^{111}In]$InCl_3$ (18 h)
Untreated (0.02 M HCl)	73%	27%	76.1%	23.9%
0.75 M NaCl in 0.02 M HCl	37%	63%	6.5%	93.5%

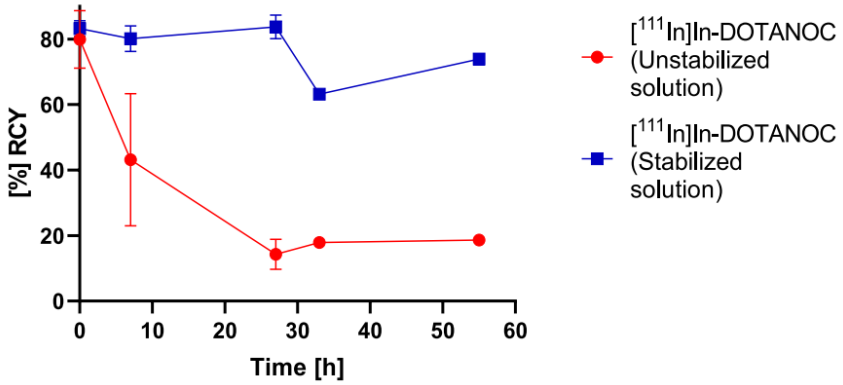

Fig. 1. Radiochemical yields of [^{111}In]In-DOTANOC using stabilized and non-stabilized stock solution of [^{111}In]$InCl_3$ at different time points after their first usage (t = 0).

were surprised to find out that the unreactive ^{111}In-species did not occur in the [^{111}In]$InCl_3$ stock solutions anymore. Radiolabeling of DOTANOC with [^{111}In]$InCl_3$ gave again high RCYs (93 ± 2%; n = 5; up to 2 weeks) even after prolonged periods of time after the opening of the stock solution. We hypothesize that a change or an optimization in the production of [^{111}In]$InCl_3$ and/or its formulation might be the reason behind our observations.

3. Conclusions

We herein report that the use of [^{111}In]$InCl_3$ stock solutions as provided by commercial suppliers for multiple radiolabeling experiments over time can be hampered by the formation of an unknown, unreactive ^{111}In-species. This leads to a dramatic decrease in RCY of radiometallation reactions with chelator-modified conjugates (e.g., DOTANOC). Increasing the chloride ion concentration in the [^{111}In]$InCl_3$ stock solution was shown to be an effective counter measurement for re-establishing acceptable radiochemical yields. The presence of the ^{111}In-species in stock solutions and DOTA-peptide radiolabeling reaction mixtures can be detected and analyzed conveniently by the described iTLC systems. We expect that our results will provide the radiochemistry/-pharmacy community with a helpful experimental protocol to resolve these issues and facilitate further investigations should they reoccur in the future.

4. Experimental

4.1. General

Sodium acetate (suprapur®), NaCl (trace metal basis), water (trace metal basis), 30% HCl (suprapur®) and sodium citrate (reagent grade) were acquired from VWR international. [^{111}In]$InCl_3$ was acquired from Curium (Petten, Netherlands) as solution in 0.02 M HCl (Usually 185 MBq in approx. 500 μL). Reactions were composed using same volumes, thus, apparent molar activity was highest during the first reaction of any series and never exceeded 20 MBq/4 nmol (or 5 MBq/nmol). As model precursor, DOTANOC (GMP-grade) was acquired from ABX (Radeberg, Germany) and used as 1 mg/mL solution in H_2O (trace select, VWR). Paper chromatography was performed using silica gel coated iTLC-SG strips from Agilent technologies GmbH (Vienna, Austria). The developed iTLC stripes were analyzed on a Canberra Packard instant imager model A2024.

4.1.1. "Glass tip experiments"

Preparation: For dispensing and spotting of the [^{111}In]$InCl_3$ stock-solution, an Eppendorf pipette (10–100 μL) with a glass tip made from a truncated Pasteur pipette was used. The glass tip was attached to the pipette and subsequently sealed/fixed with a layer of parafilm. The accuracy of the pipetted volume was checked on a balance using water and was 50 ± 5 μL. Before the experiment, the pipette tip was washed 10 times with each acetone, followed by hot (approx. 80 °C) 30% HCl and finally 0.02 M HCl. During the experiment the pipette was washed 10 times with 0.02 M HCl after each usage. A freshly prepared 0.1 M sodium acetate solution was used for pH adjustment during the experiment.

Reaction: For ^{111}In-labeling, a fresh portion of [^{111}In]$InCl_3$ in 0.02 M HCl was used. After washing the glass pipette, 50 μL of the [^{111}In]$InCl_3$ solution were pipetted to a 500 μL Eppendorf protein LoBind vessel containing 25 μL of 0.1 M sodium acetate solution mixed with 5 μL DOTANOC precursor (1 mg/mL in water). The reaction mixture was vortexed and heated at 80 °C for 30 min. Four reactions were performed at 0, 1, 2 and 3 h after the opening of the stock solution. The pH was checked using pH stripes after each reaction and was pH 4.4–4.7 for all reactions. After the reaction, iTLC samples were drawn, the iTLC plates developed in MeOH/1 M NH_4OAc 90:10 as mobile phase and subsequently analyzed using an instant imager. A more detailed procedure is provided in the SI. The stock solution was analyzed as well.

4.1.2. Experiments for the recovery of [^{111}In]$InCl_3$

50 μL of "aged" [^{111}In]$InCl_3$ stock solution were mixed with 50 μL of 1.5 M NaCl in 0.02 M HCl in an 500 μL Eppendorf vessel (final concentration was 0.75 M NaCl in 0.02 M HCl). Further, 50 μL of the "aged" [^{111}In]$InCl_3$ stock solution was mixed with 0.02 M HCl in another 500 μL Eppendorf vessel. Then, samples of both solutions were spotted on an iTLC strip, the iTLC plate developed in MeOH/1 M NH_4OAc 9:1. Subsequently, the sheets were analyzed using an instant imager. The iTLC analysis was repeated after 18 h. Afterwards, 40 μL of each solution were mixed with 20 μL NaOAc (0.1 M) and 3 μL of DOTANOC stock solution (1 mg/mL), vortexed and reacted at 90 °C for 30 min. Each reaction mixture was analyzed by iTLC using MeOH/1 M NH_4OAc 80:20 as a mobile phase.

4.1.3. Stabilization experiment/DOTANOC labeling

[^{111}In]$InCl_3$ was freshly opened and dispensed into two 1.5 mL Eppendorf vials. One solution was diluted with 0.02 M HCl while the other was diluted with 1.5 M NaCl in 0.02 M HCl (dilution: 1:1 both). For radiolabeling, 20 μL of a freshly prepared 0.1 M sodium acetate solution were mixed with 40 μL of the diluted [^{111}In]$InCl_3$ stock solution and 3 μL DOTANOC (1 mg/mL; approx. 2 nmol) and the mixture was heated at 90 °C for 30 min. All reactions were repeated at different time points over 2–3 days. For quality control, samples were drawn from each reaction mixture after the reaction as well as from the respective [^{111}In]$InCl_3$ stock solutions. For analysis of the remaining free indium, 1 μL of 0.1 M sodium citrate was added to 10 μL of the sample. The sample was

spotted on an iTLC plate. To determine the unknown ^{111}In-species, as well as RCY of the reaction, iTLC plates were spotted with undiluted samples from the reaction mixtures and [^{111}In]$InCl_3$ stock solutions. The former iTLC was developed in 0.1 M sodium citrate (pH 5.0) while the latter was developed in 80:20 MeOH:0.1M NH_4OAc.

Declaration of competing interest

The authors declare that they have no known competing financial interests or personal relationships that could have appeared to influence the work reported in this paper.

Acknowledgement

We thank Phil Blower (King's College London, United Kingdom), Martin Béhé, (Paul Scherrer Institute, Switzerland), as well as Theodosia Maina and Bert Nock (Demokritos, Greece) for sharing their experience and expertise with regards to ^{111}In-radiolabeling reactions. This research did not receive any specific grant from funding agencies in the public, commercial, or not-for-profit sectors.

Appendix A. Supplementary data

Supplementary data to this article can be found online at https://doi.org/10.1016/j.apradiso.2021.110037.

References

Baes, C.F., Mesmer, R.E., 1976. In: The Hydrolysis of Cations. John Wiley & Sons, New York. https://doi.org/10.1002/bbpc.19770810252.

Blower, J.E., Cooper, M.S., Imberti, C., Ma, M.T., Marshall, C., Young, J.D., Blower, P.J., 2019. The radiopharmaceutical chemistry of the radionuclides of gallium and indium. In: Lewis, J.S., Windhorst, A.D., Zeglis, B.M. (Eds.), Radiopharmaceutical Chemistry. Springer International Publishing, Cham, pp. 255–271. https://doi.org/10.1007/978-3-319-98947-1_14.

Blower, P.J., 2019. Personal Communication.

Brom, M., Joosten, L., Oyen, W.J.G., Gotthardt, M., Boerman, O.C., 2012. Improved labelling of DTPA- and DOTA-conjugated peptides and antibodies with ^{111}In in HEPES and MES buffer. EJNMMI Res. 2, 4. https://doi.org/10.1186/2191-219X-2-4.

Brown, P.L., Ekberg, C., 2016. Aluminium, gallium, indium and thallium. In: Brown, P.L., Ekberg, C. (Eds.), Hydrolysis of Metal Ions. Wiley-VCH Verlag GmbH & Co. KGaA, pp. 757–834. https://doi.org/10.1002/9783527656189.ch13.

Collins, D.A., Hogenkamp, H.P.C., Gebhard, M.W., 1999. Tumor imaging via indium 111–labeled DTPA– adenosylcobalamin. Mayo Clin. Proc. 74, 687–691. https://doi.org/10.4065/74.7.687.

Giersing, B.K., 2000. An Agent for Imaging Matrix Metalloproteinases. PhD Thesis, University of Kent at Canterbury, British Library DSC no, p. DXN037891.

Kurantsin-Mills, J., Jacobs, H.M., Siegel, R., Cassidy, M.M., Lessin, L.S., 1989. Indium-111 oxine labeled erythrocytes: cellular distribution and efflux kinetics of the label. Int. J. Rad. Appl. Instrum. B 16, 821–827. https://doi.org/10.1016/0883-2897(89)90167-0.

Lahiri, S., Maiti, M., Ghosh, K., 2013. Production and separation of 111In: an important radionuclide in life sciences: a mini review. J. Radioanal. Nucl. Chem. 297, 309–318.

Moerlein, S.M., Welch, M.J., 1981. The chemistry of gallium and indium as related to radiopharmaceutical production. Int. J. Nucl. Med. Biol. 8, 277–287.

Olsen, J.O., Pozderac, R.V., Hinkle, G., Hill, T., O'Dorisio, T.M., Schirmer, W.J., Ellison, E.C., O'Dorisio, M.S., 1995. Somatostatin receptor imaging of neuroendocrine tumors with indium-111 pentetreotide (Octreoscan). Semin. Nucl. Med. 25, 251–261.

Tuck, D.G., 1983. Critical survey of stability constants of complexes of indium. Pure Appl. Chem. 55, 1477–1528.

Wadas, T.J., Wong, E.H., Weisman, G.R., Anderson, C.J., 2010. Coordinating radiometals of copper, gallium, indium, yttrium, and zirconium for PET and SPECT imaging of disease. Chem. Rev. 110, 2858–2902.

Supporting information for:

Unexpected transformation of n.c.a. [^{111}In]$InCl_3$ in stock solutions into an unreactive [^{111}In]In-species

Carolina Giammei[a,b,c,#], Nedra Jouini[a,b,c,#], Marie R. Brandt[a,c] , Stefanie Frey[a,b], Thomas L. Mindt[a,b,c,*], Jens Cardinale[a]

[a] Ludwig Boltzmann Institute Applied Diagnostics, General Hospital of Vienna, Währinger Gürtel 18-20, 1090 Vienna, Austria

[b] Department of Inorganic Chemistry, Faculty of Chemistry, University of Vienna, Währinger Straße 42, 1090 Vienna, Austria

[c] Department of Biomedical Imaging and Image-Guided Therapy, Division of Nuclear Medicine, Medical University of Vienna, Währinger Gürtel 18-20, 1090 Vienna, Austria

[#] Contributed equally

* Corresponding author. Tel.: +436767620424; Email-address: Thomas.mindt@lbiad.ac.at

1. Development of the iTLC procedure

Each sample was added to 1 µL of citrate buffer (0.1 M, approx. 1:19-1:39) beforehand or spotted onto the iTLC plate undiluted. Samples were drawn from both the [^{111}In]$InCl_3$ stock solution and the reaction mixture after the reaction. Each sample was spotted on an individual iTLC sheet (in sum 8 iTLC sheets – each with spots from the 4 measured time points). After completed spotting, the iTLC plates were developed in the respective solvent.

Solvent 1: MeOH/1 M $NH_4CH_3CO_2$ 9:1

Solvent 2: 0.1 M Citrate buffer pH 5.0

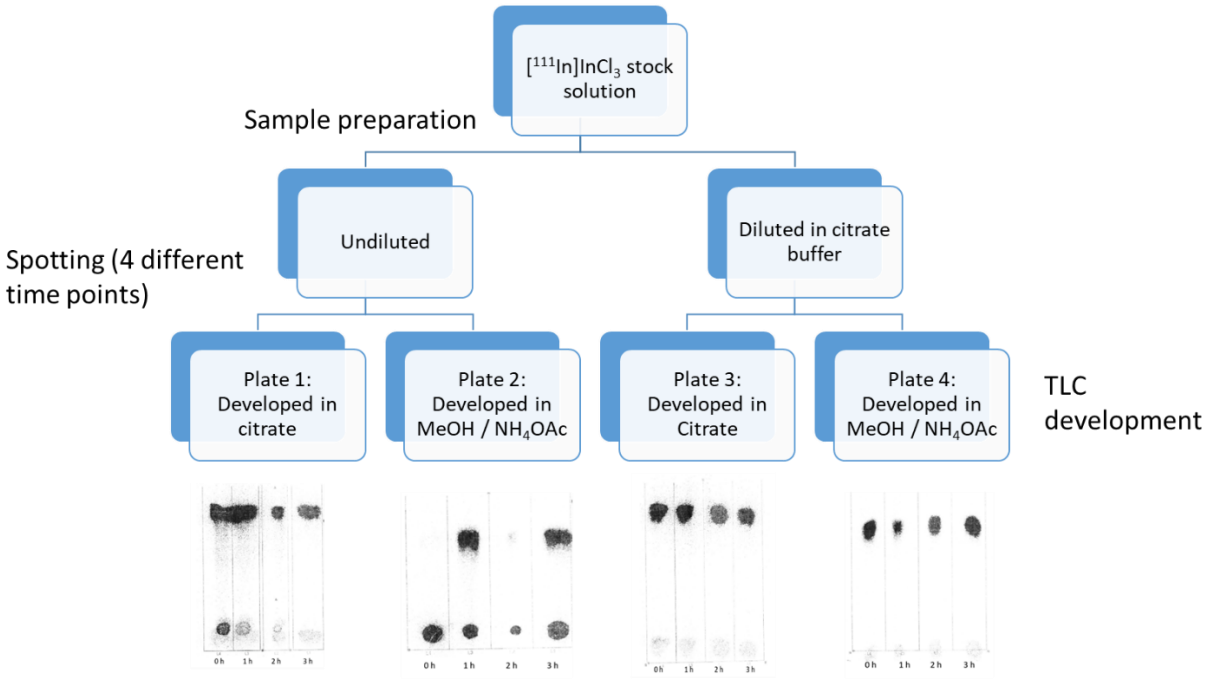

Figure S 1: Flowchart of the sample processing for the [^{111}In]$InCl_3$ stock solution, the reaction mixture samples were treated accordingly. For detailed discussion of the obtained TLC images including R_f values, see below.

2. Results of the [^{111}In]$InCl_3$ stock solution

Mobile Phase: MeOH/1 M $NH_4CH_3CO_2$

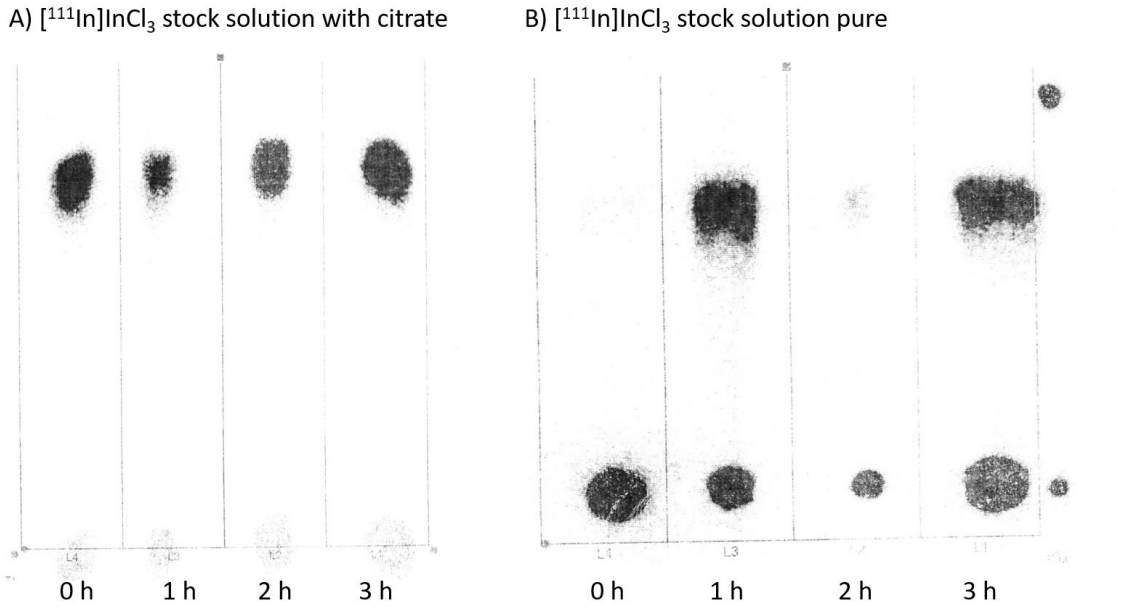

Figure S2: Instant images of the iTLC analysis of the [^{111}In]$InCl_3$ stock solution developed in MeOH/1 M NH4CH3CO2 (9:1) as mobile phase.

Table S2A Detailed results for Figure S2A

R_f/species	**0h [%]**	**1h [%]**	**2h [%]**	**3h [%]**
0.0 [^{111}In]In-radiocolloids	< LoD	< LoD	< LoD	< LoD
1.0 [^{111}In]$InCl_3$ and [^{111}In]In-species	> 99	>99	>99	>99

Table S2B: Detailed results for Figure S2B

R_f/species	**0h [%]**	**1h [%]**	**2h [%]**	**3h [%]**
0.0 [^{111}In]$InCl_3$(and radiocolloids)	96.9	44.4	65.7	64.1
0.7 [^{111}In]In-species	3.1	55.6	34.3	35.9

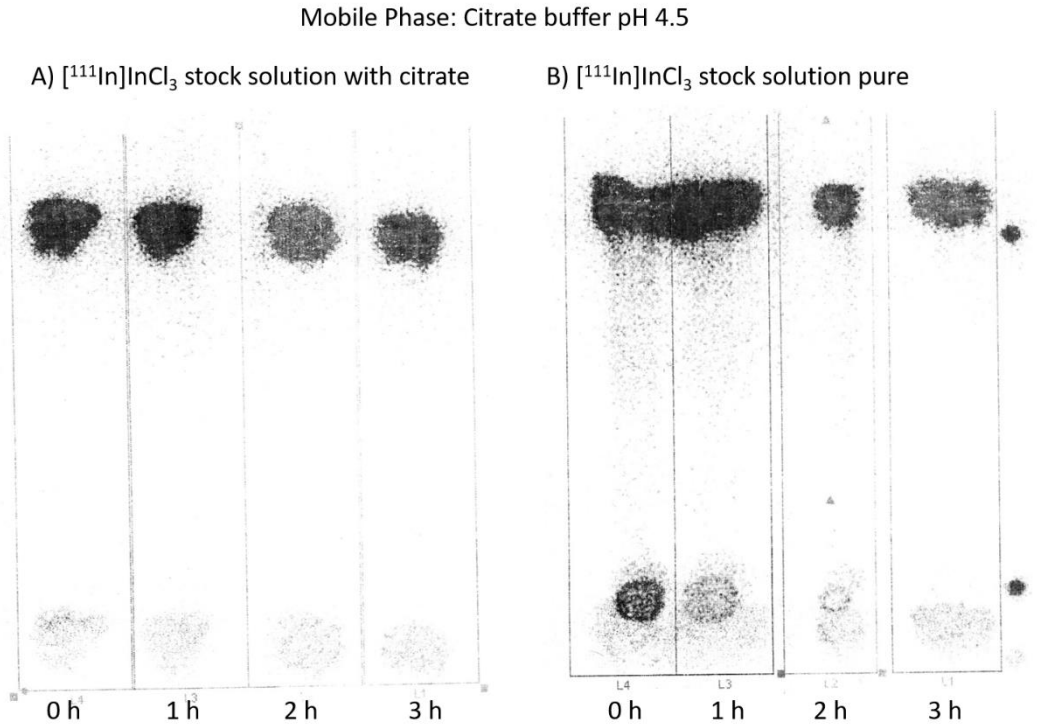

Figure S3: Instant images of the iTLC analysis of the [^{111}In]InCl$_3$ stock solution developed in citrate buffer. The "shadow" at the starting line is an artifact from the printer which was used on the PC controlling unit of the instant imager (shadows at R_f~-0.1 are an artifact from printing).

Table S3A Detailed results for Figure S3A

R_f/species	**0h [%]**	**1h [%]**	**2h [%]**	**3h [%]**
0.0 [^{111}In]In-radiocolloids	< LoD	< LoD	< LoD	< LoD
1.0 [^{111}In]InCl$_3$ and [^{111}In]In-species	> 99	>99	>99	>99

Table S3B: Detailed results for Figure S3B

R_f/species	**0h [%]**	**1h [%]**	**2h [%]**	**3h [%]**
0.0 [^{111}In]In-radiocolloids/artifacts	12.0	6.1	9.6	2.1
1.0 [^{111}In]InCl$_3$ / [^{111}In]In-species	88.0	93.9	90.4	97.9

2.1. Discussion of the results

In solvent 1, the [^{111}In]In-species (1B; R_f approx. 0.7) could be observed 1 h after the opening of the [^{111}In]InCl$_3$ stock solution. In the sample which was diluted in citrate, the impurity was not detectable. This results in the conclusion, that either the detected species is masked by citrate addition or the impurity itself is not inert and forms complexes with citrate (A; R_f 1.0).

In solvent 2, no difference between the pretreated and the undiluted sample was visible. Approx. 100 % of the activity was migrating along the TLC plate with the solvent front, which gives another hint towards the aforementioned formation of citrate complexes and/or comparable behavior of [^{111}In]In-citrate and the detected impurity. However, the TLC method could be used for the identification of potential radiocolloids, assuming that the activity on such colloids is not mobilized again by the addition of the chelator. It should be noted that an increasing amount of ^{111}In is visible at the starting line when no citrate is added to the sample. This effect can be explained by the longer residence time on the iTLC sheet before its development (irreversible binding to the silica; 12% at 0 h sample which resided 3 h on the TLC sheet; no absorbed ^{111}In at R_f = 0 is visible for the 3 h time point for which the TLC was run immediately after spotting).

3. Analysis of the [^{111}In]In-DOTANOC reaction mixture

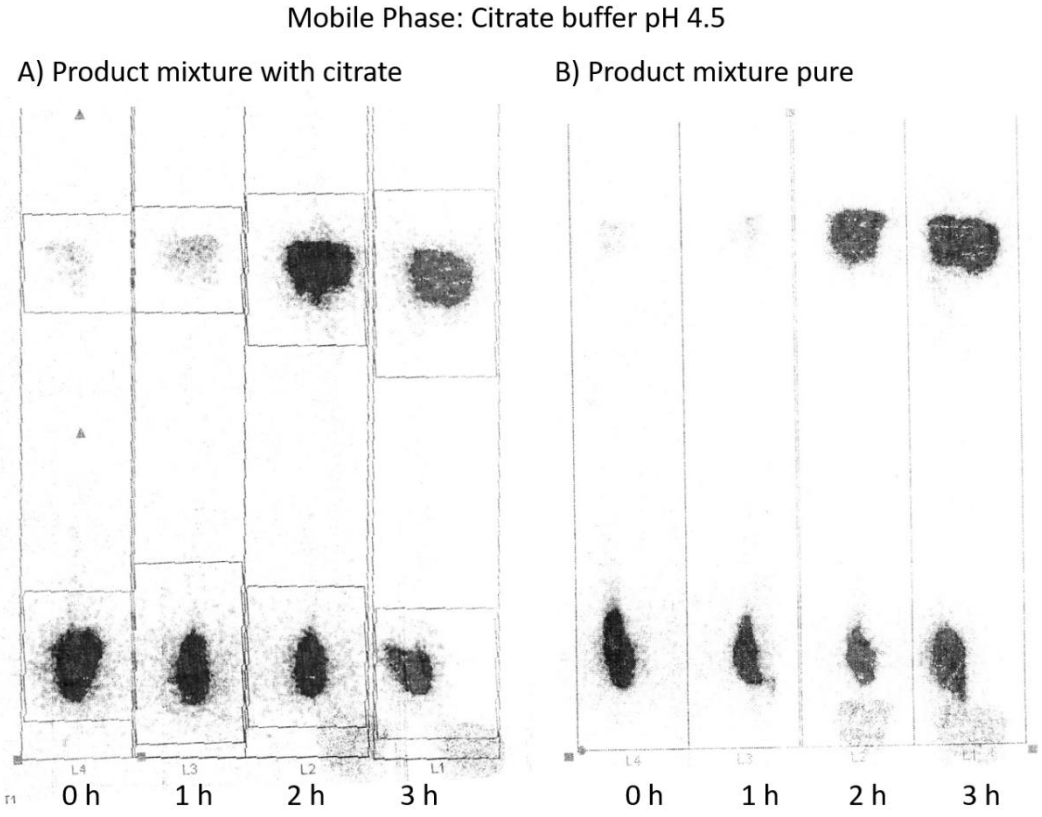

Figure S4: Instant images of the iTLC analysis of the product mixture developed in citrate buffer pH 4.5

Table S4A: Detailed results for Figure S4A

R_f/species	**0h [%]**	**1h [%]**	**2h [%]**	**3h [%]**
0.0 [^{111}In]In-DOTANOC/radiocolloids	96.2	93.0	50.0	34.2
1.0 [^{111}In]$InCl_3$ / [^{111}In]In-species	3.8	7.0	50.0	65.8

Table S4B: Detailed results for Figure S4B

R_f/species	0h [%]	1h [%]	2h [%]	3h [%]
0.0 [^{111}In]In-DOTANOC/radiocolloids	96.9	92.3	56.2	40.2
1.0 [^{111}In]$InCl_3$ / [^{111}In]In-species	3.1	7.7	43.8	59.6

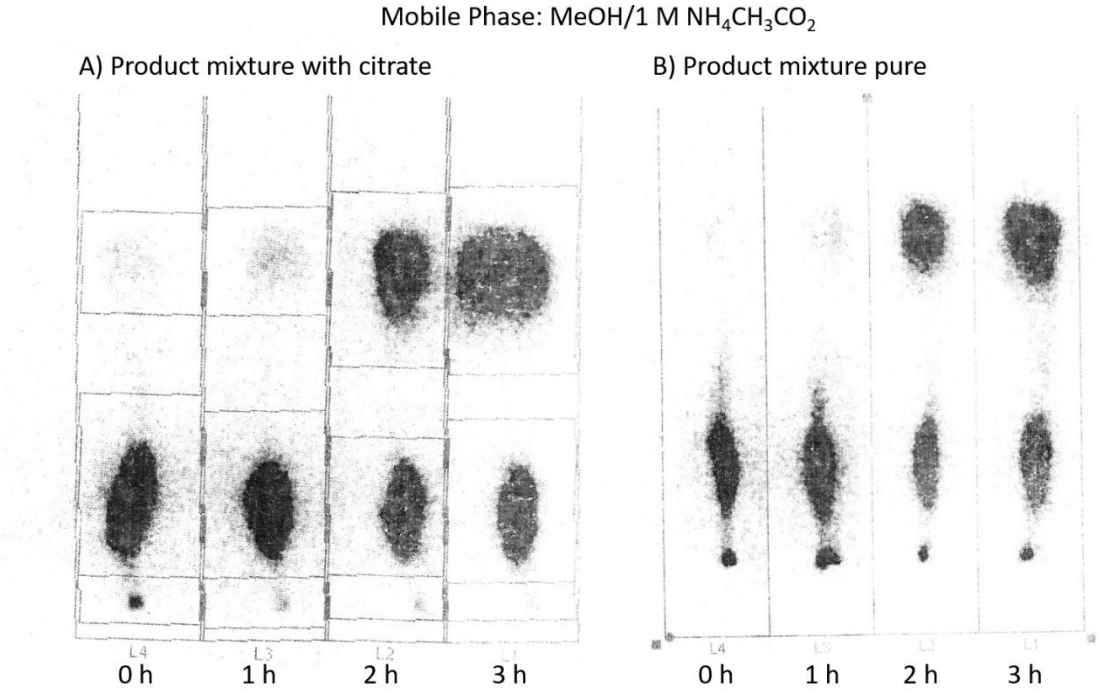

Figure S5: Images of the iTLC analysis of the product mixture developed in MeOH/1 M $NH_4CH_3CO_2$ (9:1)

Table S5A: Detailed results for Figure S5A

R_f/species	0h [%]	1h [%]	2h [%]	3h [%]
0.0 [^{111}In]In-radiocolloids/artifacts	2.9	3.0	2.3	1.4
0.2 [^{111}In]In-DOTANOC	92.5	89.5	50.5	37.2
1.0 [^{111}In]$InCl_3$ /species	4.6	7.6	47.2	61.4

Table S5B: Detailed results for Figure S5B

R_f/species	0h [%]	1h [%]	2h [%]	3h [%]
0.0 [^{111}In]$InCl_3$/radiocolloids/artifacts	7.5	8.7	5.1	3.1
0.2 [^{111}In]In-DOTANOC	89.2	85.1	52.1	41.3
0.7 [^{111}In]In-species	3.3	6.2	42.7	55.6

3.1. Discussion of the results

As before, the reaction mixtures were either diluted in citrate buffer or spotted on the TLC plate without further dilution. In solvent 2, the results of both TLC analyses are practically identical, which is in line with the TLC results from the experiment before. Also here, the [^{111}In]In-species as well as free ^{111}In ions migrate along the TLC plate with the solvent front. In contrast, the radiolabeled peptide remained at the baseline of the TLC plate. The yield of the reaction conducted with freshly opened indium was shown to be almost quantitative, whereas the yield decreased to 50% after ≈3 h with both analytical methods. However, for the present study, the method was rather inconclusive, since a differentiation between the impurity and [^{111}In]$InCl_3$ was not possible.

For solvent 1, it should be noted that the deviation between the impurity content in the analysis of the [^{111}In]$InCl_3$ stock solution at 1 h (Figure S2B) and the amount of the (assumingly) same impurity species in the reaction mixture after 1 h is remarkable (Figure 5B). This result indicates that the formation of the [^{111}In]In-species took place or is triggered during sample processing or after retrieval of the activity for the second labeling reaction (1 h) from the stock solution. Regardless where the transformation took place, the result also suggests that this transformation is a quite sudden process (since the samples for the TLC analyses were drawn directly after the labelling reaction was started). Eventually, this makes the correlation between the quality of the stock solution as measured in the experiments above and the radiochemical yield of the respective labeling reaction rather difficult.

In both cases, [^{111}In]In-DOTANOC is visible as a long spot with an R_f of approx. 0.2-0.3. Since a higher R_f would allow for a better differentiation from the spot at the baseline (R_f 0), the composition of the mobile phase was changed to 8:2 MeOH/1 M $NH_4CH_3CO_2$ (see main manuscript). Except for this, the results match the expectations arising from the experiments conducted with the stock solution (see chapter 1, Figure 2 A&B): When citrate was added, the [^{111}In]In-species is no longer visible. For a quantification of the [^{111}In]In-species, the addition of citrate to the sample has to be omitted and the latter system is suitable for the quantification of the discussed [^{111}In]In-species.

4. Conclusion of iTLC results

In summary, we developed a method suitable for the quantitation of our [^{111}In]In-species together with [^{111}In]In-DOTANOC.

The additional quantitation of radiocolloids is possible by the addition of citrate to the sample before spotting onto a second iTLC sheet. However, the highest result on radiocolloids was with approx. 3 % negligible for the present study and was, thus, not conducted in the following experiments.

Unfortunately, a clear correlation between the quality of the stock solution and the radiochemical yield of the corresponding labelling reaction was not possible.

5. Indium coordination equilibria in solution

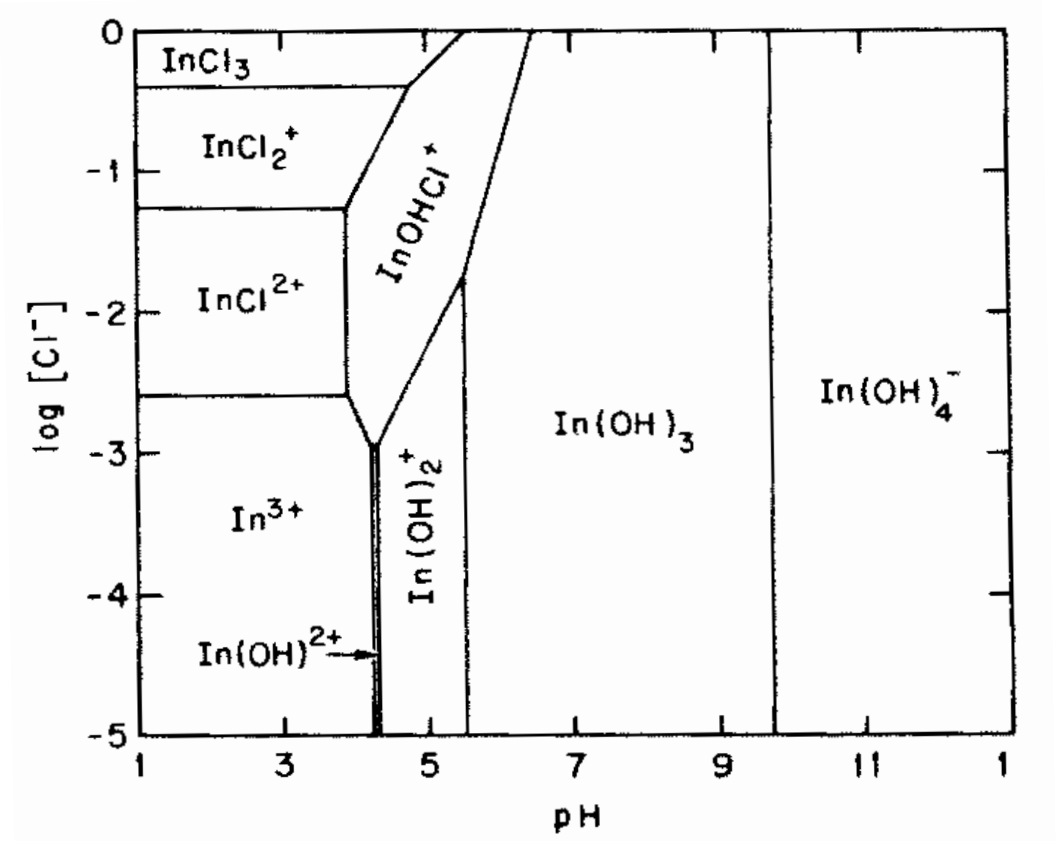

Figure S6: Predominance diagram for In^{3+}- OH^- -Cl^- species at 25 °C in 2 M $NaClO_4$. The lines represent conditions under which equal concentrations of the adjacent species occur (from Baes and Mesmer, 1976)). No information on the concentration of Indium is provided in the reference. Reprinted with permission of the publisher Wiley.

6. Literature Reference

Baes, C.F., Mesmer, R.E., 1976. The hydrolysis of cations, John Wiley & Sons, New York. https://doi.org/10.1002/bbpc.19770810252.

RESEARCHARTICLE

Immune checkpoint targeting: Inhibiting the interaction between the immune checkpoint PD-1 and its ligand PD–L1 activates the immune system to fight cancer. Detection of the expression of PD–L1 is a prerequisite for immune checkpoint inhibition therapy. We report our investigations towards the development of a PD–L1 specific nuclear imaging probe based on a macrocyclic peptide scaffold reported in the patent literature.

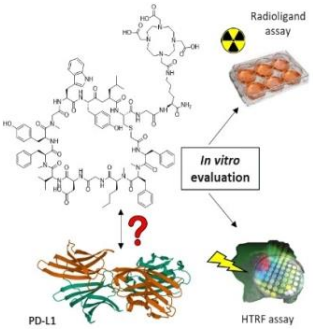

*MSc. N. Jouini, Dr. J. Cardinale, Prof. Dr. T. L. Mindt**

1 – 9

Evaluation of a Radiolabeled Macrocyclic Peptide as Potential PET Imaging Probe for PD–L1

ChemMedChem

ResearchArticle
doi.org/10.1002/cmdc.202200091

Chemistry Europe
European Chemical Societies Publishing

www.chemmedchem.org

Evaluation of a Radiolabeled Macrocyclic Peptide as Potential PET Imaging Probe for PD–L1

Nedra Jouini,[a, b, c] Jens Cardinale,[a, c] and Thomas L. Mindt*[a, b, c]

The interaction between the immune checkpoint PD-1 and PD–L1 promotes T-cell deactivation and cancer proliferation. Therefore, immune checkpoint inhibition therapy, which relies on prior assessment of the target, has been widely used for many cancers. As a non-invasive molecular imaging tool, radiotracers bring novel information on the *in vivo* expression of biomarkers (e.g., PD–L1), enabling a personalized treatment of patients. Our work aimed at the development of a PD–L1-specific, peptide-based PET radiotracer. We synthesized and evaluated a radiolabeled macrocyclic peptide adapted from a patent by Bristol Myers Squibb. Synthesis of [^{68}Ga]Ga-NJMP1 yielded a product with a radiochemical purity > 95 % that was evaluated *in vitro*. However, experiments on CHO–K1 hPD–L1 cells showed very low cell binding and internalization rates of [^{68}Ga]Ga-NJMP1 in comparison to a control radiopeptide (WL12). Non-radioactive cellular assays using time-resolved fluorescence energy transfer confirmed the low affinity of the reported parent peptide and the DOTA-derivatives towards PD–L1. The results of our studies indicate that the macrocyclic peptide scaffold reported in the patent literature is not suitable for radiotracer development due to insufficient affinity towards PD–L1 and that C-terminal modifications of the macrocyclic peptide interfere with important ligand/receptor interactions.

Introduction

The inhibitory immune checkpoint Programmed cell Death receptor 1 (PD-1) and its ligand Programmed cell Death Ligand 1 (PD–L1) is widely researched since its discovery in the early nineties.[1] The interaction between PD-1 and PD–L1 inhibits T-cell signaling, therefore rendering the immune system ineffective for fighting diseases. PD-1 (CD 279) is a membrane receptor critical for the regulation of adaptive immune cells such as T-lymphocytes.[2] PD–L1 (CD274) is a transmembrane protein that is expressed on immune-related lymphocytes and overexpressed by cancer cells, thus, allowing for their efficient evasion from the host immune system. To activate the immune system, the inhibition of the interaction between PD-1 and PD–L1 can be achieved on either target and is now a clinical option for immune-oncology therapies.[3] To date, several well-established compounds for immune checkpoint inhibition (ICI) therapy have been developed, such as antibodies like Atezolizumab (targeting PD–L1) and Nivolumab (targeting PD-1).[4] Early reports on the different therapeutic antibodies that successfully received approval by the Food and Drug Administration (FDA) demonstrated the efficacy of PD-1/PD–L1 inhibition therapy in different types of cancers including non-small cell lung carcinoma (NSCLC) and melanoma.[5] To benefit from an immune checkpoint blockade therapy, the expression of the target (e.g., PD–L1) should be evaluated beforehand. The most frequently applied method for this is immunohistochemistry (IHC) staining of formalin-fixed, paraffin-embedded biopsy samples. However, there is considerable variability in the used techniques: differences in the binding sites of the used anti-PD–L1 staining antibodies, the choice of the staining method (automatic versus manual), and the technical protocols are all factors that give rise to incomparable results. The absence of a standardized method for staining and scoring of PD–L1 leads to an incomplete picture of the heterogeneously expressed target.[6] The non-invasive molecular imaging modality Positron Emission Tomography (PET) offers a promising alternative to the current IHC for detecting the PD–L1 expression and therefore predicting the response to immunotherapy treatment.[7–8] ImmunoPET, which employs antibody-based PET radiotracers for the imaging of immune checkpoints, has witnessed an increased usage over the past years.[9] However, radiolabeled antibodies can present unfavorable characteristics such as low tissue penetration, costly production, slow pharmacokinetics and thus, longer diagnosis time (days to weeks). Smaller molecules with faster pharmacokinetics that are able to target protein-protein interactions, in this case PD-1/PD–L1, have recently gained attention in the field of radiopharmaceutical development.[10] In comparison to bulkier PD–L1 inhibitors (e.g., antibodies and other proteins), synthetically readily accessible peptides exhibit several advantages such as excellent specificity, low toxicity, good tissue penetration,

[a] MSc. N. Jouini, Dr. J. Cardinale, Prof. Dr. T. L. Mindt
Ludwig Boltzmann Institute Applied Diagnostics
General Hospital of Vienna
Währinger Gürtel 18–20, 1090 Vienna (Austria)
E-mail: thomas.mindt@univie.ac.at
[b] MSc. N. Jouini, Prof. Dr. T. L. Mindt
Faculty of Chemistry, University of Vienna
Währinger Strasse 42, 1090 Vienna (Austria)
[c] MSc. N. Jouini, Dr. J. Cardinale, Prof. Dr. T. L. Mindt
Division of Nuclear Medicine, Medical University of Vienna
Währinger Gürtel 18–20, 1090 Vienna (Austria)

Supporting information for this article is available on the WWW under https://doi.org/10.1002/cmdc.202200091

fast pharmacokinetics, and low production costs. All these features make peptides promising candidates for the development of PD–L1 imaging probes.[11–13] Our study focused on the synthesis, characterization and evaluation of a novel peptide-based radiotracer which targets PD–L1. The 14-mer macrocyclic peptide (BMS78), adapted from a library of peptides published in a patent by Bristol Myers Squibb (BMS),[14] was equipped with the universal chelator 2,2′,2″,2‴-(1,4,7,10-tetraazacyclo-dodecane-1,4,7,10-tetrayl)tetraacetic acid (DOTA) at its C-terminus for ^{68}Ga-labelling (**NJMP1**) and the conjugate was evaluated *in vitro* using the Chinese Hamster Ovary cell line expressing human PD–L1 (CHO–K1 hPD–L1). The reported and established radiolabeled PD–L1-targeting macrocyclic peptide WL12 was used as a reference compound.

Results and Discussion

Selection of the PD–L1 targeting peptide

Protein-protein interactions (PPI) have been shown to play a vital role in regulating biological processes within the co-stimulatory and inhibitory immune checkpoints. However, targeting PPIs with small molecules presents its own challenges since the PD-1/PD–L1 interaction surface is quite large (1,97 Å^2) and featureless.[15] In the past years, BMS published multiple patents disclosing structures of immunomodulatory macrocyclic peptides that inhibit the interaction between PD-1 and PD–L1. The corresponding *in vitro* data was also disclosed, revealing several promising compounds with reportedly high affinities towards the target protein PD–L1.[16] Research conducted by other teams based on structures included in these patents have narrowed down the library to a couple of potential macrocyclic peptides with 13 to 15 amino acid sequences, able to inhibit the PD-1/PD–L1 interaction.[17] The X-ray analysis of two of these peptides (BMS71 and BMS57) bound to PD–L1 have meanwhile been published, providing resourceful information in determining our choice of peptides for the development of a PD–L1 radiotracer.[17] Based on the available information at the onset of our studies, BMS71 was chosen because of its reported low IC_{50} value (7 nM) and different favorable interactions of its amino acid residues with PD–L1. Beforehand, we reviewed the published co-crystal structure of BMS71/PD–L1 (Protein Data Bank (PDB) ID: 5O45; see Supporting Information (SI) Figure S13) where the C-terminal amino acid amide (Gly^{14}-NH_2) was reported to point away from the PPI interface and not to form important interactions with the receptor PD–L1. Thus, it appeared that the C-terminus offers an easily accessible conjugation site for the modification of the peptide with chelators for radiometal labelling.[17] Although, as discussed below, this notion had to be revised at a later time point after new structural data became available.[18]

The well-established macrocyclic peptide WL12 was equipped with the chelator DOTAGA, radiolabeled with [^{68}Ga]$GaCl_3$ and used as a reference PD–L1 radiotracer for *in vitro* assays. WL12 is a PD–L1 targeting peptide that has been demonstrated to bind with high affinity to PD–L1 (IC_{50} = 23 nM).[13,19] It is among the first macrocyclic peptides that has shown promising *in vitro* and *in vivo* results after being radiolabeled with various radionuclides (copper-64, gallium-68 and fluorine-18).[13,19,20] Currently, WL12 is being investigated in clinical trials as a PD–L1 targeting PET-tracer in gastrointestinal and lung cancer (*NCT04304066*[21]). [^{64}Cu]Cu-WL12 has also been recently used as a quantifying tool for target engagement of therapeutic anti-PD–L1 antibodies, improving therefore the therapeutic doses applied to the patients in clinics.[22] Manual Fmoc-Solid Phase Peptide Synthesis (SPPS) was used to synthesize the linear 14/15-amino acid sequence of BMS71, BMS78, and NJMP1 (Table 1, SI Figure S10).

Synthesis of macrocyclic peptides and their derivatives

After the first attempts to synthesize BMS71, we observed an instability in the *N*-methyl amide rich peptide sequence (^{m}Phe^2-^{m}Nle^3-^{m}Gly^4). It has been reported that for peptides containing several consecutive *N*-methylated amino acids, fragmentation during the trifluoroacetic acid-mediated cleavage from the resin can occur at the N-terminal positions.[23–25] This made the synthesis of BMS71 by standard SPPS very challenging. The low yields of the synthesis of BMS71 (approx. 5%) and the difficult separation of multiple side products prompted us to choose another sequence, BMS78. The latter is only one-amino acid different from the first peptide (Gly^4 instead of ^{m}Gly^4) and it was reported to show a good binding affinity towards PD–L1 in the published BMS patent (IC_{50} = 14 nM).[14]

With an *N*-methyl amide less, it could be assumed that BMS78 is not prone to degradation during standard SPPS. Indeed, the synthesis of BMS78 and NJMP1 (Table 1, Figure 1) on a Rink amide resin proceeded without problems. For NJMP1, the synthesis started with the coupling of the Fmoc-Lys(DOTA(O*t*Bu)$_3$)-OH to the resin in order to place the chelator at the *C*-terminal amino acid of the peptide. Even though the coupling of Fmoc-Lys(DOTA)–OH to the resin has been reported to be challenging due to steric reasons, the reaction proceeded smoothly in our hands.[26] Once the linear sequences were

Table 1. Amino acid sequences of investigated peptides and peptide conjugates and corresponding yields.

Peptide	Sequences[a]	Yields	Purity (HPLC)
BMS71	Cyclo(AcPhe–^{m}Phe–^{m}Nle–^{m}Gly–Asp–Val–^{m}Phe–Tyr–^{m}Gly–Trp–Tyr–Leu–Cys)-Gly–NH_2	5%	83%
BMS78	Cyclo(AcPhe–^{m}Phe–^{m}Nle–Gly–Asp–Val–^{m}Phe–Tyr–^{m}Gly–Trp–Tyr–Leu–Cys)-Gly–NH_2	50%	98%
NJMP1	Cyclo(AcPhe–^{m}Phe–^{m}Nle–Gly–Asp–Val–^{m}Phe–Tyr–^{m}Gly–Trp–Tyr–Leu–Cys)-Gly–Lys(DOTA)-NH_2	42%	98%
WL12	Cyclo(AcTyr–^{m}Ala–Asn–Pro–His–Leu–Hyp–Trp–Ser–Trp(Me)-^{m}Nle–^{m}Nle–Orn(DOTAGA)-Cys)-Gly–NH_2	68%	97%

[a] The thioether bridge is located between Cys^{13} and Ac–Phe^1 for NJMP1, BMS71, BMS78, and between Cys^{14} and Ac–Tyr^1 for WL12.

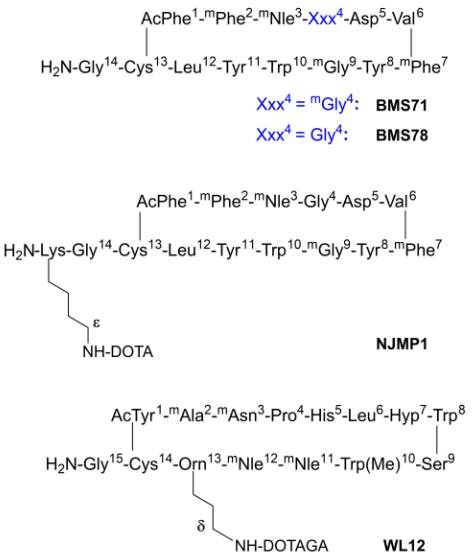

Figure 1. Structures of the peptides and peptide-conjugates investigated in this work.

elongated, chloroacetic acid was coupled to the last amino acid (Phe[1]). The peptides were then cleaved from the resin and deprotected, and the cyclization between the thiol group of Cys[13] and the chloroacetylated Phe[1] was carried out.[17] Both compounds BMS78 and NJMP1 were obtained in higher yields than BMS71 (Table 1) and in excellent purities. Electrospray Ionization Mass Spectrometry (ESI-MS) of the HPLC-purified compounds confirmed their structures (SI Table S1, Figures S1, S2 and S3). The conjugation of 2,2′,2″-(10-(2,6-dioxotetrahydro-2H-pyran-3-yl)-1,4,7,10-tetraazacyclododecane-1,4,7-triyl)triacetic acid (DOTAGA-anhydride) to Orn[13] of the commercial WL12 peptide was conducted according to a published procedure.[13] The crude product was purified by Reverse Phase (RP)–HPLC and the structure of the conjugate was confirmed by ESI-MS (Table S1, Figure S6).

^{nat}Ga- and ^{68}Ga-labelling of NJMP1 and WL12

Metalation reactions of NJMP1 and WL12 with $^{nat}Ga(NO_3)_3$ and [^{68}Ga]$GaCl_3$ were performed according to literature procedures yielding the desired products in quantitative yields and high purities (>95%).[27–28] ^{nat}Ga-NJMP1 and ^{nat}Ga-WL12 were purified by RP-HPLC, lyophilized, and analysis by ESI-MS confirmed their structures (SI Table S1 and Figures S4, S7). [^{68}Ga]Ga-NJMP1 and [^{68}Ga]Ga-WL12 were prepared with a radiochemical purity (RCP) and radiochemical yield (RCY) of >95% (SI Figures S5 and S8).

$LogD_{pH\ 7.4}$ and human serum stability assay

The lipophilicity of a radiolabeled compound is an important indicator for potential unspecific binding to non-targeted tissues. $LogD_{pH7.4}$ of [^{68}Ga]Ga-NJMP1 and [^{68}Ga]Ga-WL12 were determined using the Shake-flask method (n=3 in triplicate) and are given as mean values±standard deviation (SD).[29–30] [^{68}Ga]Ga-NJMP1 displayed a $LogD_{pH\ 7.4}$ of 0.795±0.22 indicating a rather lipophilic character of the compound. For [^{68}Ga]Ga-WL12, a calculated value of LogP=−5.99 has been reported.[13] Our shake-flask experiments showed that [^{68}Ga]Ga-WL12 is less hydrophilic with a $LogD_{pH\ 7.4}$ of −1.22±0.23. This value falls in the range of the reported $LogD_{pH\ 7.4}$ for [^{64}Cu]Cu-NOTA-WL12 (−0.818±0.026) demonstrating the hydrophilicity of the radiolabeled peptide.[31] Overall, WL12 presents more charged amino acids in its cyclic structure than NJMP1 (Figure 1) and thus, the observed differences in $LogD_{pH\ 7.4}$ were to be expected.

The stability of [^{68}Ga]Ga-NJMP1 was evaluated in human serum at 37 °C. [^{68}Ga]Ga-NJMP1 was stable in serum after 2 h (> 93% as determined by γ-HPLC; Figure S14). As the results of the lipophilic character of NJMP1, a substantial amount of radioactivity was found associated with the protein pellet (approx. >50% after 90 min).

Receptor binding and cell internalization assays

Receptor binding and cell internalization assays were performed with CHO–K1 hPD–L1 and CHO–K1 as a negative control. The CHO–K1 hPD–L1 cell line was passaged fewer than ten times in order to avoid a decrease in the efficiency of the hPD–L1 transfection while maintaining reliable results.[32] To our surprise, the receptor binding and uptake of [^{68}Ga]Ga-NJMP1 in the CHO–K1 hPD–L1 cell line was <2% AD (applied dose)/10^6 cells after 90 min (Figure 2, Table 2). Cell binding and uptake of [^{68}Ga]Ga-NJMP1 in CHO–K1 cell line was negligible. The time point t=90 min was chosen as a reference point after initial cell experiments with [^{68}Ga]Ga-NJMP1 during which the cell binding and internalization rates did not change after two hours (SI Figure S11).

Various cell lines have been used for the *in vitro* evaluation of PD–L1 radiotracers. Despite the lack of a standardized method and a commonly used PD–L1-expressing cell line, we decided to validate our own set-up for the evaluation of NJMP1. We therefore performed the same cell binding and internalization assays with [^{68}Ga]Ga-WL12 (Figure 2, Table 2, SI Fig-

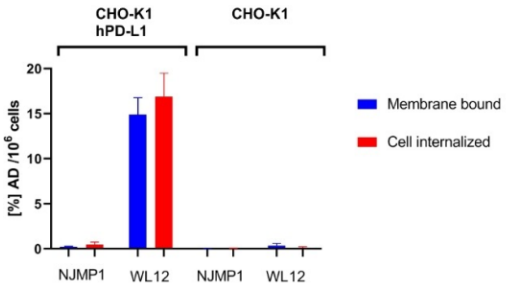

Figure 2. A comparison of receptor binding and cell internalization between [^{68}Ga]Ga-NJMP1 and [^{68}Ga]Ga-WL12 on CHO–K1 hPD–L1 and CHO–K1 cells at 90 min. Data are presented as mean values±SD (n=3 in triplicate).

Table 2. Membrane bound and cell internalized fractions in CHO–K1 and CHO–K1 hPD–L1 cell line for [68Ga]Ga-WL12 and [68Ga]Ga-NJMP1 after 90 min. Data are presented as mean values ± SD (n = 3 in triplicate).

Cell line		[^{68}Ga]Ga-NJMP1	[^{68}Ga]Ga-WL12
CHO–K1 hPD–L1	Membrane bound %AD/10^6 cells	0.36 ± 0.06	18.17 ± 1.75
	Cell internalization %AD/10^6 cells	1.68 ± 0.19	19.18 ± 1.6
CHO–K1 (negative control)	Membrane bound %AD/10^6 cells	0.133 ± 0.01	3.5 ± 0.30
	Cell internalization %AD/10^6 cells	1.18 ± 0.04	3.07 ± 0.43

ure S12). Each approx. 18% AD/10^6 cells were found membrane bound and internalized, respectively, in the CHO–K1 hPD–L1 cells after 90 min indicating a high affinity of [^{68}Ga]Ga-WL12 towards PD–L1. Experiments with [^{68}Ga]Ga-WL12 and the PD–L1 negative control cell line CHO–K1 resulted in a reduced cell binding and internalization of each approx. < 4% AD/10^6 cells, therefore demonstrating the specificity of [^{68}Ga]Ga-WL12 towards PD–L1. For complete *in vitro* data of [^{68}Ga]Ga-WL12 including results of blocking experiments see the SI, Figure S12. We were able to generate good and reproducible *in vitro* results for the binding and internalization of [^{68}Ga]Ga-WL12 to PD–L1 as well as provide proof of its specificity to the target in accordance with published data.[20,33]

The CHO–K1 and CHO–K1 hPD–L1 cell lines that constituted the used *in vitro* test system were therefore validated and the unfavourable low binding and internalization of [^{68}Ga]Ga-NJMP1 could only be on account of the intrinsic characteristics of the parent peptide BMS78 and/or the structural modifications that were introduced. The lack of binding of [^{68}Ga]Ga-NJMP1 to PD–L1 *in vitro* led us to resort to non-radioactive assays for quantitative measurement of the affinity (IC_{50}) of BMS78 and its derivatives towards PD–L1 as well as to test the extent of the loss of affinity that could be ascribed to its C-terminal modification with DOTA. For this purpose, we used the homogenous time-resolved fluorescence PD-1/PD–L1 biochemical binding assay (HTRF). This method is comparable to the one utilized by BMS,[14] although the specific assay conditions were not fully disclosed in the patents. We first measured the IC_{50} of known PD–L1 blockers such as Atezolizumab (IC_{50} = 2.25 nM) and Inhibitor 3^{TM}, a commercially available PD–L1 inhibiting peptide (IC_{50} = 186 nM). The measured IC_{50} of both compounds were in good agreement with literature values (Table 3, Figure 3A).[34–35] However, the IC_{50} value for BMS78 was found an order of magnitude higher than what was reported in the

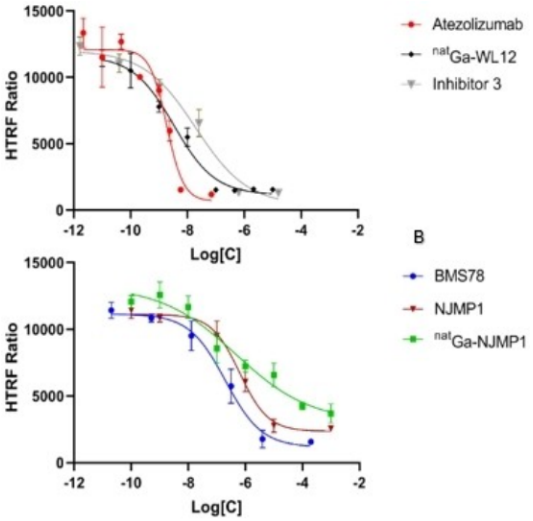

Figure 3. PD-1/PD–L1 blockade HTRF bioassay. A) Concentration-dependent inhibition curves for Atezolizumab, inhibitor 3^{TM} and ^{nat}Ga-WL12, which were used as reference compounds for this assay. B) Concentration-dependent inhibition curves for BMS78, NJMP1, and ^{nat}Ga-NJMP1. Data are presented as mean values ± SD (n = 2–3 in triplicate).

patent (Table 3, Figure 3B).[14] Similarly, another report on PD–L1-targeting macrocyclic BMS peptides (e.g., BMS57) also discloses lower binding affinities towards PD–L1 than those presented in the BMS patents.[36] C-terminal modified NJMP1 and ^{nat}Ga-NJMP1 displayed even higher values than BMS78, with an increase of the IC_{50} from the nM to the μM range. While the attachment of Lys(DOTA)NH_2 to the C-terminus of BMS78 resulted in a doubling of the IC_{50} compared to BMS78, loading the chelator with ^{nat}Ga had even a bigger impact and further increased the IC_{50} by two orders of magnitude. We can currently not provide an explanation for this phenomenon. However, the (positive or negative) impact of radiometalation as well as the influence of different radiometals on the binding affinity of peptide-chelator conjugates towards their respective molecular targets has previously been reported.[37–39] Although the co-crystal structure of BMS71/PD–L1 indicated a C-terminal Gly^{14}-NH_2 that was pointing away from the main hydrophobic binding site of PD–L1 (SI Figure S13),[17] our results suggest that the modification in this position could have either altered the binding mechanism of the peptide or, alternatively, interfered with important ligand-receptor interactions.

Table 3. IC_{50} values measured by the Homogenous Time resolved Fluorescence (HTRF) PD-1/PD–L1 assay. Data are presented as mean values ± SD (n = 2–3 in triplicate).

Compound	Measured IC_{50} [nM]	95% CI [nM]	Reported IC_{50} [nM]
Atezolizumab	2.25 ± 0.36	1.292–7.667	3.83[35]
BMS78	133 ± 1.23	106.3–166.9	14[14]
NJMP1	242 ± 0.89	218.2–278.7	–
^{nat}Ga-NJMP1	25945 ± 1450	15320–54990	–
^{nat}Ga-WL12	12.41 ± 0.25	10.09–16.08	^{nat}Cu-WL12 = 2.3[13]
Inhibitor 3^{TM}	186 ± 1.69	165.1–209.5	146[35]

With the substantial decrease in PD–L1 affinity from BMS78 (IC_{50} 133 nM) to NJMP1 (IC_{50} 242 nM) and ^{nat}Ga-NJMP1 (IC_{50} 26 μM), the observed lack of binding of [^{68}Ga]Ga-NJMP1 to CHO–K1 hPD–L1 cells became obvious. Thus, our hypothesis that the modification of the C-terminal amino acid of BMS78 (Gly^{14}) negatively impacts the overall binding of NJMP1 to PD–L1 could be confirmed.

In the course of our investigations, Zhong et al. reported a pharmacophore mapping study with the macrocyclic peptide BMS71 which complements our observations.[18,40] The interaction of BMS71/PD–L1 is driven by major hydrophobic interactions between the non-polar amino acids of the peptide (e.g., Phe^1, $^m Nle^3$, Val^6) and the "hot spots" of PD–L1.[41] However, few polar interactions and hydrogen bonds were also found to be important, especially since hydrogen bonds from the backbone amides contribute to the stabilization of the cyclic structure of the peptide. Few of the amino acid residues found within the PD–L1 "hot-spots" (e.g., Glu^{58}) were shown to form important hydrogen bonds with the C-terminal Gly^{14}-NH_2 of BMS71 (and therefore BMS78). By attaching a Lys(DOTA)NH_2 to the Gly^{14} of BMS78, we have likely interfered with some important polar interactions and, in addition, added more steric bulk. All these factors in turn impacted the binding of the peptide-conjugate NJMP1 to PD–L1. It might be possible to improve the PD–L1 binding properties of radiolabeled derivatives of BMS71/BMS78 (e.g., by choosing a different site for DOTA conjugation), however, the currently limited binding affinity of the parent macrocyclic peptides renders them unsuitable lead structures for the development of PD–L1 targeting PET radiopharmaceuticals.

Experimental Section

Unless stated otherwise, all reagents and solvents were purchased from Iris Biotech (Marktredwitz, Germany), and Merck (Darmstadt, Germany) and used without further purification. Fmoc-amino acids, *N*-methylated Fmoc-amino acids, Rink Amide MBHA LL resin (100–200 mesh), N,N-diisopropylcarbodiimide (DIC) and ethyl cyano(hydroxyimino)acetate (OXYMA Pure) were purchased from Merck Biosciences (Nottingham, UK) or Iris Biotech (Marktredwitz, Germany). Solid Phase Peptide Synthesis (SPPS) was performed manually. Fmoc-Lys(DOTA(O*t*Bu)$_3$)-OH was purchased from Macrocyclics (Texas, USA). Polypropylene syringes fitted with polypropylene frits and a polypropylene plunger were obtained from Multi-Syntech (Witten, Germany) and teflon taps from Biotage (Uppsala, Sweden). PD–L1 inhibitor 3™, a commercially available macrocyclic peptide targeting PD–L1 used for the validation of the HTRF assay, was purchased from SelleckChem (Texas, USA). WL12, a macrocyclic peptide used as a reference compound for *in vitro* experiments (structure shown in SI Figure S9) was purchased from BioVision (California, USA). Atezolizumab was purchased from Evidentic GmbH (Berlin, Germany). The Human PD1/PD–L1 biochemical binding assay HTRF was purchased from Cisbio Perkin Elmer (Massachusetts, USA). HPLC analysis was carried out with an Agilent system (Vienna, Austria) equipped with Autosampler Agilent 1100 Series, Iso Pump Agilent 1200 Series G1310 A, UV-Monitor Agilent 1200 Series G1314B Variable Wavelength Detector (VWD) and Radioactivity Detector Elysia Raytest Gabi Star. Data acquisition and gradient control were performed using GINA Star™, version 5.9. HTRF assay read-outs were performed on a Molecular Devices FlexStation 3 Multi-mode micro-plate reader (San José, USA). The γ-counter used in this work was a 2480 Wizard2, PerkinElmer (Waltham, USA). The Centrifuge was a Hettich Universal 30 RF with Hettich rotor 1412 24×3 g/24×1,5–2,2 mL (Tuttlingen, Germany). Data and statistical analysis were carried with GraphPad Prism5 ®. Low resolution (LR)–Mass Spectrometry (MS) was performed on a Bruker maXis (UHR-TOF, Vienna, Austria) equipped with Electrospray ionization (ESI) ion source and 3D ion trap and High resolution (HR)–MS was recorded on a Bruker maXis UHR-TOF spectrometer. HPLC solvents were 0.1% trifluoroacetic acid (TFA) in H_2O (A) and acetonitrile (MeCN) (B). Semi-preparative separation of the peptide derivatives was performed using Chromolith® SemiPrep RP-18 endcapped column (100–10 mm), followed by analytical HPLC on the Chromolith® Performance RP-18 endcapped column (100–4.6 mm) and a linear gradient from 70% to 30% of eluent (A) in 13 min (20 min for BMS71), flow rate 0.6 mL/min. Quality control of the radiolabeled peptides was performed using a Chromolith® Performance RP-18 endcapped column (100–4.6 mm) and a linear gradient from 70% to 30% of eluent (A) in 13 min with a flow rate of 0.6 mL/min.

Peptide synthesis of BMS71 and BMS78

BMS71 and BMS78[14] both comprise a common cyclic 14-mer amino acid sequence with one amino acid difference (Sar^4 versus Gly^4) as shown in Table 1 and in Figure 1. The resin (Rink Amide MBHA LL, 0.015 mmol) was swollen in 3 mL of N, N-dimethylformamide (DMF) in a syringe fitted with a polypropylene frit and a teflon tap. Standard coupling procedure (a) consisted of adding the Fmoc-protected amino acid (0.06 mmol, 4.0 equiv.), OXYMA Pure (0.06 mmol, 4.0 equiv.) and DIC (0.06 mmol, 4.0 equiv.), mixed in 1 mL of DMF to the resin, and the suspension was shaken for 15 min at 75 °C. Double coupling procedures (b) were used for *N*-methylated amino acids; the *N*-methyl-Fmoc-protected amino acid (0.06 mmol, 4.0 equiv.), OXYMA Pure (0.06 mmol, 4.0 equiv.) and DIC (0.06 mmol, 4.0 equiv.) mixed in 1 mL of DMF, were added to the resin, and the suspension was shaken for 15 min at 75 °C. The solvent was removed by filtration, and the resin was washed three times with 3 mL of DMF and 3 mL of dichloromethane (CH_2Cl_2). Then the second coupling was performed by the same procedure. After the second coupling, the reaction mixture was left shaking for 6 hours at room temperature (RT). The solvent was removed by filtration, and the resin was washed three times with 3 mL of DMF and 3 mL of CH_2Cl_2. Completion of the reaction was monitored by Kaiser Test or *n*-Chloranil Test (for secondary amines). For Fmoc deprotection, 20% piperidine in 3 mL DMF was added to the resin and left to react for 3 min at RT. The deprotection agent was then filtered off, and this process was repeated three times. The resin was then washed three times with 3 mL of DMF and 3 mL CH_2Cl_2. The yield of the deprotection was determined by UV measurement ($\lambda = 301$ nm) of the fluorenylmethylpiperidine adduct ($\varepsilon = 7800\ mol^{-1}\ dm^3\ cm^{-1}$). After completion of the elongation of the amino acid sequence, and before cleaving the peptide from the resin, chloroacetic acid (0.06 mmol, 4.0 equiv.) was coupled to the N-terminus using the standard amino acid coupling procedure (a). The peptide sequences were cleaved and deprotected by a treatment of 2 h with 2 mL of 90% TFA and 10% triisopropylsilane mixture that was afterward removed by evaporation with a stream of air. The crude peptides were then precipitated by the addition of ice-cold diethyl ether Et_2O (15 mL). After centrifugation (4000 rpm, 3×5 min, 4 °C) and two washing steps with cold Et_2O, the linear peptide sequences were used for the cyclization procedure as described below.

NJMP1 synthesis

NJMP1 (BMS78 C-terminally conjugated to Lys(DOTA)NH_2) was synthesized according to the following procedure. Fmoc-Lys(DOTA(O*t*Bu)$_3$)-OH (0.02 mmol, 1.0 equiv.) was added to OXYMA and DIC (each 0.06 mmol, 3.0 equiv.) in 1 mL of DMF, then coupled to the resin prior to the elongation of the peptide sequence according to the coupling procedure (a). The reaction mixture was reacted for 15 min at 75 °C and then left shaking overnight at RT. The completion of the reaction was monitored with a Kaiser test. Acetylation of the unreacted amines of the resin was performed with 2.5 mL of a mixture of 90% DMF, 5% DIPEA, 5% Ac_2O by agitating for 10 min at RT. The elongation of the sequence and final coupling of chloroacetic acid followed the procedures described above.

Cyclization procedure

1 mg of the crude linear peptides were dissolved in a (1:2, v/v) mixture of acetonitrile and aqueous ammonium bicarbonate buffer (0.1 M, pH 8.5, 24 mL) and the solution was afterwards left shaking overnight at RT. The reaction mixture was then concentrated and the obtained products were dissolved in 500 μL (1:1, v/v) of a mixture of acetonitrile/water and purified by RP-HPLC. The analytical HPLC of the cyclized BMS71 had a retention time of and t_R = 9,13 min. The cyclized peptides BMS78 and NJMP1 had a retention time of t_R = 6,43 min and t_R = 6,33 min, respectively. The obtained lyophilized peptides were characterized by ESI-MS.

Synthesis of WL12

4 mg (2 μmol, 1.0 equiv.) of WL12 peptide and DOTAGA-anhydride (10 μmol, 5.0 equiv.) were dissolved in 1 mL of DMF and N,N-diisopropylethylamine (DIPEA, 5.0 equiv.) was added to the mixture that was left shaking overnight at RT. After the completion of the reaction, DMF was removed *in vacuo* and the residue was dissolved in a mixture (1:1, v/v) of H_2O and MeCN for RP-HPLC purification. The analytical HPLC of WL12 resulted in a retention time of t_R = 7,94 min. The obtained lyophilized compound was characterized by ESI-MS.

^{nat}Ga-labelling of peptide NJMP1 and WL12

The DOTAGA- and DOTA-conjugated peptides (0.08 μmol, 1.0 equiv.) were dissolved in 50 μL of HEPES buffer (pH = 3) and $Ga(NO_3)_3 \cdot 6H_2O$ (0.39 μmol, 5.0 equiv.) dissolved in 50 μL HEPES buffer was added. The mixtures were stirred for 30 min at 75 °C and afterwards purified with RP-HPLC. ^{nat}Ga-NJMP1 was collected at t_R = 7,12 min and ^{nat}Ga-WL12 at t_R = 8,2 min with a purity of 98% for the final peptide conjugates. The obtained lyophilized peptides were characterized by ESI-MS and stored at 4 °C for later use.

^{68}Ga-labelling of peptide NJMP1 and WL12

A ^{68}Ge/^{68}Ga generator (IRE Elit Radiopharma) was eluted with approx. 1 mL of 0.1 M HCl yielding an eluate of approx. 1 mL (450 MBq). In the reaction mixture, we added the peptide precursors (1.7 nmol, 4 μL) from 1 mg/mL stock solutions prepared in a H_2O/MeCN mixture (1:1, v/v), to sodium acetate buffer (22 μL, 1 M, pH 4.5) and 44 μL of the eluted [^{68}Ga]$GaCl_3$. The mixture, with a final pH 4.3, was reacted for 13 min at 95 °C. Quality control of the obtained radiolabeled peptides (A_s = 2.5 MBq/μg) consisted of analytical radio-HPLC to check the radiochemical purity of the compound. The retention time for the [^{68}Ga]Ga-NJMP1 was t_R = 7,4 min and t_R = 8,7 min for [^{68}Ga]Ga-WL12 (SI Figures S5, S8).

PD-1/PD–L1 biochemical binding assay

Cisbio (Perkin Elmer) provides a commercially available competitive inhibition assay, promoted to discover novel inhibitors for the immune checkpoint PD-1/PD–L1. The assay relies on time-resolved fluorescence resonance energy transfer (TR-FRET) and uses PD–L1-6His-tag and PD-1-Ig that can be detected by anti-human IgG-Eu^{3+} cryptate and anti-6HIS-XL665 monoclonal antibody, respectively. For the plating of the compounds, the instructions in the leaflet of the assay provided by the company were followed.

Cell lines

Chinese Hamster Ovary cell line CHO–K1 (CHO) were purchased from the American Type Culture Collection (ATCC, Manassas, VA), and passaged less than ten times before the experiments. CHO–K1 cells were maintained in Ham's F-12 medium with 10% Fetal Bovine Serum (FBS, Gibco) and 1% Penicillin/Streptomycin (P/S). Recombinant CHO–K1 cells stably expressing human PD–L1 (hPD–L1), henceforth referred to as CHO–K1 hPD–L1, were purchased from BPS Bioscience (San Diego, California) and were maintained in F-12 K medium with 10% FBS, 1% P/S, and 2 mg/mL G418. The cells were cultured in an incubator at 37 °C in an atmosphere containing 5% CO_2 and passaged less than ten times before seeding out for cell internalization experiments.

Cell internalization and receptor binding assay

Internalization studies were performed as previously published.[42,43] Briefly, approx. 10^6 CHO–K1 hPD–L1 or CHO–K1 cells were seeded in F-12 K medium containing 10% FBS, 1% P/S and 2 mg/mL G418 in 6-well plates on the day before the experiment and incubated overnight in a humidified incubator (37 °C, 5% CO_2). Approx. one hour before the experiment, the medium was replaced with 1.3 mL fresh 1% FBS F-12 K medium. Subsequently, 100 μL of the radio-labeled peptide [^{68}Ga]Ga-NJMP1 or [^{68}Ga]Ga-WL12 were added to each well (100 μL per well; 15 pmol; ~1.0 kBq) and cells were incubated for different time points (30, 60, 90 and 120 min). After the respective incubation times, the supernatant was collected and the cells were washed twice with 1 mL ice-cold Dulbecco's phosphate-buffered saline (PBS). The combined fractions represent the unbound radioligand. The receptor-bound radioactivity was obtained by incubating the cells twice for 5 min with an ice-cold acidic glycine solution (100 mM NaCl, 50 mM glycine, pH 2.8; 1 mL) on ice followed by the removal of the supernatant. Finally, the internalized fraction was collected after cell lysis using 1 M NaOH (1 mL; 10 min; 37 °C; 5% CO_2) and the wells containing the cell lysate were washed twice with NaOH (1 M, 1 mL). Standards of the radio-labeled peptides [^{68}Ga]Ga-NJMP1 and [^{68}Ga]Ga-WL12, for the determination of the applied dose, were prepared in triplicate. All fractions were measured in a γ-counter (409–613 keV energy window) and calculated as a percentage of the applied dose (AD) per one million cells.

$LogD_{pH7.4}$ determination

The lipophilicity (LogD) of [^{68}Ga]Ga-NJMP1 and [^{68}Ga]Ga-WL12 was determined by the partition coefficient between n-octanol and PBS (pH 7.4) utilizing the "shake-flask method".[28–29] PBS and n-octanol were shaken overnight to saturate each phase. After the separation of the layers by centrifugation at 4500 rpm for 5 min at 23 °C, equal volumes (500 μL) of each layer were taken and transferred into an Eppendorf tube and 5 μL (~5 kBq) of the radiolabeled peptide solutions (formulated in saline solution) were added to the PBS/n-octanol mixture. The resulting solutions were left shaking for

20 min, then centrifuged at 3000 rpm for 10 min. Aliquots of 300 μL were removed from the n-octanol and PBS phases and the radioactivity was measured in the γ-counter (n = 3 in triplicates). The lipophilicity was calculated as the LogD value of the average ratio between the radioactivity in the organic (n-octanol) and the PBS fractions.

Stability assay in human serum

For the determination of the serum stability, the radiopeptide [^{68}Ga]Ga-NJMP1 (100 μL; 15 pmol, 0.105 MBq) was added to 900 μL of fresh human blood serum and incubated (37 °C, 5 % CO_2). 100 μL of acetonitrile were dispensed into three tubes and at preselected time points (30, 60, and 90 min) samples of 100 μL serum were taken and added to the solvents in the tube to precipitate the proteins. The tube was thoroughly vortexed for 2 min at 5200 rpm, then 75 μL were taken from the supernatant and diluted with 75 μL of MilliQ Water. The mixture was then analyzed by γ-HPLC to determine the formation of potential metabolites. The protein pellet was washed 3 times with saline, centrifuged and measured in a gamma counter in order to quantify the protein-bound fraction of radioactivity.

Conclusion

In summary, we have synthesized and evaluated *in vitro* some $^{68/nat}$Ga-labeled peptide conjugates based on a macrocyclic scaffold described in patents of BMS. The radiolabeled [^{68}Ga]Ga-NJMP1 as well as ^{nat}Ga-NJMP1 were tested *in vitro* using cell binding experiments and HTRF screening assays and compared with the corresponding WL12 reference compounds. The results from our investigations indicate that the parent peptide BMS78 (lacking the chelator) has a much lower affinity towards PD–L1 than what was reported in the patent literature. In addition, C-terminal modification of the macrocyclic peptide with a DOTA chelator further decreased its affinity towards PD–L1 likely due to disturbance of important hydrogen bonding interactions with the receptor. On the other hand, the reference compound used in our studies, ^{68}Ga-labeled macrocyclic peptide WL12 with the chelator DOTAGA attached to an amino acid within the macrocycle (Orn^{13}), exhibited better properties. We also describe the first validation of a PD–L1 *in vitro* test system composed of CHO–K1 hPD–L1/CHO–K1 cells, which can be used in the future for the reliable evaluation of other PD–L1 targeted radiotracers. We conclude that the macrocyclic parent peptides BMS71 and BMS78 show potential in inhibiting the PD-1/PD–L1 interaction, but their low binding affinity towards PD–L1 makes them unsuitable lead structures for the development of PET radiotracers for the imaging of PD–L1.

Acknowledgements

We thank the Mass Spectrometry Service Centre of the University of Vienna, Dr. Barbara Lieder (Institute of Physiological Chemistry, University of Vienna) for help with the HTRF measurements, Dr. Marie Brandt, Anna Stingender, and Katarína Benčurová (Ludwig Boltzmann Institute Applied Diagnostics) as well as Dr. Verena Pichler and Karsten Bamminger (Department of Biomedical Imaging and Image-guided Therapy (Division of Nuclear Medicine) of the general hospital of Vienna) for their general and technical support. Open Access Funding was provided by the University of Vienna.

Conflict of Interest

The authors declare no conflict of interest.

Data Availability Statement

The data that support the findings of this study are available in the supplementary material of this article.

Keywords: radiopharmaceuticals · peptides · immune checkpoint blockade · PET · PD-1/PD–L1

[1] K. Bardhan, T. Anagnostou, V. A. Boussiotis, *Front. Immunol.* **2016**, *7*, 550.
[2] B. T. Fife, K. E. Pauken, *Ann. N. Y. Acad. Sci.* **2011**, *1217*, 45–59.
[3] L. Chen, X. Han, *J. Clin. Invest.* **2015**, *125*, 3384–3391.
[4] K. M. Hargadon, C. E. Johnson, C. J. Williams, *Int. Immunopharmacol.* **2018**, *62*, 29–39.
[5] Y. Jiang, M. Chen, H. Nie, Y. Yuan, *Hum. Vaccines Immunother.* **2019**, *15*, 1111–1122.
[6] X. Meng, Z. Huang, F. Teng, L. Xing, J. Yu, *Cancer Treat. Rev.* **2015**, *41*, 868–876.
[7] S. Nimmagadda, *Cancers (Basel).* **2020**, *12*.
[8] F. Bensch, E. L. van der Veen, M. N. Lub-de Hooge, A. Jorritsma-Smit, R. Boellaard, I. C. Kok, S. F. Oosting, C. P. Schroder, T. J. N. Hiltermann, A. J. van der Wekken, H. J. M. Groen, T. C. Kwee, S. G. Elias, J. A. Gietema, S. S. Bohorquez, A. de Crespigny, S. P. Williams, C. Mancao, A. H. Brouwers, B. M. Fine, E. G. E. de Vries, *Nat. Med.* **2018**, *24*, 1852–1858.
[9] W. Wei, Z. T. Rosenkrans, J. Liu, G. Huang, Q. Y. Luo, W. Cai, *Chem. Rev.* **2020**, *120*, 3787–3851.
[10] M. Konstantinidou, T. Zarganes-Tzitzikas, K. Magiera-Mularz, T. A. Holak, A. Domling, *Angew. Chem. Int. Ed.* **2018**, *57*, 4840–4848; *Angew. Chem.* **2018**, *130*, 4932–4940.
[11] A. Signore, A. Annovazzi, M. Chianelli, F. Corsetti, C. Van de Wiele, R. N. Watherhouse, *Eur. J. Nucl. Med.* **2001**, *28*, 1555–1565.
[12] U. Hennrich, M. Benešová, *Pharmaceuticals* **2020**, *13*, 38.
[13] S. Chatterjee, W. G. Lesniak, M. S. Miller, A. Lisok, E. Sikorska, B. Wharram, D. Kumar, M. Gabrielson, M. G. Pomper, S. B. Gabelli, S. Nimmagadda, *Biochem. Biophys. Res. Commun.* **2017**, *483*, 258–263.
[14] M. M. Miller, C. Mapelli, M. P. Allen, M. S. Bowsher, E. P. Gillis, D. R. Langley, E. Mull, M. A. Poirier, N. Sanghvi, L.-Q. Sun, D. J. Tenney, K.-S. Yeung, J. Zhu, K. W. Gillman, Q. Zhao, K. A. Grant-Young, P. M. Scola (Bristol Myers Squibb), WO2016039749 A1, **2016**.
[15] K. M. Zak, R. Kitel, S. Przetocka, P. Golik, K. Guzik, B. Musielak, A. Domling, G. Dubin, T. A. Holak, *Structure* **2015**, *23*, 2341–2348.
[16] X. Lin, X. Lu, G. Luo, H. Xiang, *Eur. J. Med. Chem.* **2020**, *186*, 111876.
[17] K. Magiera-Mularz, L. Skalniak, K. M. Zak, B. Musielak, E. Rudzinska-Szostak, L. Berlicki, J. Kocik, P. Grudnik, D. Sala, T. Zarganes-Tzitzikas, S. Shaabani, A. Domling, G. Dubin, T. A. Holak, *Angew. Chem. Int. Ed.* **2017**, *56*, 13732–13735; *Angew. Chem.* **2017**, *129*, 13920–13923.
[18] Y. Zhong, X. Li, H. Yao, K. Lin, *Molecules* **2019**, *24*, 1940.
[19] W. G. Lesniak, R. C. Mease, S. Chatterjee, D. Kumar, A. Lisok, B. Wharram, V. R. Kalagadda, L. A. Emens, M. G. Pomper, S. Nimmagadda, *Mol. Imaging* **2019**, *18*, 1-9.
[20] R. A. De Silva, D. Kumar, A. Lisok, S. Chatterjee, B. Wharram, K. Venkateswara Rao, R. Mease, R. F. Dannals, M. G. Pomper, S. Nimmagadda, *Mol. Pharm.* **2018**, *15*, 3946–3952.

[21] H. Zhu, '' Research for the Molecular Imaging of the PD–L1 Targeting Tracer", can be found under https://clinicaltrials.gov/ct2/show/NCT04304066, **2020**.
[22] D. Kumar, A. Lisok, E. Dahmane, M. McCoy, S. Shelake, S. Chatterjee, V. Allaj, P. Sysa-Shah, B. Wharram, W. G. Lesniak, E. Tully, E. Gabrielson, E. M. Jaffee, J. T. Poirier, C. M. Rudin, J. V. Gobburu, M. G. Pomper, S. Nimmagadda, *J. Clin. Invest.* **2019**, *129*, 616–630.
[23] M. J. O. Anteunis, C. Auwera, *Int. J. Pept. Protein Res.* **2009**, *31*, 301–310.
[24] Y. Yang, in: *Side Reactions in Peptide Synthesis* (Ed.: Y. Yang), Academic Press, **2016**, pp. 1–31.
[25] M. Teixido, F. Albericio, E. Giralt, *J. Pept. Res.* **2005**, *65*, 153–166.
[26] M. W. Pennington, M. E. Byrnes, *Methods Mol. Biol.* **1994**, *35*, 1–16.
[27] M. A. Green, M. J. Welch, *Nuclear Medicine and Biology* **1989**, *16*, 435–448.
[28] D. Mueller, W. A. Breeman, I. Klette, M. Gottschaldt, A. Odparlik, M. Baehre, I. Tworowska, M. K. Schultz, *Nat. Protoc.* **2016**, *11*, 1057–1066.
[29] C. A. Fischer, S. Vomstein, T. L. Mindt, *Pharmaceuticals* **2014**, *7*, 662–675.
[30] C. Vraka, L. Nics, K. H. Wagner, M. Hacker, W. Wadsak, M. Mitterhauser, *Nucl. Med. Biol.* **2017**, *50*, 1–10.
[31] J. Jiang, D. Li, T. Liu, L. Xia, X. Guo, X. Meng, F. Liu, F. Wang, Z. Yang, H. Zhu, *Bioorg. Med. Chem. Lett.* **2021**, *40*, 127901.
[32] P. Hughes, D. Marshall, Y. Reid, H. Parkes, C. Gelber, *BioTechniques* **2007**, *43*, 575–586..
[33] H. Z. A. Z. Y. Jiang Jinquan, *J. Nucl. Med.* **2020**, *61*, 1022.
[34] Cisbio, "Human PD1/PD–L1 biochemical binding assay", can be found under https://www.cisbio.eu/human-pd1-pd-l1-biochemical-binding-assay-44666, **2020**.
[35] X. Lin, X. Lu, G. Luo, H. Xiang, *Eur. J. Med. Chem.* **2020**, *186*, 111876.
[36] B. Musielak, J. Kocik, L. Skalniak, K. Magiera-Mularz, D. Sala, M. Czub, M. Stec, M. Siedlar, T. A. Holak, J. Plewka, *Molecules* **2019**, *24*, 2804.
[37] A. Poschenrieder, M. Schottelius, M. Schwaiger, H. Kessler, H. J. Wester, *EJNMMI Res.* **2016**, *6*, 36.
[38] P. Antunes, M. Ginj, H. Zhang, B. Waser, R. P. Baum, J. C. Reubi, H. Maecke, *Eur. J. Nucl. Med. Mol. Imaging* **2007**, *34*, 982–993.
[39] J. C. Reubi, J. C. Schar, B. Waser, S. Wenger, A. Heppeler, J. S. Schmitt, H. R. Macke, *Eur. J. Nucl. Med.* **2000**, *27*, 273–282.
[40] C. Mejias, O. Guirola, *J. Mol. Graphics Modell.* **2019**, *91*, 105–111.
[41] H. Lim, J. Chun, X. Jin, J. Kim, J. Yoon, K. T. No, *Sci. Rep.* **2019**, *9*, 16727.
[42] C. A. Kluba, A. Bauman, I. E. Valverde, S. Vomstein, T. L. Mindt, *Org. Biomol. Chem.* **2012**, *10*, 7594–7602.
[43] N. M. Grob, S. Schmid, R. Schibli, M. Behe, T. L. Mindt, *J. Med. Chem.* **2020**, *63*, 4496–4505.

Manuscript received: February 17, 2022
Accepted manuscript online: April 7, 2022
Version of record online: ■■, ■■■

ChemMedChem

Supporting Information

Evaluation of a Radiolabeled Macrocyclic Peptide as Potential PET Imaging Probe for PD–L1

Nedra Jouini, Jens Cardinale, and Thomas L. Mindt*

Table S1: Molecular formula and ESI-MS results for the compounds.

Compound	Molecular Formula	Calculated M_w g.mol^{-1}	ESI-MS (+) *m/z*
BMS71	$C_{93}H_{118}N_{16}O_{19}S$	1795.85	$[M+2H^+]^{2+}$: 898.98
BMS78	$C_{92}H_{116}N_{16}O_{19}S$	1781.84	$[M+2H^+]^{2+}$: 891.92
NJMP1	$C_{114}H_{154}N_{22}O_{27}S$	2296.11	$[M+2H^+]^{2+}$: 1149.11
^{nat}Ga-NJMP1	$C_{114}H_{152}GaN_{22}O_{27}S$	2364.35	$[M+2H^+]^{2+}$: 1182.58
WL12-DOTAGA	$C_{110}H_{158}N_{26}O_{29}S$	2340.65	$[M+2H^+]^{2+}$: 1171.08
^{nat}Ga-WL12	$C_{110}H_{156}GaN_{26}O_{29}S$	2408.05	$[M+2H^+]^{2+}$: 803.36

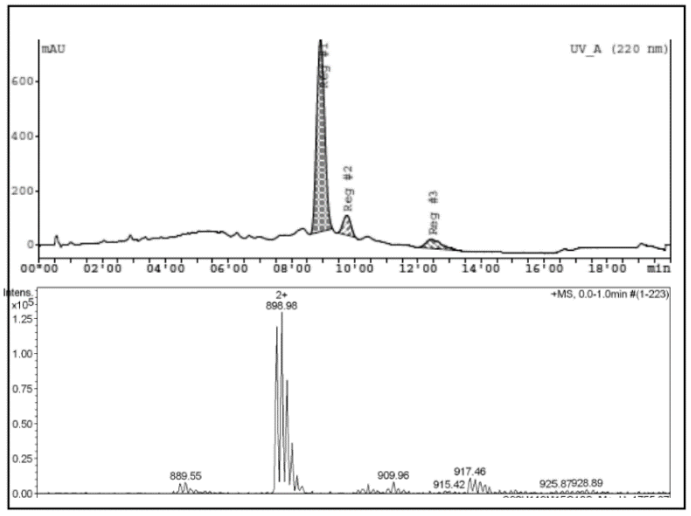

Figure S1: UV-HPLC/ESI-MS characterization of BMS71

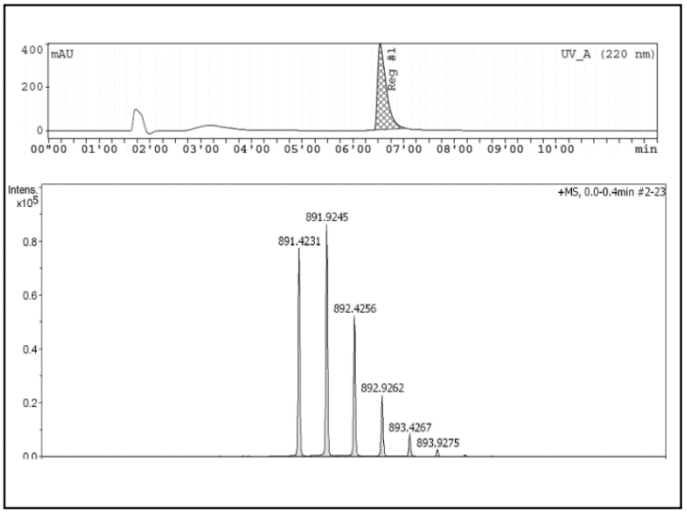

Figure S2: UV-HPLC/ESI-MS characterization of BMS78.

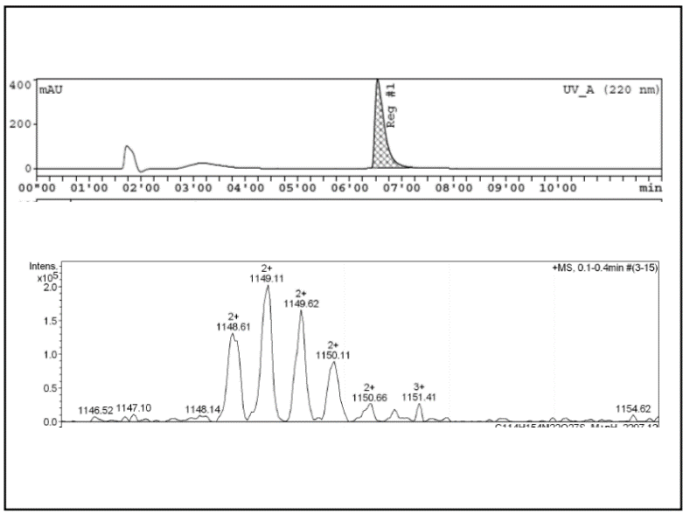

Figure S3: UV-HPLC/ESI-MS characterization of NJMP1.

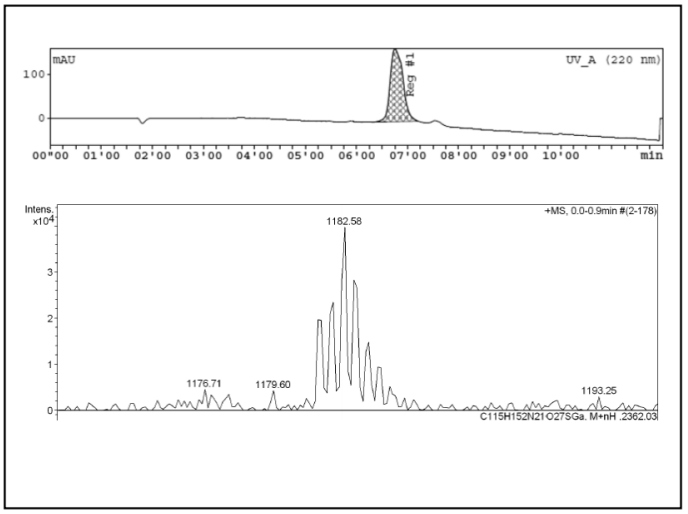

Figure S4: UV-HPLC/ESI-MS characterization of ^{nat}Ga-NJMP1.

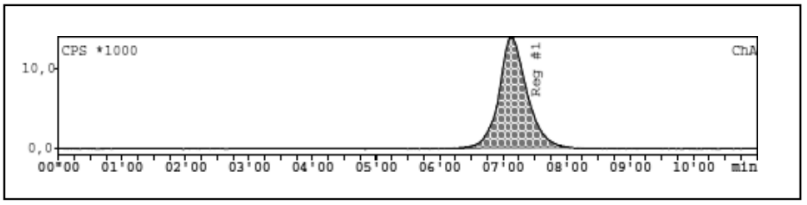

Figure S5: Radio-HPLC of [^{68}Ga]Ga-NJMP1.

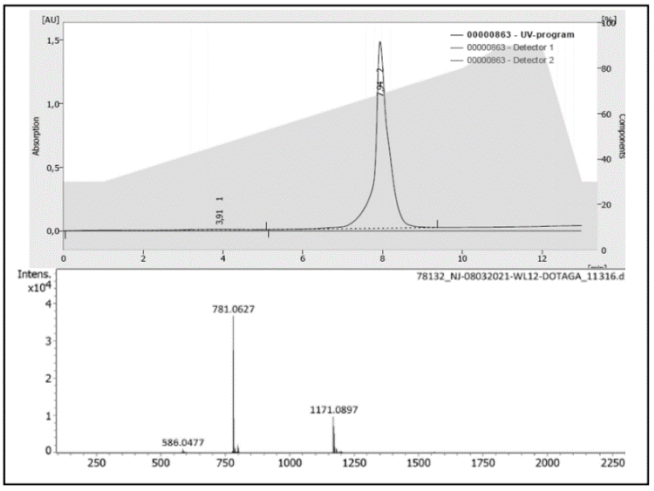

Figure S6: UV-HPLC/ESI-MS characterization of WL12.

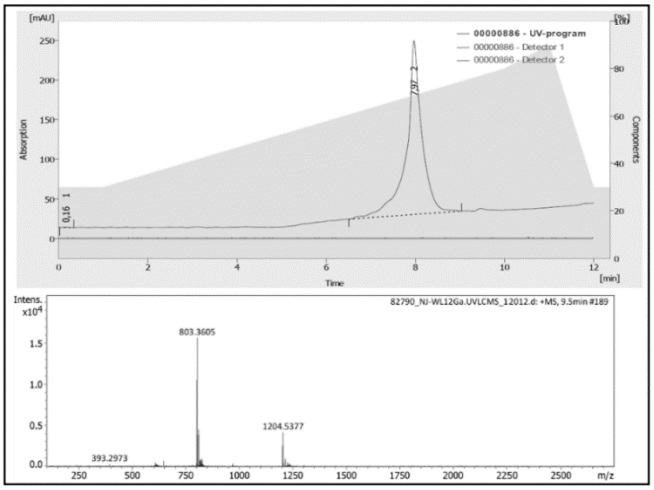

Figure S7: UV-HPLC/ESI-MS characterization of ^{nat}Ga-WL12.

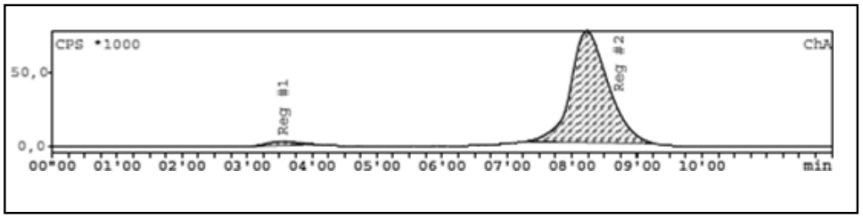

Figure S8: Radio-HPLC/ESI-MS characterization of [^{68}Ga]Ga-WL12.

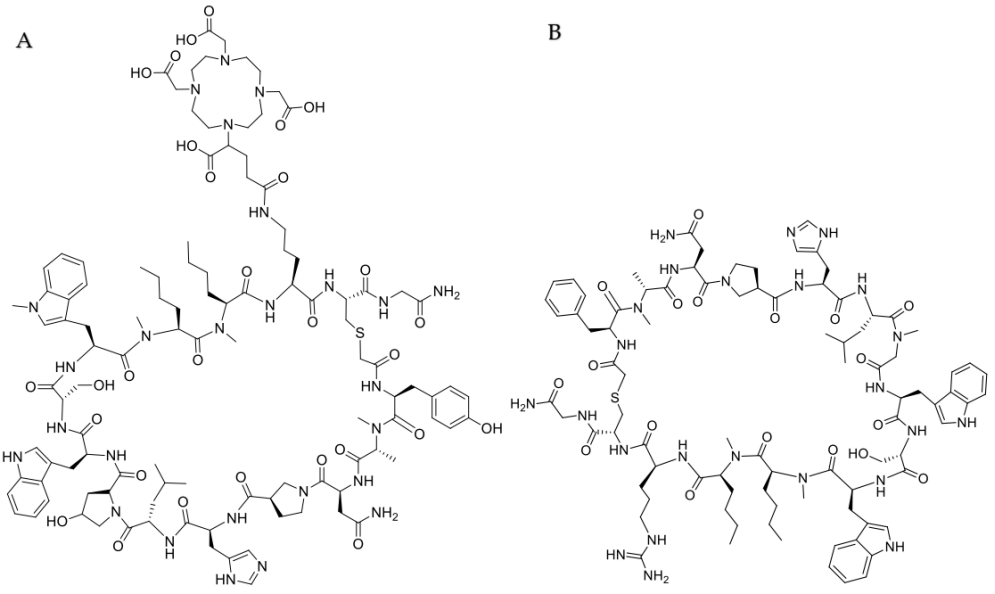

Figure S9: A) Structure of DOTAGA-WL12 and B) Inhibitor 3™ (SelleckChem).

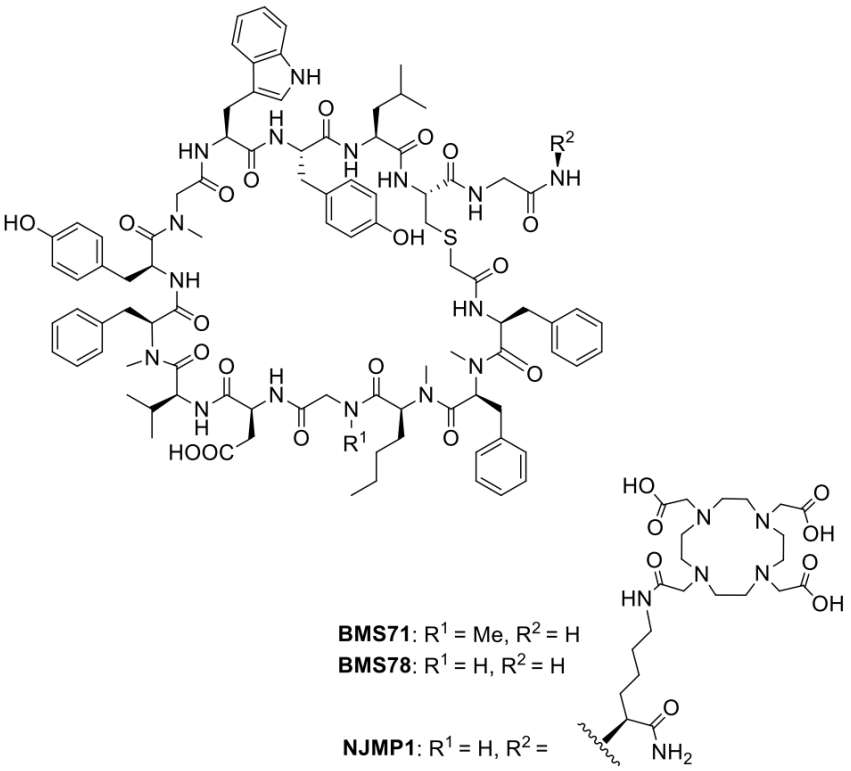

Figure S10: Structure of BMS71, BMS78 and NJMP1

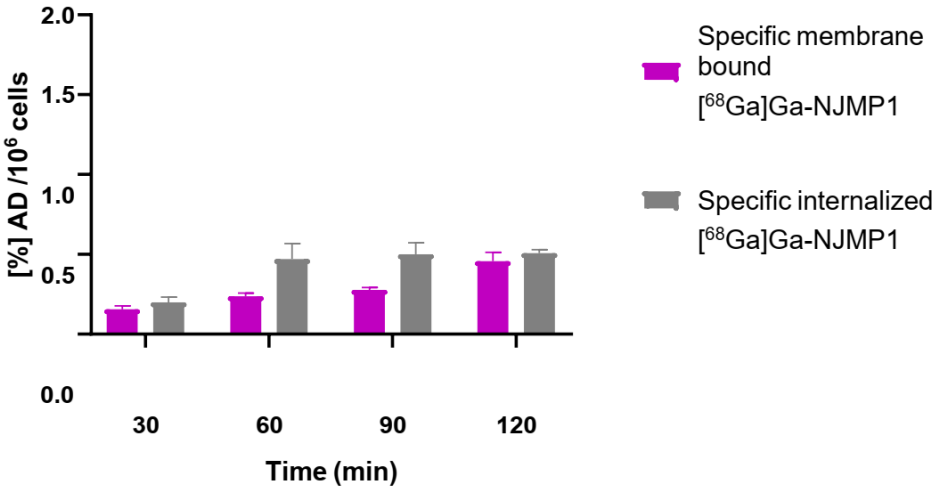

Figure S11: Specific cell internalization and receptor binding of [^{68}Ga]Ga-NJMP1 in CHO-K1 hPD-L1 cells.

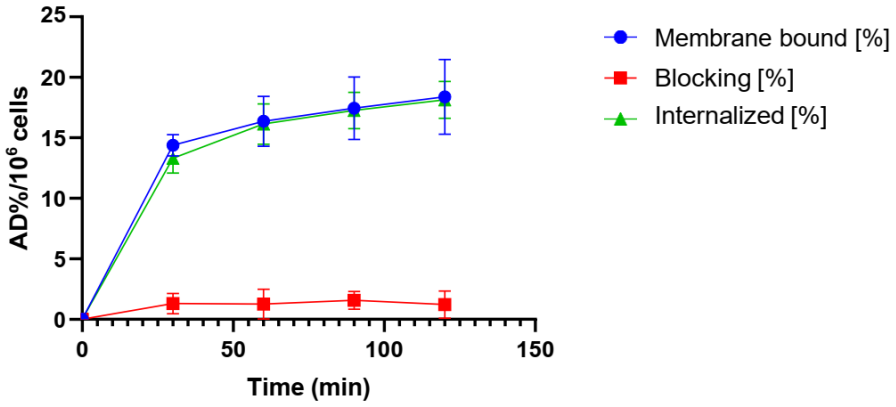

Figure S12: Cell internalization, receptor binding and blocking experiment of [^{68}Ga]Ga-WL12 on CHO-K1 hPD-L1 cells. Blocking was determined by incubating the cells with the radiotracers and a 1000-fold excess of reference WL12 (15 nmol; 100 µL per well) as the receptor blocking agent.

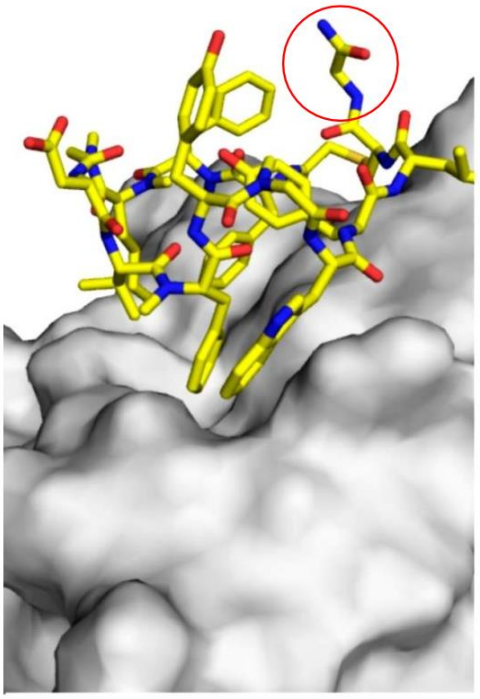

Figure S13: Co-crystal structure of BMS78/PD-L1. The position of the C-terminus Gly^{14}-NH_2 (red circle) is not involved in the hydrophobic interactions that constituted the main type of binding to the PD-L1 pocket. Image reprinted with permission from the publisher Wiley-VCH [1].

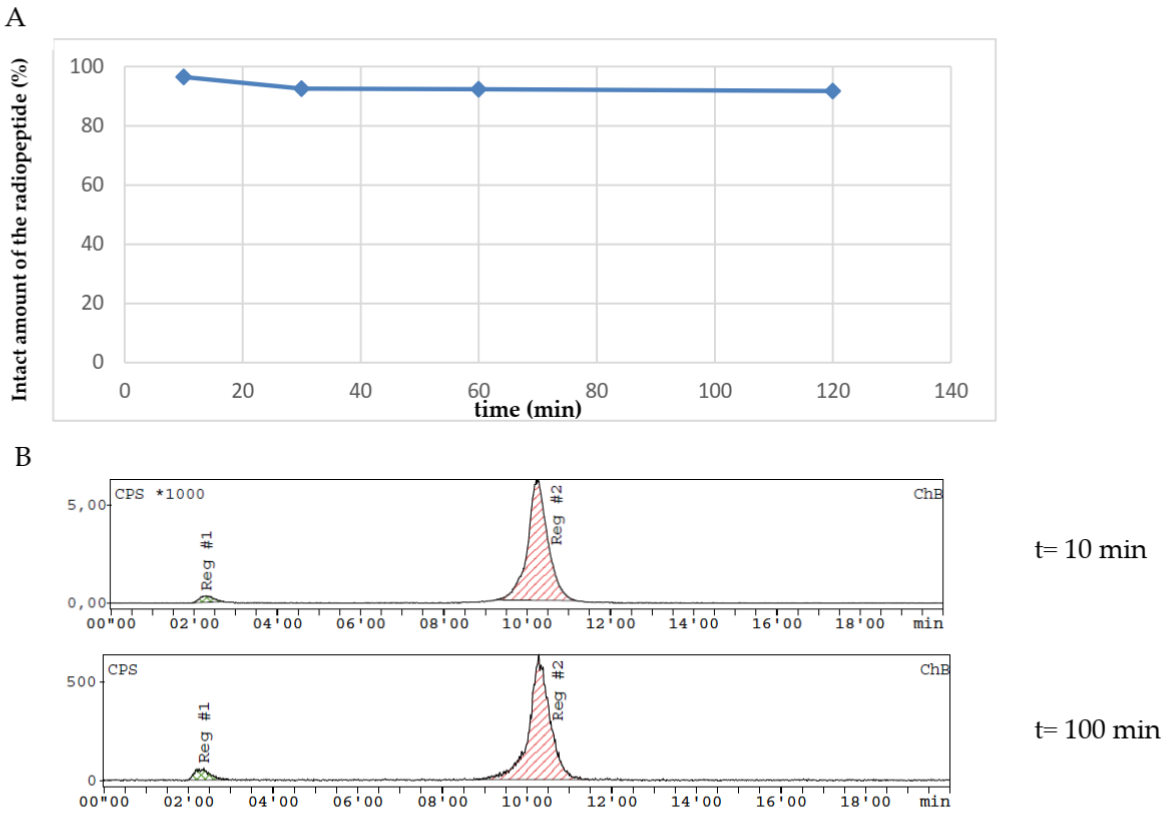

Figure S14: A) Stability curve of the radiopeptide NJMP1, B) Radio-HPLC of [^{68}Ga]Ga-NJMP1 after incubation with human serum at 37 °C (t = 10 min and 100 min).

References:

1. K. Magiera-Mularz, L. Skalniak, K. M. Zak, B. Musielak, E. Rudzinska-Szostak, Ł. Berlicki, J. Kocik, P. Grudnik, D. Sala, T. Zarganes-Tzitzikas, S. Shaabani, A. Dömling, G. Dubin, TA. Holak, *Angew. Chem. Int. Ed.* **2017**, 56, 13732–13735.

Concluding Remarks

Developing a novel radiotracer is a multi-step process. Many efforts and strategies are implemented in the various steps: from the initial identification of a promising biomolecule candidate, its synthesis, radiolabeling, till its preclinical evaluation *in vitro* and *in vivo*. Nevertheless, unforeseen setbacks and negative results often require iterative approaches that rely on multidisciplinary techniques. However, pioneers of the field took on this challenge and investigated an important class of molecules (peptides) targeting the immune checkpoint PD-1/PD-L1 as a potential radiotracer for PD-L1 imaging with PET and SPECT.

In this work, the development of a PET/SPECT peptide-based radiotracer (NJMP1) targeting the immune checkpoint ligand PD-L1 has been first met with some adversity in synthesizing its parent peptide (BMS 71). The instability of multiple consecutive *N*-methylated amide bonds led to poor synthesis yields. This was overcome by omitting methylation on one of the N-terminal amino acids without affecting the overall binding affinity (IC_{50} values were reported to still be in the nanomolar range), leading to the synthesis of BMS 78. The macrocyclic peptide was successfully obtained in better yields and higher stability. Further modifications were introduced to the parent peptide (BMS78) by conjugating a universal chelator DOTA to its C-terminal Gly-NH_2. In the evaluation of a novel PD-L1 radiotracer, the following steps to be taken consisted of establishing the radiosynthesis of the ^{68}Ga-labeled and ^{111}In-labeled radiopeptides to optimize the specific molar activity while maintaining high radiochemical yield (RCY) and purity.

During the radiolabeling experiments with the SPECT radionuclide ^{111}In, low radiochemical yields were observed when the [^{111}In]$InCl_3$ stock solution was used for multiple radiolabelling reactions at different time points. We identified, using an iTLC system, an unknown [^{111}In]In-species in the stock solution and the peptide-conjugates radiolabeling mixtures. DOTANOC was used as a valid test compound for the ^{111}In labelling. Our investigations have distinguished between the radiocolloids and the formed unknown [^{111}In]In-species , confirming therefore the cause of the poor RCYs. The restoration of the initial stock solution and the reactivity of ^{111}In was made possible by reversing the reaction and increasing the concentration of chloride ions in [^{111}In]$InCl_3$ in accordance with the Law of Mass Action. Nevertheless, we proceeded with the radiolabeling experiments of NJMP1 with ^{68}Ga out of convenience, which gave a product of high radiochemical purity and yield.

The evaluation of both $^{68/nat}$Ga-labeled NJMP1 *in vitro* relied on radioligand binding assays with CHO-K1 hPD-L1 cells and fluorescence-based cellular assays (HTRF). The reported corresponding PD-L1 radiopeptide, WL12, was used as a reference compound for comparison. We found that the parent peptide (BMS 78; without the chelator) exhibited a lower affinity towards PD-L1 than what was reported in the BMS patent. Furthermore, an additional decrease of affinity was observed after the C-terminal modification of the macrocyclic peptide with the chelator DOTA and after the metalation with $^{nat/68}$Ga.

We tentatively ascribe this observation to the disturbance of the reported necessary hydrogen bonding between PD-L1 and the C-terminal Gly^{14}-NH_2.

As the research in the field of PD-L1 targeting radiotracers expands, the validated *in vitro* test system consisting of CHO-K1 hPD-L1 and CHO-K1 cells developed during this work is available to the research community as a reliable tool to assess novel PD-L1 radiotracers. This system would allow the community to generate well-grounded results and progress in promoting research with medium-sized peptides and molecules.

Despite the low binding affinity of BMS 78 and the peptide conjugates, its potential to inhibit the interaction between PD-1 and PD-L1 has been proven. Our findings would pave the path for the anti-PD-L1 peptides in the pipelines. It lays the groundwork for further optimization of this class of biomolecules, and their evaluation in a validated *in vitro* set-up. Moreover, investigating and overcoming the formation of unknown radioactive [^{111}In]In-species during the radiolabelling experiments with ^{111}In is a valuable discovery that can save time and efforts spent on troubleshooting. Instead, the focus would be directed towards increasing radiochemical yields. Regardless of the discontinued development of a novel PET /SPECT radiotracer, the conclusions of this doctoral thesis had no precedent and shall play an essential role in the progress of research in the field of radiopharmacy, immune-oncology and drug development.

Abbreviations

%	Percentage
°C	Degree Celsius
µ	Micro
Å	ångström
α	Alpha
B	Beta
Γ	Gamma
AA	Amino acid
Ac	Acetyl
Aq.	Aqueous
BFCA	Bifunctional chelating agent
Bq	Becquerel
BMS	Bristol Myers Squibb
CHO-K1	Chinese hamster ovary cell
CNS	Central nervous system
CT	Computed tomography
DIPEA	Diisopropylethylamine
DMF	Dimethylformamide
DOTA	1,4,7,10-tetraazacyclododecane-1,4,7,10- tetraacetic acid
DOTAGA	1,4,7,10-tetraazacyclododecane- 4,7,10-triacetic acid-1-[2-glutaric acid]
DOTATE	DOTA-(Tyr^3)-octreotate
DOTATOC	DOTA-(Phe^1)-(Tyr^3)-octreotide
DTPA	Diethylenetriaminepentaacetic acid
EC	Electron capture
EDTA	Ethylenediaminetetracetic acid
e.g.	*Exempli gratia*
Equiv.	Equivalent
ESI	Electrospray ionization
eV	Electron volt
FDA	Food and Drug Administration
FDG	Fluorodesoxyglucose
Fmoc	9-fluorenylmethoxycarbonyl
G	Giga
HPLC	High-performance liquid chromatography
IC_{50}	Half maximal inhibitory concentration
iTLC	Instant thin layer chromatography
IHC	Immunohistochemistry
K_D	Dissociation constant
K_{on}	Rate of association

K_{off}	Rate of dissociation
kDa	Kilo Dalton
keV	Kilo-electronvolt
LET	Linear energy transfer
LogD	Water/octanol distribution coefficient
M	Molarity
m/z	Mass to charge ratio
mAb	Monoclonal antibody
Me	Methyl
MeOH	Methanol
MRI	Magnetic resonance imaging
nat	Natural
NET	Neuroendocrine tumor
OI	Optical imaging
PD-1	Programmed cell death receptor 1
PD-L1	Programmed cell death ligand 1
PET	positron emission tomography
PK	Pharmacokinetic
RCY	Radiochemical yields
RIT	Radioimmunotherapy
RP	Reversed phase
SAR	Structure-activity relationship
SPECT	Single photon emission computed tomography
SPPS	Solid phase peptide synthesis
SST	Somatostatin
Sv	Sievert
US	Ultrasound
$t_{1/2}$	Half-life
*t*Bu	*tert*-Butyl
TFA	Trifluoracetic acid
TIS	Triisopropylsilane
UV	Ultraviolet

List of Figures

List of Tables

References

1. James ML, Gambhir SS. A molecular imaging primer: modalities, imaging agents, and applications. Physiol Rev. 2012;92(2):897-965.
2. Chen ZY, Wang YX, Lin Y, Zhang JS, Yang F, Zhou QL, et al. Advance of molecular imaging technology and targeted imaging agent in imaging and therapy. Biomed Res Int. 2014;2014:819324.
3. Martin Pomper HV, Carolyn Anderson; SNM Molecular Imaging Center of Excellence. What is molecular imaging? Journal of Nuclear Medicine. 2008;49:163.
4. Weissleder R, Pittet MJ. Imaging in the era of molecular oncology. Nature. 2008;452(7187):580-9.
5. Paulus MJ, Gleason SS, Kennel SJ, Hunsicker PR, Johnson DK. High resolution X-ray computed tomography: an emerging tool for small animal cancer research. Neoplasia. 2000;2(1-2):62-70.
6. Pysz MA, Gambhir SS, Willmann JK. Molecular imaging: current status and emerging strategies. Clin Radiol. 2010;65(7):500-16.
7. Kim HL. Optical imaging in oncology. Urol Oncol. 2009;27(3):298-300.
8. Gonzalez Hernando C, Esteban L, Canas T, Van den Brule E, Pastrana M. The role of magnetic resonance imaging in oncology. Clin Transl Oncol. 2010;12(9):606-13.
9. Kufe DW, Holland JF, Frei E, Society AC. Cancer Medicine 6: BC Decker; 2003.
10. Reedijk J. Reference Module in Chemistry, Molecular Sciences and Chemical Engineering: Elsevier; 2013.
11. Berger A. How does it work? Positron emission tomography. BMJ. 2003;326(7404):1449.
12. Hutton BF. The origins of SPECT and SPECT/CT. Eur J Nucl Med Mol Imaging. 2014;41 Suppl 1:S3-16.
13. Deshpande N, Pysz MA, Willmann JK. Molecular ultrasound assessment of tumor angiogenesis. Angiogenesis. 2010;13(2):175-88.
14. Belkić D BK. Molecular imaging in the framework of personalized cancer medicine. The Israel Medical Association Journal 2013;15(11):665-72.
15. Townsend DW. Positron emission tomography/computed tomography. Semin Nucl Med. 2008;38(3):152-66.
16. Kostakoglu L, Hardoff R, Mirtcheva R, Goldsmith SJ. PET-CT fusion imaging in differentiating physiologic from pathologic FDG uptake. Radiographics. 2004;24(5):1411-31.
17. Ritt P, Kuwert T. Quantitative SPECT/CT. Recent Results Cancer Res. 2013;187:313-30.
18. Zhao T, Su L, Xia W. Optical Ultrasound Generation and Detection for Intravascular Imaging: A Review. J Healthc Eng. 2018;2018:3182483.
19. Pimlott SL, Sutherland A. Molecular tracers for the PET and SPECT imaging of disease. Chem Soc Rev. 2011;40(1):149-62.
20. Barsanti C, Lenzarini F, Kusmic C. Diagnostic and prognostic utility of non-invasive imaging in diabetes management. World J Diabetes. 2015;6(6):792-806.
21. Thurman JM, Serkova NJ. Non-invasive imaging to monitor lupus nephritis and neuropsychiatric systemic lupus erythematosus. F1000Research. 2015;4:153.
22. Sadeghi MM, Glover DK, Lanza GM, Fayad ZA, Johnson LL. Imaging atherosclerosis and vulnerable plaque. J Nucl Med. 2010;51 Suppl 1:51S-65S.
23. Bolus NE, George R, Washington J, Newcomer BR. PET/MRI: the blended-modality choice of the future? J Nucl Med Technol. 2009;37(2):63-71; quiz 2-3.
24. Vértes A, Nagy S, Klencsár Z, Lovas RG, Rösch F. Handbook of Nuclear Chemistry2011.
25. Hicks RJ, Hofman MS. Is there still a role for SPECT-CT in oncology in the PET-CT era? Nat Rev Clin Oncol. 2012;9(12):712-20.
26. Boellaard R. Standards for PET image acquisition and quantitative data analysis. J Nucl Med. 2009;50 Suppl 1:11S-20S.
27. Bateman TM. Advantages and disadvantages of PET and SPECT in a busy clinical practice. J Nucl Cardiol. 2012;19 Suppl 1:S3-11.
28. Rahmim A, Zaidi H. PET versus SPECT: strengths, limitations and challenges. Nucl Med Commun. 2008;29(3):193-207.
29. Anger HO. Scintillation Camera. Review of Scientific Instruments. 1958;29(1):27-33.
30. Saha GB. Scintillation and Semiconductor Detectors. Physics and Radiobiology of Nuclear Medicine. New York, NY: Springer New York; 2006. p. 81-107.
31. Saha GB. Performance Parameters of Gamma Cameras. Physics and Radiobiology of Nuclear Medicine. New York, NY: Springer New York; 2006. p. 118-38.
32. Cherry SS, James & Phelps, Michael. Tomographic Reconstruction in Nuclear Medicine2012.

33. Qwerty123uiop. Photomultiplier Tube: Wikipedia; 2013 [Available from: https://commons.wikimedia.org/wiki/File:PhotoMultiplierTubeAndScintillator.svg#/media/File:PhotoMultiplierTubeAndScintillator.svg
34. Lapa C, Nestle U, Albert NL, Baues C, Beer A, Buck A, et al. Value of PET imaging for radiation therapy. Nuklearmedizin. 2021;60(5):326-43.
35. Dahlbom SRC. PET: Physics, Instrumentation, and Scanners. 1 ed: Springer, New York, NY; 2006. 130 p.
36. Vardi Y, Shepp LA, Kaufman L. A Statistical Model for Positron Emission Tomography. Journal of the American Statistical Association. 1985;80(389):8-20.
37. Dagogo-Jack I, Shaw AT. Tumour heterogeneity and resistance to cancer therapies. Nat Rev Clin Oncol. 2018;15(2):81-94.
38. Marusyk A, Polyak K. Tumor heterogeneity: causes and consequences. Biochim Biophys Acta. 2010;1805(1):105-17.
39. Janku F. Tumor heterogeneity in the clinic: is it a real problem? Ther Adv Med Oncol. 2014;6(2):43-51.
40. Bailly C, Bodet-Milin C, Bourgeois M, Gouard S, Ansquer C, Barbaud M, et al. Exploring Tumor Heterogeneity Using PET Imaging: The Big Picture. Cancers (Basel). 2019;11(9).
41. Alic L, Niessen WJ, Veenland JF. Quantification of heterogeneity as a biomarker in tumor imaging: a systematic review. PLoS One. 2014;9(10):e110300.
42. Sharma M, Soni SL, Kumar D, Jain S, Shrivastava S. A Review on Theranostics: An Approach to Targeted Diagnosis and Therapy. Asian Journal of Pharmaceutical Research and Development. 2019;7(2):63-9.
43. Kelkar SS, Reineke TM. Theranostics: combining imaging and therapy. Bioconjug Chem. 2011;22(10):1879-903.
44. Silberstein EB. Radioiodine: the classic theranostic agent. Semin Nucl Med. 2012;42(3):164-70.
45. Gomes Marin JF, Nunes RF, Coutinho AM, Zaniboni EC, Costa LB, Barbosa FG, et al. Theranostics in Nuclear Medicine: Emerging and Re-emerging Integrated Imaging and Therapies in the Era of Precision Oncology. Radiographics. 2020;40(6):1715-40.
46. Bockisch A. Matched pairs for radionuclide-based imaging and therapy. Eur J Nucl Med Mol Imaging. 2011;38 Suppl 1:S1-3.
47. Mikolajczak R, Huclier-Markai S, Alliot C, Haddad F, Szikra D, Forgacs V, et al. Production of scandium radionuclides for theranostic applications: towards standardization of quality requirements. EJNMMI Radiopharm Chem. 2021;6(1):19.
48. Borrego-Soto G, Ortiz-Lopez R, Rojas-Martinez A. Ionizing radiation-induced DNA injury and damage detection in patients with breast cancer. Genet Mol Biol. 2015;38(4):420-32.
49. Herzog H. Dosimetry related to SPECT and PET applications. Radiochimica Acta. 2001;89(4-5):215-22.
50. Flux G, Bardies M, Monsieurs M, Savolainen S, Strands SE, Lassmann M, et al. The impact of PET and SPECT on dosimetry for targeted radionuclide therapy. Z Med Phys. 2006;16(1):47-59.
51. Cinca J, Garcia-Burillo A, Carreño A, Castell J, Warren M, Candell-Riera J, et al. Differential uptake of myocardial perfusion radiotracers in normal, infarcted, and acutely ischemic peri-infarction myocardium. Cardiovascular Research. 1998;38(1):91-7.
52. Moka D, Voth E, Dietlein M, Larena-Avellaneda A, Schicha H. Technetium 99m-MIBI-SPECT: A highly sensitive diagnostic tool for localization of parathyroid adenomas. Surgery. 2000;128(1):29-35.
53. Edward Deutsch KL, Carolyn B. Becker, Marion D. Francis, Andrew J. Tofe, Debra L. Ferguson and Lionel D. McCreary. Preparation and Biological Distribution of Technetium Diphosphonate Radiotracers Synthesized Without Stannous Ion. Society of Nuclear Medicine. 1980;21(9):859-66.
54. Handley MG, Medina RA, Mariotti E, Kenny GD, Shaw KP, Yan R, et al. Cardiac hypoxia imaging: second-generation analogues of 64Cu-ATSM. J Nucl Med. 2014;55(3):488-94.
55. Cherry SR, Jones T, Karp JS, Qi J, Moses WW, Badawi RD. Total-Body PET: Maximizing Sensitivity to Create New Opportunities for Clinical Research and Patient Care. J Nucl Med. 2018;59(1):3-12.
56. Poeppel TD, Binse I, Petersenn S, Lahner H, Schott M, Antoch G, et al. 68Ga-DOTATOC versus 68Ga-DOTATATE PET/CT in functional imaging of neuroendocrine tumors. J Nucl Med. 2011;52(12):1864-70.
57. Werner RA, Derlin T, Lapa C, Sheikbahaei S, Higuchi T, Giesel FL, et al. (18)F-Labeled, PSMA-Targeted Radiotracers: Leveraging the Advantages of Radiofluorination for Prostate Cancer Molecular Imaging. Theranostics. 2020;10(1):1-16.
58. Pruis IJ, van Dongen G, Veldhuijzen van Zanten SEM. The Added Value of Diagnostic and Theranostic PET Imaging for the Treatment of CNS Tumors. Int J Mol Sci. 2020;21(3).
59. Kumar K. Radiolabeled Compounds for Diagnosis and Treatment of Cancer. Molecules. 2021;26(20).
60. Chemistry of Organic Radionuclides (C, N, and O). Molecular Imaging: Radiopharmaceuticals for PET and SPECT. Berlin, Heidelberg: Springer Berlin Heidelberg; 2009. p. 167-77.
61. Brandt M, Cardinale J, Aulsebrook ML, Gasser G, Mindt TL. An Overview of PET Radiochemistry, Part 2: Radiometals. J Nucl Med. 2018;59(10):1500-6.

62. Pichler V, Berroteran-Infante N, Philippe C, Vraka C, Klebermass EM, Balber T, et al. An Overview of PET Radiochemistry, Part 1: The Covalent Labels (18)F, (11)C, and (13)N. J Nucl Med. 2018;59(9):1350-4.
63. Burke JF. Radiometals in diagnosis and therapy. Met Based Drugs. 1997;4(3):153-8.
64. Jacobson O, Kiesewetter DO, Chen X. Fluorine-18 radiochemistry, labeling strategies and synthetic routes. Bioconjug Chem. 2015;26(1):1-18.
65. Law WP. Molecular Imaging of Brain Tumours. InTech; 2016.
66. Kostakoglu L, Agress H, Jr., Goldsmith SJ. Clinical role of FDG PET in evaluation of cancer patients. Radiographics. 2003;23(2):315-40; quiz 533.
67. Nagarajah J, Janssen M, Hetkamp P, Jentzen W. Iodine Symporter Targeting with (124)I/(131)I Theranostics. J Nucl Med. 2017;58(Suppl 2):34S-8S.
68. Tolmachev V. Radiobromine-labelled tracers for positron emission tomography: possibilities and pitfalls. Curr Radiopharm. 2011;4(2):76-89.
69. Market Ra. Global Radiopharmaceuticals Market Report 2021 Globenewswire2021 [Available from: https://www.globenewswire.com/news-release/2021/05/24/2234505/28124/en/Global-Radiopharmaceuticals-Market-Report-2021-High-Cost-of-Radiopharmaceuticals-is-Anticipated-to-Limit-the-Growth-of-the-Market.html.
70. Lewis JS, Windhorst AD, Zeglis BM. Radiopharmaceutical Chemistry2019.
71. Bhattacharyya S, Dixit M. Metallic radionuclides in the development of diagnostic and therapeutic radiopharmaceuticals. Dalton Trans. 2011;40(23):6112-28.
72. Synowiecki MA, Perk LR, Nijsen JFW. Production of novel diagnostic radionuclides in small medical cyclotrons. EJNMMI Radiopharm Chem. 2018;3(1):3.
73. Chemistry of Aluminium, Gallium, Indium and Thallium: Springer Dordrecht; 1993. 526 p.
74. Sneddon D, Cornelissen B. Emerging chelators for nuclear imaging. Curr Opin Chem Biol. 2021;63:152-62.
75. Martell AE. The Chelate Effect. Werner Centennial. Advances in Chemistry. 62: AMERICAN CHEMICAL SOCIETY; 1967. p. 272-94.
76. Vallet V, Wahlgren U, Grenthe I. Chelate effect and thermodynamics of metal complex formation in solution: a quantum chemical study. J Am Chem Soc. 2003;125(48):14941-50.
77. Hancock RD, McDougall GJ. The macrocyclic effect in tetraaza-macrocyclic ligands. Advances in Molecular Relaxation and Interaction Processes. 1980;18(2):99-108.
78. Cabbiness DK, Margerum DW. Macrocyclic effect on the stability of copper(II) tetramine complexes. Journal of the American Chemical Society. 2002;91(23):6540-1.
79. Okoye NC, Baumeister JE, Najafi Khosroshahi F, Hennkens HM, Jurisson SS. Chelators and metal complex stability for radiopharmaceutical applications. Radiochimica Acta. 2019;107(9-11):1087-120.
80. Price EW, Orvig C. Matching chelators to radiometals for radiopharmaceuticals. Chem Soc Rev. 2014;43(1):260-90.
81. Rey AM. Radiometal complexes in molecular imaging and therapy. Curr Med Chem. 2010;17(31):3673-83.
82. Wangler B, Schirrmacher R, Bartenstein P, Wangler C. Chelating agents and their use in radiopharmaceutical sciences. Mini Rev Med Chem. 2011;11(11):968-83.
83. Sarko D, Eisenhut M, Haberkorn U, Mier W. Bifunctional chelators in the design and application of radiopharmaceuticals for oncological diseases. Curr Med Chem. 2012;19(17):2667-88.
84. Poschenrieder A, Schottelius M, Schwaiger M, Kessler H, Wester HJ. The influence of different metal-chelate conjugates of pentixafor on the CXCR4 affinity. EJNMMI Res. 2016;6(1):36.
85. Shpinkova LG, Carbonari AW, Nikitin SM, Mestnik-Filho J. Influence of electron capture after-effects on the stability of 111In(111Cd)-complexes with organic ligands. Chemical Physics. 2002;279(2-3):255-63.
86. Bjørnstad T, Portela JI, Brisset P, Chankow N, Charlton JS, Solis MA, et al. Radiotracer generators for industrial applications, IAEA Radiation Technology Series No. 52013.
87. Hunt F. Radionuclides of gallium and indium : new applications in nuclear medicine. Chemistry in Australia. 1987;54(10):368-70.
88. Maecke HR, Andre JP. 68Ga-PET radiopharmacy: A generator-based alternative to 18F-radiopharmacy. Ernst Schering Res Found Workshop. 2007(62):215-42.
89. Hofman MS, Lau WF, Hicks RJ. Somatostatin receptor imaging with 68Ga DOTATATE PET/CT: clinical utility, normal patterns, pearls, and pitfalls in interpretation. Radiographics. 2015;35(2):500-16.
90. Rinne S, Vorobyeva A. Radiometals—Chemistry and radiolabeling. 2021.
91. Hasegawa T, Okada K, Morimoto Y, Okita Y. Indium-111-oxine-labeled platelet scintigraphic images in the assessment of thrombogenicity in small-caliber prosthetic vascular grafts. ASAIO J. 2006;52(2):140-4.
92. Lahiri S, Maiti M, Ghosh K. Production and separation of 111In: an important radionuclide in life sciences: a mini review. Journal of Radioanalytical and Nuclear Chemistry. 2012;297(3):309-18.
93. Wadas TJ, Wong EH, Weisman GR, Anderson CJ. Coordinating radiometals of copper, gallium, indium, yttrium, and zirconium for PET and SPECT imaging of disease. Chem Rev. 2010;110(5):2858-902.

94. Luigi Camera SK, Kayhan Garmestani, Chuanchu Wu, Martin W. Brechbiel, Lee H. Pai, Thomas J. McMurry, Otto A. Gansow, Ira Pastan, Chang H. Paik and Jorge A. Carrasquillo. Evaluation of the Serum Stability and In Vivo Biodistribution of CHX-DTPA and Other Ligands for Yttrium Labeling of Monoclonal Antibodies. Journal of Nuclear Medicine. 1994;35(5):882-9.
95. von Witting E, Garousi J, Lindbo S, Vorobyeva A, Altai M, Oroujeni M, et al. Selection of the optimal macrocyclic chelators for labeling with (111)In and (68)Ga improves contrast of HER2 imaging using engineered scaffold protein ADAPT6. Eur J Pharm Biopharm. 2019;140:109-20.
96. Roosenburg S, Laverman P, Joosten L, Cooper MS, Kolenc-Peitl PK, Foster JM, et al. PET and SPECT imaging of a radiolabeled minigastrin analogue conjugated with DOTA, NOTA, and NODAGA and labeled with (64)Cu, (68)Ga, and (111)In. Mol Pharm. 2014;11(11):3930-7.
97. Tsionou MI, Knapp CE, Foley CA, Munteanu CR, Cakebread A, Imberti C, et al. Comparison of macrocyclic and acyclic chelators for gallium-68 radiolabelling. RSC Adv. 2017;7(78):49586-99.
98. Berry DJ, Ma Y, Ballinger JR, Tavare R, Koers A, Sunassee K, et al. Efficient bifunctional gallium-68 chelators for positron emission tomography: tris(hydroxypyridinone) ligands. Chem Commun (Camb). 2011;47(25):7068-70.
99. Moerlein SM, Welch MJ. The chemistry of gallium and indium as related to radiopharmaceutical production. International Journal of Nuclear Medicine and Biology. 1981;8(4):277-87.
100. Frank C, Winter G, Rensei F, Samper V, Brooks AF, Hockley BG, et al. Development and implementation of ISAR, a new synthesis platform for radiopharmaceutical production. EJNMMI Radiopharmacy and Chemistry. 2019;4(1).
101. Sharma R, Aboagye E. Development of radiotracers for oncology--the interface with pharmacology. Br J Pharmacol. 2011;163(8):1565-85.
102. Kunos CA, Mankoff DA, Schultz MK, Graves SA, Pryma DA. Radiopharmaceutical Chemistry and Drug Development-What's Changed? Semin Radiat Oncol. 2021;31(1):3-11.
103. Use ICfHoTRfPfH. Efficacy Guidelines 2021 [Available from: https://www.ich.org/page/efficacy-guidelines.
104. Hughes JP, Rees S, Kalindjian SB, Philpott KL. Principles of early drug discovery. Br J Pharmacol. 2011;162(6):1239-49.
105. Hulme EC, Trevethick MA. Ligand binding assays at equilibrium: validation and interpretation. British Journal of Pharmacology. 2010;161(6):1219-37.
106. Motulsky HJ, Neubig RR. Analyzing binding data. Curr Protoc Neurosci. 2010;Chapter 7:Unit 7 5.
107. Degorce F, Card A, Soh S, Trinquet E, Knapik GP, Xie B. HTRF: A technology tailored for drug discovery - a review of theoretical aspects and recent applications. Curr Chem Genomics. 2009;3:22-32.
108. Devices M. TRF / TR-FRET (HTRF) Overview 2020 [Available from: https://www.moleculardevices.com/technology/time-resolved-fluorescence-trf-tr-fret-htrf
109. Jia Y, Quinn CM, Gagnon AI, Talanian R. Homogeneous time-resolved fluorescence and its applications for kinase assays in drug discovery. Anal Biochem. 2006;356(2):273-81.
110. Cisbio. Human PD1/PD-L1 biochemical binding assay 2018 [Available from: https://www.cisbio.eu/human-pd1-pd-l1-biochemical-binding-assay-44666.
111. 2020 G. Estimated age-standardized incidence rates (World) in 2020, all cancers, both sexes, all ages 2020 [Available from: https://www.uicc.org/news/globocan-2020-new-global-cancer-data.
112. Sung H, Ferlay J, Siegel RL, Laversanne M, Soerjomataram I, Jemal A, et al. Global Cancer Statistics 2020: GLOBOCAN Estimates of Incidence and Mortality Worldwide for 36 Cancers in 185 Countries. CA Cancer J Clin. 2021;71(3):209-49.
113. Arem H, Loftfield E. Cancer Epidemiology: A Survey of Modifiable Risk Factors for Prevention and Survivorship. Am J Lifestyle Med. 2018;12(3):200-10.
114. Hennessy B BR, Gonzalez-Angulo AM, Mills GB. Early Detection of Cancer: Molecular Screening. In The Molecular Basis of Cancer Elsevier Inc. 2009:335-47.
115. Henry NL, Hayes DF. Cancer biomarkers. Mol Oncol. 2012;6(2):140-6.
116. Abbas Z, Rehman S. An Overview of Cancer Treatment Modalities. InTech; 2018.
117. Ayoub NM, Al-Shami KM, Yaghan RJ. Immunotherapy for HER2-positive breast cancer: recent advances and combination therapeutic approaches. Breast Cancer (Dove Med Press). 2019;11:53-69.
118. Mayer AT, Gambhir SS. The Immunoimaging Toolbox. J Nucl Med. 2018;59(8):1174-82.
119. Baumeister SH, Freeman GJ, Dranoff G, Sharpe AH. Coinhibitory Pathways in Immunotherapy for Cancer. Annu Rev Immunol. 2016;34:539-73.
120. Unterrainer M, Ruzicka M, Fabritius MP, Mittlmeier LM, Winkelmann M, Rubenthaler J, et al. PET/CT imaging for tumour response assessment to immunotherapy: current status and future directions. Eur Radiol Exp. 2020;4(1):63.
121. Zhao B, Zhao H, Zhao J. Efficacy of PD-1/PD-L1 blockade monotherapy in clinical trials. Ther Adv Med Oncol. 2020;12:1758835920937612.
122. Huang Z, Su W, Lu T, Wang Y, Dong Y, Qin Y, et al. First-Line Immune-Checkpoint Inhibitors in Non-Small Cell Lung Cancer: Current Landscape and Future Progress. Front Pharmacol. 2020;11:578091.

123. Liberini V, Laudicella R, Capozza M, Huellner MW, Burger IA, Baldari S, et al. The Future of Cancer Diagnosis, Treatment and Surveillance: A Systemic Review on Immunotherapy and Immuno-PET Radiotracers. Molecules. 2021;26(8).
124. Iyalomhe O, Farwell MD. Immune PET Imaging. Radiol Clin North Am. 2021;59(5):875-86.
125. Sharpe AH, Pauken KE. The diverse functions of the PD1 inhibitory pathway. Nature Reviews Immunology. 2018;18(3):153-67.
126. Nasser NJ, Gorenberg M, Agbarya A. First line Immunotherapy for Non-Small Cell Lung Cancer. Pharmaceuticals (Basel). 2020;13(11).
127. Bensch F, van der Veen EL, Lub-de Hooge MN, Jorritsma-Smit A, Boellaard R, Kok IC, et al. 89Zr-atezolizumab imaging as a non-invasive approach to assess clinical response to PD-L1 blockade in cancer. Nature Medicine. 2018;24(12):1852-8.
128. McLaughlin J, Han G, Schalper KA, Carvajal-Hausdorf D, Pelekanou V, Rehman J, et al. Quantitative Assessment of the Heterogeneity of PD-L1 Expression in Non-Small-Cell Lung Cancer. JAMA Oncol. 2016;2(1):46-54.
129. Kerr KM, Tsao MS, Nicholson AG, Yatabe Y, Wistuba, II, Hirsch FR, et al. Programmed Death-Ligand 1 Immunohistochemistry in Lung Cancer: In what state is this art? J Thorac Oncol. 2015;10(7):985-9.
130. Khedri M, Abnous K, Rafatpanah H, Ramezani M. An optimized protocol for the in vitro generation and functional analysis of human PD1/PD-L1 signal. J Recept Signal Transduct Res. 2018;38(1):31-6.
131. Li K, Tian H. Development of small-molecule immune checkpoint inhibitors of PD-1/PD-L1 as a new therapeutic strategy for tumour immunotherapy. J Drug Target. 2019;27(3):244-56.
132. Konstantinidou M, Zarganes-Tzitzikas T, Magiera-Mularz K, Holak TA, Domling A. Immune Checkpoint PD-1/PD-L1: Is There Life Beyond Antibodies? Angew Chem Int Ed Engl. 2018;57(18):4840-8.
133. Niemeijer AN, Leung D, Huisman MC, Bahce I, Hoekstra OS, van Dongen G, et al. Whole body PD-1 and PD-L1 positron emission tomography in patients with non-small-cell lung cancer. Nat Commun. 2018;9(1):4664.
134. Leung D, Bonacorsi S, Smith RA, Weber W, Hayes W. Molecular Imaging and the PD-L1 Pathway: From Bench to Clinic. Front Oncol. 2021;11:698425.
135. Broos K, Keyaerts M, Lecocq Q, Renmans D, Nguyen T, Escors D, et al. Non-invasive assessment of murine PD-L1 levels in syngeneic tumor models by nuclear imaging with nanobody tracers. Oncotarget. 2017;8(26):41932-46.
136. Wong NC, Cai Y, Meszaros LK, Biersack H-J, Cook G, Jr., Ting HH, et al. Preclinical development and characterisation of (99m)Tc-NM-01 for SPECT/CT imaging of human PD-L1. Am J Nucl Med Mol Imaging. 2021;11(3):154-66.
137. Lv G, Miao Y, Chen Y, Lu C, Wang X, Xie M, et al. Promising potential of a (18)F-labelled small-molecular radiotracer to evaluate PD-L1 expression in tumors by PET imaging. Bioorg Chem. 2021;115:105294.
138. Liu H, Hu M, Deng J, Zhao Y, Peng D, Feng Y, et al. A Novel Small Cyclic Peptide-Based (68)Ga-Radiotracer for Positron Emission Tomography Imaging of PD-L1 Expression in Tumors. Mol Pharm. 2022;19(1):138-47.
139. Lee AC, Harris JL, Khanna KK, Hong JH. A Comprehensive Review on Current Advances in Peptide Drug Development and Design. Int J Mol Sci. 2019;20(10).
140. Sun X, Li Y, Liu T, Li Z, Zhang X, Chen X. Peptide-based imaging agents for cancer detection. Adv Drug Deliv Rev. 2017;110-111:38-51.
141. Fernandez L, Bustos RH, Zapata C, Garcia J, Jauregui E, Ashraf GM. Immunogenicity in Protein and Peptide Based-Therapeutics: An Overview. Curr Protein Pept Sci. 2018;19(10):958-71.
142. Fani M, Maecke HR, Okarvi SM. Radiolabeled peptides: valuable tools for the detection and treatment of cancer. Theranostics. 2012;2(5):481-501.
143. Fani M, Maecke HR. Radiopharmaceutical development of radiolabelled peptides. Eur J Nucl Med Mol Imaging. 2012;39 Suppl 1:S11-30.
144. Lau JL, Dunn MK. Therapeutic peptides: Historical perspectives, current development trends, and future directions. Bioorg Med Chem. 2018;26(10):2700-7.
145. Krecisz P, Czarnecka K, Krolicki L, Mikiciuk-Olasik E, Szymanski P. Radiolabeled Peptides and Antibodies in Medicine. Bioconjug Chem. 2021;32(1):25-42.
146. Zak KM, Kitel R, Przetocka S, Golik P, Guzik K, Musielak B, et al. Structure of the Complex of Human Programmed Death 1, PD-1, and Its Ligand PD-L1. Structure. 2015;23(12):2341-8.
147. Lin X, Lu X, Luo G, Xiang H. Progress in PD-1/PD-L1 pathway inhibitors: From biomacromolecules to small molecules. Eur J Med Chem. 2020;186:111876.
148. Chen T, Li Q, Liu Z, Chen Y, Feng F, Sun H. Peptide-based and small synthetic molecule inhibitors on PD-1/PD-L1 pathway: A new choice for immunotherapy? Eur J Med Chem. 2019;161:378-98.
149. Pan C, Yang H, Lu Y, Hu S, Wu Y, He Q, et al. Recent advance of peptide-based molecules and nonpeptidic small-molecules modulating PD-1/PD-L1 protein-protein interaction or targeting PD-L1 protein degradation. Eur J Med Chem. 2021;213:113170.

150. Guzik K, Tomala M, Muszak D, Konieczny M, Hec A, Blaszkiewicz U, et al. Development of the Inhibitors that Target the PD-1/PD-L1 Interaction-A Brief Look at Progress on Small Molecules, Peptides and Macrocycles. Molecules. 2019;24(11).
151. Gurung S, Khan F, Gunassekaran GR, Yoo JD, Poongkavithai Vadevoo SM, Permpoon U, et al. Phage display-identified PD-L1-binding peptides reinvigorate T-cell activity and inhibit tumor progression. Biomaterials. 2020;247:119984.
152. Li W, Zhu X, Zhou X, Wang X, Zhai W, Li B, et al. An orally available PD-1/PD-L1 blocking peptide OPBP-1-loaded trimethyl chitosan hydrogel for cancer immunotherapy. J Control Release. 2021;334:376-88.
153. Zhou X, Jiang J, Yang X, Liu T, Ding J, Nimmagadda S, et al. First-in-Humans Evaluation of a PD-L1-Binding Peptide PET Radiotracer in Non-Small Cell Lung Cancer Patients. J Nucl Med. 2022;63(4):536-42.
154. Miller MMM, C.; Allen, M. P.; Bowsher, M. S.; Boy, K. M.; Gillis, E. P.; Langley, D. R.; Mull, E.; Poirier, M. A.; Sanghvi, N.; Sun, L.-Q.; Tenney, D. J.; Yeung, K.-S.; Zhu, J.; Reid, P. C.; Scola, P. M, inventorMacrocyclic Inhibitors of the Pd-1/Pd-L1 and Cd80(B7-1)/Pd-L1 Protein/Protein Interactions. USA2014.
155. Magiera-Mularz K, Skalniak L, Zak KM, Musielak B, Rudzinska-Szostak E, Berlicki L, et al. Bioactive Macrocyclic Inhibitors of the PD-1/PD-L1 Immune Checkpoint. Angew Chem Int Ed Engl. 2017;56(44):13732-5.
156. Surmiak E, Magiera-Mularz K, Musielak B, Muszak D, Kocik-Krol J, Kitel R, et al. PD-L1 Inhibitors: Different Classes, Activities, and Mechanisms of Action. Int J Mol Sci. 2021;22(21).
157. Shaabani S, Huizinga HPS, Butera R, Kouchi A, Guzik K, Magiera-Mularz K, et al. A patent review on PD-1/PD-L1 antagonists: small molecules, peptides, and macrocycles (2015-2018). Expert Opin Ther Pat. 2018;28(9):665-78.
158. Musielak B, Kocik J, Skalniak L, Magiera-Mularz K, Sala D, Czub M, et al. CA-170 - A Potent Small-Molecule PD-L1 Inhibitor or Not? Molecules. 2019;24(15).
159. Zhong Y, Li X, Yao H, Lin K. The Characteristics of PD-L1 Inhibitors, from Peptides to Small Molecules. Molecules. 2019;24(10).
160. Yin H, Zhou X, Huang YH, King GJ, Collins BM, Gao Y, et al. Rational Design of Potent Peptide Inhibitors of the PD-1:PD-L1 Interaction for Cancer Immunotherapy. J Am Chem Soc. 2021;143(44):18536-47.